UNIVERSITÉ DE
SHERBROOKE

Faculté de Génie
Département de Génie Civil

GFRP- REINFORCED CONCRETE COLUMNS UNDER SIMULATED SEISMIC LOADING

COLONNES EN BÉTON ARMÉ RENFORCÉES DE PRFV SOUS UN CHARGEMENT SISMIQUE SIMULÉ

Thèse de doctorat
Spécialité: génie civil

Mohammed Gaber Elshamandy Mohammed

A dissertation submitted in partial fulfillment
of the requirements for the degree of
Doctor of Philosophy
(Civil Engineering)

Jury: Prof. Brahim Benmokrane (Directeur de recherche)
Prof. Murat Saatcioglu (Examinateur)
Prof. Amr ElRagaby (Examinateur)
Prof. Sébastien Langlois (Examinateur et rapporteur)

Sherbrooke (Québec) Canada March 2017

ABSTRACT

Steel and fiber-reinforced-polymer (FRP) materials have different mechanical and physical characteristics. High corrosion resistance, high strength to weight ratio, non-conductivity, favorable fatigue enable the FRP to be considered as alternative reinforcement for structures in harsh environment. Meanwhile, FRP bars have low modulus of elasticity and linear-elastic stress-strain curve. These features raise concerns about the applicability of using such materials as reinforcement for structures prone to earthquakes. The main demand for the structural members in structures subjected to seismic loads is dissipating energy without strength loss which is known as ductility. In the rigid frames, columns are expected to be the primary elements of energy dissipation in structures subjected to seismic loads.

The present study addresses the feasibility of reinforced-concrete columns totally reinforced with glass-fiber-reinforced-polymer (GFRP) bars achieving reasonable strength and the drift requirements specified in various codes. Eleven full-scale reinforced concrete columns—two reinforced with steel bars (as reference specimens) and nine totally reinforced with GFRP bars—were constructed and tested to failure. The columns were tested under quasi-static reversed cyclic lateral loading and simultaneously subjected to compression axial load. The columns are 400 mm square cross-section with a shear span 1650 mm. The specimen simulates a column with 3.7 m in height in a typical building with the point of contra-flexure located at the column mid-height. The tested parameters were the longitudinal reinforcement ratio (0.63, 0.95 and 2.14), the spacing of the transverse stirrups (80, 100, 150), tie configuration (C1, C2, C3 and C4), and axial load level (20%, 30% and 40%).

The test results clearly show that properly designed and detailed GFRP-reinforced concrete columns could reach high deformation levels with no strength degradation. An acceptable level of energy dissipation compared with steel-reinforced concrete columns is provided by GFRP reinforced concrete columns. The dissipated energy of GFRP reinforced concrete columns was 75% and 70% of the counter steel columns at 2.5% and 4% drift ratio respectively. High drift capacity achieved by the columns up to 10% with no significant loss in strength. The high drift capacity and acceptable dissipated energy enable the GFRP columns to be part of the moment resisting frames in regions prone to seismic activities. The experimental

ultimate drift ratios were compared with the estimated drift ratios using the confinement Equation in CSA S806-12. It was found from the comparison that the confinement Equation underestimates values of the drift ratios thus the experimental drift ratios were used to modify transverse FRP reinforcement area in CSA S806-12. The hysteretic behavior encouraged to propose a design procedure for the columns to be part of the moderate ductile and ductile moment resisting frames. The development of design guidelines, however, depends on determining the elastic and inelastic deformations and on assessing the force modification factor and equivalent plastic-hinge length for GFRP-reinforced concrete columns. The experimental results of the GFRP-reinforced columns were used to justify the design guideline, proving the accuracy of the proposed design equations.

Keywords: Concrete columns, GFRP bars, hysteretic response, ductility parameters, energy dissipation, drift capacity, displacement-based design

RÉSUMÉ

L'acier et les matériaux à base de polymères renforcés de fibres (PRF) ont des caractéristiques physiques et mécaniques différentes. La résistance à la haute corrosion, le rapport résistance vs poids, la non-conductivité et la bonne résistance à la fatigue font des barres d'armature en PRF, un renforcement alternatif aux barres d'armature en acier, pour des structures dans des environnements agressifs. Cependant, les barres d'armature en PRF ont un bas module d'élasticité et une courbe contrainte-déformation sous forme linéaire. Ces caractéristiques soulèvent des problèmes d'applicabilité quant à l'utilisation de tels matériaux comme renforcement pour des structures situées en forte zone sismique. La principale exigence pour les éléments structuraux des structures soumises à des charges sismiques est la dissipation d'énergie sans perte de résistance connue sous le nom de ductilité. Dans les structures rigides de type cadre, on s'attend à ce que les colonnes soient les premiers éléments à dissiper l'énergie dans les structures soumises à ces charges.

La présente étude traite de la faisabilité des colonnes en béton armé entièrement renforcées de barres d'armature en polymères renforcés de fibres de verre (PRFV), obtenant une résistance et un déplacement latéral raisonnable par rapport aux exigences spécifiées dans divers codes. Onze colonnes à grande échelle ont été fabriquées: deux colonnes renforcées de barres d'acier (comme spécimens de référence) et neuf colonnes renforcées entièrement de barres en PRFV. Les colonnes ont été testées jusqu'à la rupture sous une charge quasi-statique latérale cyclique inversée et soumises simultanément à une charge axiale de compression. Les colonnes ont une section carrée de 400 mm avec une portée de cisaillement de 1650 mm pour simuler une colonne de 3,7 m de hauteur dans un bâtiment typique avec le point d'inflexion situé à la mi-hauteur. Les paramètres testés sont : le taux d'armature longitudinal (0,63%, 0,95% et 2,14 %), l'espacement des étriers (80mm, 100mm, 150 mm), les différentes configurations (C1, C2, C3 et C4) et le niveau de charge axiale (20%, 30 % et 40%).

Les résultats des essais montrent clairement que les colonnes en béton renforcées de PRFV et bien conçues peuvent atteindre des niveaux de déformation élevés sans réduction de résistance. Un niveau acceptable de dissipation d'énergie, par rapport aux colonnes en béton armé avec de l'armature en acier, est atteint par les colonnes en béton armé de PRFV.

L'énergie dissipée des colonnes en béton armé de PRFV était respectivement de 75% et 70% des colonnes en acier à un rapport déplacement latéral de 2,5% et 4%. Un déplacement supérieur a été atteint par les colonnes en PRFV jusqu'à 10% sans perte significative de résistance. La capacité d'un déplacement supérieur et l'énergie dissipée acceptable permettent aux colonnes en PRFV de participer au moment résistant dans des régions sujettes à des activités sismiques. Les rapports des déplacements expérimentaux ultimes ont été comparés avec les rapports estimés en utilisant l'Équation de confinement du code CSA S806-12. À partir de la comparaison, il a été trouvé que l'Équation de confinement sous-estime les valeurs des rapports de déplacement, donc les rapports de déplacement expérimentaux étaient utilisés pour modifier la zone de renforcement transversal du code CSA S806-12. Le comportement hystérétique encourage à proposer une procédure de conception pour que les colonnes fassent partie des cadres rigides à ductilité modérée et résistant au moment. Cependant, l'élaboration de guides de conception dépend de la détermination des déformations élastiques et inélastiques et de l'évaluation du facteur de modification de la force sismique et de la longueur de la rotule plastique pour les colonnes en béton armé renforcées de PRFV. Les résultats expérimentaux des colonnes renforcées de PRFV étudiées ont été utilisés pour justifier la ligne directrice de conception, ce qui prouve l'efficacité des équations de conception proposées.

Mots clés: Colonnes en béton, barres en PRFV, réponse hystérétique, paramétres de ductilité, énergie de dissipation, capacité de déplacement.

ACKNOWLEDGEMENT

Thanks to ***Almighty ALLAH*** for blessing and mercy and to be always beside me when I need and for all the life which I have, starting from choosing for me; my parents, uncle, all my family, teachers, friends and Colleagues.

I would like to express my deepest and sincere gratitude to my supervisor Professor ***Brahim Benmokrane*** not just for giving me the opportunity to work on such project in his large research group or for his patience, kindness, advices and continuous support but also for giving me a clear example for the difference between the leader and the boss.

I would like to express my deepest and sincere gratitude to Dr. ***Ahmed Farghaly*** for his patience and advices, helping, co-operation and guidance during my program starting from first step to the last one which even included participating in the experimental work and analysis.

Deep thanks for my colleagues and friends ***Ahmed Arafa***, ***Ahmed Hassanien, Fareed Elgabbas***, and ***Khaled Mohamed*** for helping me during the cages fabrication and casting.

Thanks for all my colleagues in Civil Engineering Department and our research group technical staff ***Martin Bernard.***

Thanks cannot be described for ***my parents; my mother and my father*** and my uncle ***Abdelnasser*** for their love, kindness, teaching, support, advices, and consolation and also for being a real good example I tried to follow.

Thanks for my ***brothers*** and ***sister*** who I cannot imagine my life without them, who really sharing me all my memories including happiness and sadness who setting with them and with our parents means all happiness to me.

Thanks for my GOD that I have my wife ***Karmen Mohammed*** in my life who was really a great support for me during my work. Really thanks for her sacrifices, co-operation, kindness, understanding and love.

Finally thanks for GOD for having my kids ***Adam*** and ***Nour*** who just looking at their eyes when they smile, give me all happiness in the world.

TABLE OF CONTENTS

TABLE OF CONTENTS

TABLE OF CONTENTS

TABLE OF CONTENTS

LIST OF TABLES

LIST OF TABLES

LIST OF FIGURES

CHAPTER 1: INTRODUCTION

1.1 General

Using of Fiber Reinforced Polymers-FRP- reinforcement as alternative to steel reinforcement is being explored in all members of the new concrete structures such as slabs, beams, columns, shear walls, squat walls and shear walls. The reasons for increase in demand and usage of FRP reinforcement in the civil engineering industry are as follows:

1. FRP reinforcement possess many desirable features including high strength to weight ratio, non-conductivity, electro-magnetic transparency, favorable fatigue strength and low relaxation characteristics.
2. The long term cost and effectiveness of FRP reinforcement when used in corrosive environments like chemical plants, waste-water treatment plants, marine structures and industrial cooling towers encouraged structures owners and governments to use these kind of materials.
3. The deterioration state of the infrastructures which requires restoration and maintenance proceedings, opens the door for FRP reinforcement not just in rehabilitation and strengthening of existing structures but also as alternative to steel reinforcement in the new structures.

All the previous characteristics enabled FRP bars and stirrups to be good replacement to steel bars and stirrups respectively, however, the stress-strain relationship for FRP bars is linear elastic up to failure without a yielding plateau as happens in the case of steel bars. This raises concerns about the applicability of using FRP bars in reinforcing concrete structural members exposed to seismic activities. Inquiries for the behavior of FRP reinforced concrete structures regarding the deformability, strength, and energy dissipation need to be explored. These characteristics are essential for concrete structural members exposed to seismic actions like earthquakes and wind loads.

The ductility of earthquake resistant structures assures the ability and capacity of the structural elements to absorb and dissipate energy under seismic loads without a significant loss of strength. Due to the inelastic behavior of the structural element, the plastic hinge might be developed. The plastic hinge is the region where the inelastic deformations appear and in return dissipate the

absorbed energy. Consequently, reinforced concrete columns have to provide an important inelastic response without a significant decrease of strength capacity. In order to guarantee the ductile behavior of the columns, codes specify the transverse reinforcement ratio provisions to be included in critical zones where a plastic hinge could be developed. In spite of all previous favorable characteristics of FRP reinforcement in new structures, there is a lack in informations regarding the performance of FRP–reinforced columns subjected to lateral reversed loads as in case of earthquakes resistant elements. The present study investigates the performance of GFRP-reinforced concrete columns.

1.2 Research objectives

The main objective of the current research is to investigate the behavior of GFRP-reinforced concrete columns subjected to quasi-static reversed cyclic loading, and to develop design equations for such structural element. Experimental research is needed to verify the applicability of GFRP-reinforced concrete columns under seismic loading. The objectives of the current study can be summarized as follows:

- Design the GFRP-reinforced concrete columns with a dominant flexural behavior in accordance with previous works and design codes guidelines.
- Investigate the ultimate load capacity.
- Investigate the lateral drift ratio, deformability and energy dissipation.
- Assess the seismic behavior and the deformability within the inelastic range of concrete.
- Evaluate the plastic hinge length and ductility related force modification factors needed in the design.
- Propose simplified equation for calculating the deformation capacity and compare the calculated deformation capacity with the needed deformation demand.

1.3 Methodology

To achieve the objectives of this research, the following steps are followed:

- Review the design guidelines in available codes concerning the seismic design of laterally loaded FRP-reinforced concrete elements.
- Review of previous researches on the behavior of concrete columns reinforced with steel and FRP bars.

- Design, constructing, and testing nine large-scale GFRP reinforced concrete columns in addition to two steel reinforced concrete columns which serve as control specimens.
- Analyze the experimental results regarding hysteretic response, lateral drift ratio, deformability, energy dissipation, ultimate load capacity.

1.4 Thesis outlines

The thesis includes six chapters; chapter 1 presents general information on GFRP reinforcement including the advantages of using these materials. The objectives and the methodology of the present study are also included in this chapter. Chapter 2 reports the literature review on steel and FRP reinforced structural members. Chapter 3 includes the experimental program and the followed design philosophy of FRP reinforced concrete elements. Chapter 4 shows the experimental results and analysis. Chapter 5 provides proposed equations for designing GFRP reinforced concrete columns based on displacement capacity. Chapter 6 includes conclusions and recommendations for the future studies based on present study.

CHAPTER 2: LITERATURE REVIEW

2.1 FRP Composite Materials

2.1.1 General

FRPs are being used in many fields like the aeronautical, aerospace and automotive fields since five decades. The use of FRPs in civil engineering started in 1950s when GFRP bars were considered. However, it was not until the 1970s that FRP was finally considered for structural engineering applications. Since their early application, many different types of fibers have been developed including aramid, polyvinyl, carbon and improved glass fibers. Also different shapes and forms have been manufactured such as bars, fabric, 2D grids, 3D grids or standard structural shape.

2.1.2 Constituents

FRP products are composite materials consisting of a matrix (resin) and reinforcing fibers. The fibers have higher strength than the matrix as shown in Figure 2-1. For reinforcing demands, the fiber-volume fraction should be more than 55 percent for FRP bars and rods and 35 percent for FRP grids (ISIS 2007). The mechanical properties of the final FRP product depend on the fiber quality, orientation, shape, volumetric ratio, adhesion to the matrix, and on the manufacturing process.

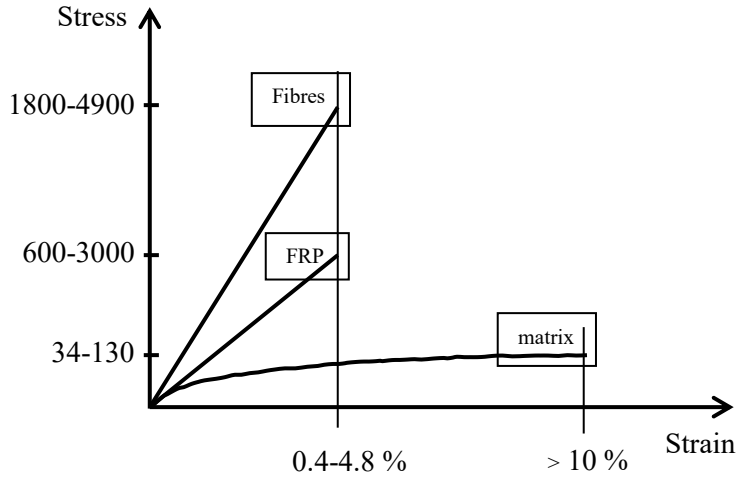

Figure 2-1: Stress-strain relationships for fibrous reinforcement and matrix (ISIS2007)

2.1.2.1 Fibers

High strength and stiffness, toughness, durability and low cost are the main characteristics for the fibers used in manufacturing FRP composite materials. The performances of fibers depend on the fibers length, cross-sectional shape and the chemical composition. Different types, cross-sectional shapes and sizes of fibers are available. The most common fibers are carbon, glass and aramid fibers.

2.1.2.2 Resins

The physical and thermal properties of the matrix significantly affect the final mechanical properties as well as the manufacturing process. To achieve the full strength of the fibers, the matrix should be able to develop a higher ultimate strain than the fibers (Phillips, 1989). Matrix is used for coating the fibers and protecting them from mechanical abrasion, transferring stresses between the fibers, transferring inter-laminar and in-plane shear in the composite, also providing lateral support against fibers buckling. There are two types of polymeric matrices used for FRP composites; namely, thermosetting and thermoplastic.

2.1.3 Manufacturing Process

There are three common manufacturing processes for FRP materials; pultrusion, braiding, and filament winding. Pultrusion is a common technique for manufacturing continuous lengths of FRP bars that are of constant or nearly constant profile. A schematic representation of this technique is shown in Figure 2-2. Continuous strands of reinforcing material are drawn from creels, through a resin tank, and then through a number of wiper rings into the mouth of a heated die. To ensure good bond with concrete, the surface of the bars is usually braided or sand-coated. Braiding is a term used for interlocking two or more yarns to form an integrated structure. Filament winding is a process whereby continuous fibers are impregnated with matrix resin and wrapped around a mandrel (ISIS2007).

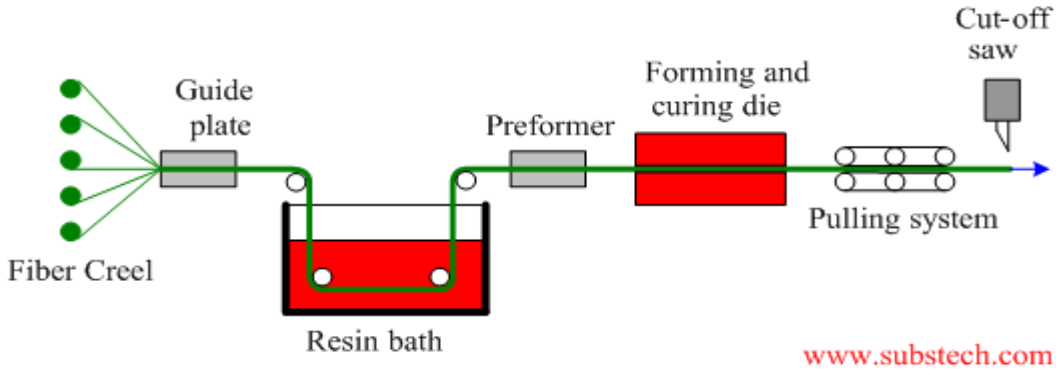

Figure 2-2: Pultrusion process

2.1.4 Physical properties

2.1.4.1 Density

FRP bars have a density ranging from 1.25 to 2.1 g/cm^3, one-sixth to one-fourth of that of steel. Reduced weight lowers transportation costs and may ease handling of the cages during construction. Table 2.1 lists different types of FRP bars densities.

Table 2.1: Typical densities of different FRP bars (ACI 440.1R-15)

Steel	GFRP	CFRP	AFRP
7.9	1.25 to 2.10	1.50 to 1.60	1.25 to 1.40

2.1.4.2 Coefficient of thermal expansion

The coefficients of thermal expansion of FRP bars vary in the longitudinal and transverse directions depending on the types of fiber, resin, and volume fraction of fiber. The longitudinal coefficient of thermal expansion is dominated by the properties of the fibers, while the transverse coefficient is dominated by the resin (Bank 1993). Table 2.2 lists the longitudinal and transverse coefficients of thermal expansion for typical FRP and steel bars.

Table 2.2: Typical Coefficient of thermal expansion for reinforcing bars (ACI 440.1R-15)

Direction	Steel	GFRP	CFRP	AFRP
Longitudinal $\alpha L \times 10^{-6}$/°C	11.7	6.0 to 10	-9.0 to 0.0	-6 to -2
Transverse $\alpha T \times 10^{-6}$/°C	11.7	21 to 23	74 to 104	60 to 80

2.1.5 Mechanical properties

2.1.5.1 Tensile behavior

The tensile behavior of FRP bars consisting of one type of fiber material is characterized by a linearly elastic stress-strain relationship until failure. The tensile properties of some commonly used FRP bars are summarized in Table 2.3. The tensile strength and stiffness of an FRP bar are dependent on several factors. Because the fibers in an FRP bar are the main load-carrying constituent, the ratio of the volume of fiber to the overall volume of the FRP (fiber-volume fraction) significantly affects the tensile properties of an FRP bar (Wu 1990).

Table 2.3 - Tensile properties of reinforcing bars (ACI 440.1R-15)

Properties	Steel	GFRP	CFRP	AFRP
Nominal yield stress, MPa	276 to 517	N/A	N/A	N/A
Tensile Strength, MPa	483 to 690	483 to 1600	600 to 3690	1720 to 2540
Elastic Modulus, GPa	200	35.0 to 51.0	120.0 to 580	41 to 125
Yield strain, %	0.14 to 0.25	N/A	N/A	N/A
Rupture strain, %	6.0 to 12.0	1.2 to 3.1	0.5 to 1.7	1.9 to 4.4

2.1.5.2 Compressive behavior

While it is not recommended to rely on FRP bars to resist compressive stresses, the following researches are presented to fully characterize the behavior of FRP bars. Tests on FRP bars with a length-diameter ratio from 1:1 to 2:1 have shown that the compressive strength is lower than the tensile strength (Wu 1990). The mode of failure for FRP bars subjected to longitudinal compression can include transverse tensile failure, fiber micro-buckling, or shear failure. The mode of failure depends on the type of fiber, the fiber-volume fraction, and the type of resin. Compressive strengths of 55, 78, and 20% of the tensile strength have been reported for GFRP, CFRP, and AFRP, respectively (Mallick 1988; Wu 1990). In general, compressive strengths are higher for bars with higher tensile strengths, except in the case of AFRP, where the fibers exhibit nonlinear behavior in compression at a relatively low level of stress.

2.1.5.3 Shear behavior

Most FRP bar composites are relatively weak in inter-laminar shear where layers of unreinforced resin lie between layers of fibers. Because there is usually no reinforcement across layers, the inter-laminar shear strength is governed by the relatively weak polymer matrix. Orientation of the fibers in an off-axis direction across the layers of fiber will increase the shear resistance, depending upon the degree of offset. If the shear properties of a particular FRP bar are needed, these should be obtained from the bar manufacturer. The manufacturer should provide a description of the test method used to obtain the reported shear values (ACI 440.1 R-15).

2.1.5.4 Bond behavior

Bond performance of an FRP bar is dependent on the design, manufacturing process, mechanical properties of the bar itself, and the environmental conditions (Al-Dulaijan et al. 1996; Nanni et al. 1997; Bakis et al. 1998; Bank et al. 1998; Freimanis et al. 1998). The bond properties of FRP bars have been extensively investigated by numerous researchers through different types of tests, such as pullout tests, splice tests, and cantilever beams, to determine an empirical equation for embedment length (Faza and GangaRao 1990; Ehsani et al. 1996; Benmokrane 1997; Shield et al. 1999; Mosley 2002; Wambeke and Shield 2006; Tighiouart et al. 1999).

2.2 Literature Review

2.2.1 General

The use of GFRP reinforcement in concrete members like columns under seismic loading is suffering lack and shortage of data and guidelines in codes due to lack in researches. Few researches were conducted on axial compression columns reinforced with FRP bars (Pantelides et al. 2013, Tobbi et al. 2012). Also, FRP jackets and sheets were used as a confinement for the columns (Purba and Mufti 1999, Deniaud and Neale 2005). FRP materials were used also for rehabilitation and strengthening of existing structures (Zafra and Kawashima 2013, Shan et al. 2006). Beam-column joints were studied by Mady et al. (2011), and Said and Nehdi (2004). FRP-reinforced structural walls had been studied by Yamakawa and Fujisaki (1995), Mohamed et al. (2014). Previous researches for FRP reinforced concrete columns under seismic loading are limited (Tavassoli et al. 2015 and Ali and El-Salakawy

2016), therefore the following section summarizes the available conducted researches on steel and FRP reinforced concrete columns.

2.2.2 Steel reinforced concrete columns under simulated seismic loading

Many experimental and analytical studies were carried out on steel reinforced concrete columns under different types of loading; concentric and eccentric compression, monotonic lateral loading, reversed lateral loading and simulated seismic loading (axial compression and reversed lateral deformations). Many codes and specifications include guidelines and provisions for columns' design; involve equations to determine the section dimensions and the required amount of steel reinforcement. The main demand for structures in seismic zones is the ductility capacity, the structures with ductile behavior have the ability to absorb and dissipate energy under seismic loads without significant loss in strength through plastic hinges. The capacity of ductile structures to dissipate energy is taken into account in the seismic design of concrete structures in all codes. A safe ductile behavior and failure for a structure can be reached by guarantee strong column-weak beam concept. However, according to Hwang and Yun (2004), it has been stated that hinges appear at the ends of the columns after an earthquake.

Caballero et al. (2012) performed an experimental study on the behavior of slender columns subjected to combinations of constant axial and lateral cyclic loads. Figure 2-3 shows the concrete dimensions and reinforcement details. Fourteen specimens were constructed and tested. The researchers used the results to calibrate numerical models and to validate simplified methods. The studied parameters were: slenderness, axial load level, transverse reinforcement ratio, and volumetric steel-fiber ratio. The strength and deformation capacity of the columns are analyzed. It was concluded that the deformation capacity depends on the chosen parameters. Using steel fibers and the minimum transverse reinforcement into the concrete mixture increases the deformation capacity. Also the slenderness of the column influences the deformation capacity.

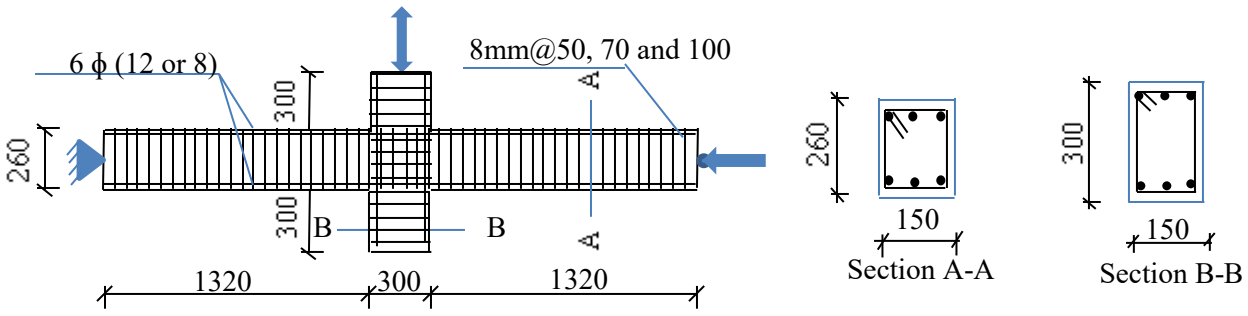

Figure 2-3: Slender concrete columns details. (Caballero et al. 2012)

Grira and Saatcioglu (1998) tried to develop economically feasible new techniques for columns confinement. Thirty one full scale reinforced concrete columns were constructed and tested under simulated seismic loading. Thirteen columns confined with welded steel grids, of which 3 columns were built of high strength concrete, 4 columns confined with steel hoops and double head studs, and 14 columns confined with fiber reinforced plastic grids. The columns specimens were chosen to be representatives of a lower portion of a first floor column between the footing and the point of inflection with a 1645 mm shear span and cross-sectional dimensions of 350×350 mm. The dimensions of the columns were chosen to guarantee flexural dominant behavior. The columns were confined following the spacing requirements of ACI 318 (1995). The studied parameters were compressive strength of concrete, arrangement of longitudinal bars, volumetric ratio of transverse reinforcement, vertical spacing of grids and level of the axial load. The authors concluded that the welded reinforcement grids can be used effectively as confinement reinforcement provided that the steel has sufficient ductility and without noticeable loss in strength. The specimens showed 7 to 10% strain prior to failure and producing lateral drift ratios (the lateral displacement divided by the shear span) in excess of 3% with volumetric ratios less than those required by ACI 318 (1995) building code. For the concrete columns confined with double head studs and conventional perimeter hoops also showed ductile behavior, developing lateral drifts of 4 to 6% prior to a significant loss moment capacity. The concrete column properly confined with FRP grids showed ductile response and behaved as well as the companion columns confined with welded steel grids. The failure of those columns was caused mostly by crushing of compression concrete but in few columns, premature failure of FRP grids at the joints had happened.

Saatcioglu and Baingo (1999) studied the behavior of high strength steel reinforced concrete columns under simulated seismic loading. The studied parameters were the concrete strength, axial load level, confinement steel grade, volumetric ratio of transverse reinforcement and spacing. The authors concluded that the increased confinement required for HSC columns can be provided by increasing the volumetric ratio and/or yield strength of transverse steel. Deformability of HSC columns decreases with increasing axial compression. Individual circular hoops are as effective as continuous circular spirals in confining HSC columns; however, the spiral reinforcement appears to be more effective in improving stability of longitudinal reinforcement at later stages of inelastic deformations. Figure 2-4 shows the concrete dimension and reinforcement details.

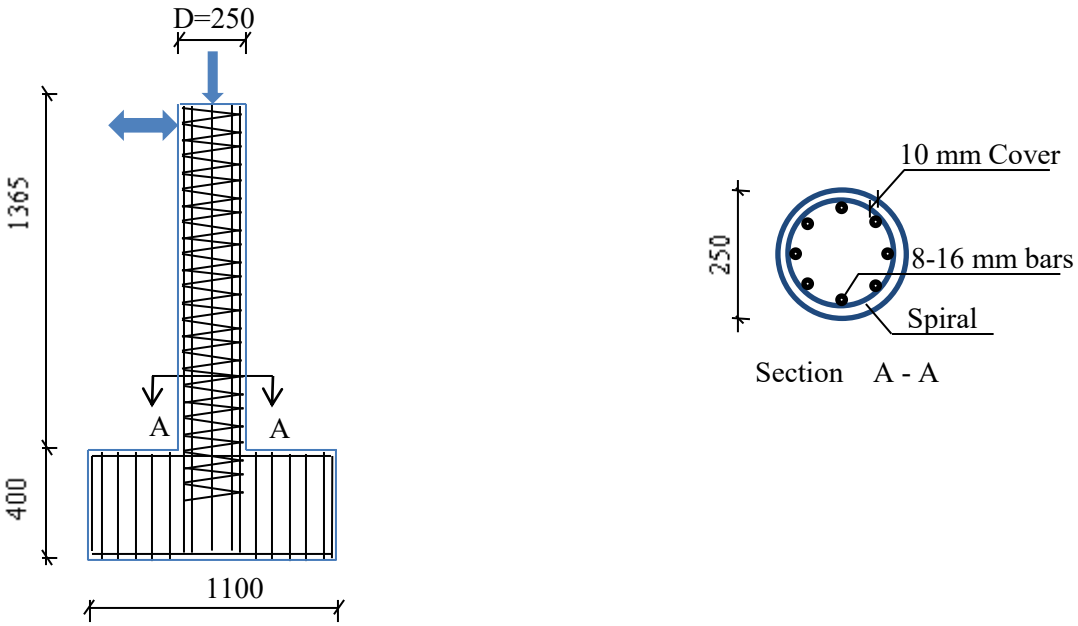

Figure 2-4: High strength circular concrete columns details (Saatcioglu and Baingo 1999)

Samuel et al. (2011) designed and constructed 600 mm square cross section columns and 1200 mm in length with 10 different steel configurations as shown in Figure 2-5 to study the effect of tie configuration on column seismic behavior.

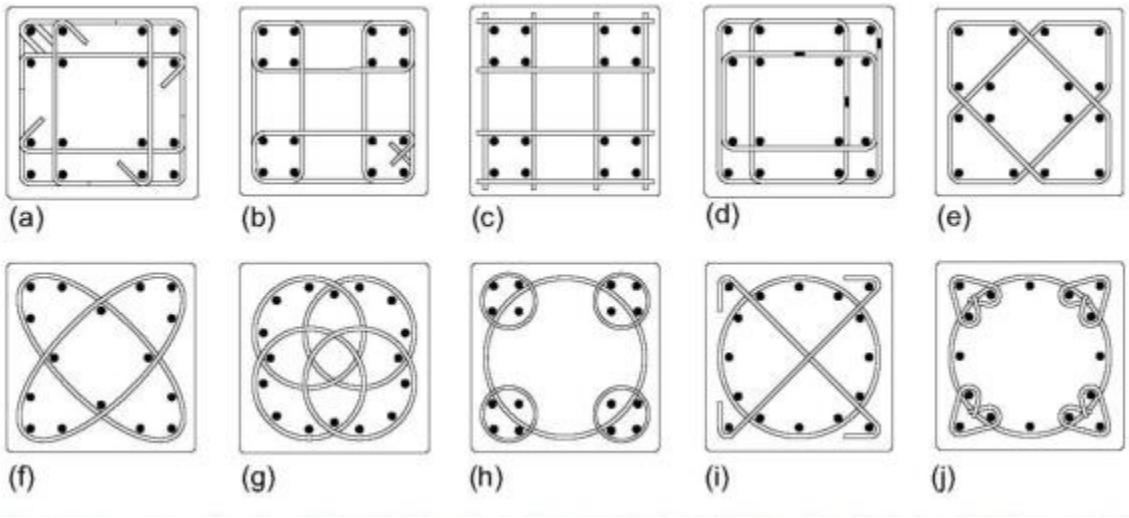

Figure 2.5 - Confinement Configuration details (Samuel et al. 2011)

(a) conventional; (b) single bar; (c) welded wire grid; (d) three welded hoops; (e) twin hexagonal; (f) twin elliptical; (g) four spiral; (h) five spiral; (i) spiral plus cross ties; and (j) spiral plus four ears.

Sixteen No. 8 (area = 506.7 mm2) longitudinal bars with a yield strength of 412 MPa were used for all specimens. The results clearly verified that columns with interlocking multi-spiral confinement design exhibited higher compressive strength and ductility when compared to columns with conventional rectilinear hoop design.

Yeh and Shamim (1990) studied the seismic behavior of steel reinforced concrete columns, confined by rectilinear ties. 305 mm square cross section columns with length 2740 mm were tested under flexure to large inelastic deformations while simultaneously subjected to constant axial load. The studied parameters were distribution of longitudinal and lateral reinforcement, the axial load level, and amount of lateral reinforcement and spacing of ties. The result showed that large number of laterally supported longitudinal bars results in higher flexural strength and ductility. At small tie spacing for the same amount of transverse reinforcement, higher strength and ductility were found with precautions of lateral steel anchorage. 26% excess in flexural capacity was observed due to the confinement. The maximum values of curvature ductility factor and the compressive concrete strain corresponding to the maximum moment were above 50 and 0.019, respectively. In case of unsupported longitudinal bars, the

bars suffered buckling at large deformations, resulting in brittle failure due to losing the needed confinements. Higher axial load reduces strength and ductility of confined concrete sections very significantly. Flexural behavior enhancement could be obtained at case of increasing the amount of lateral reinforcement.

Bayrak and Shamim (1998) studied experimentally the confinement of high-strength concrete (HSC) and ultrahigh-strength concrete (UHSC) column with lateral steel reinforcement on columns seismic behavior. 305 mm square cross section columns with 1473 mm in length tested under different axial load levels and reversed cyclic displacement. The studied parameters were the concrete strength, axial load level, steel configuration, and amount of lateral steel. A comparison between the behavior of normal strength concrete column and HSC and UHSC columns was done. The authors reported that HSC and UHSC could behave in ductile manner if a sufficient amount of confinement is used in an efficient configuration. A high confined 102 MPa concrete columns displayed a very ductile behavior showing a curvature ductility factor of 14 and displacement ductility factor of 6.3. The authors concluded that the rectilinear ties had high effect on the columns ductility. Better distribution of reinforcement and better lateral support to the longitudinal bars provided tougher response of UHSC columns, which is similar to the ones observed for NSC and HSC columns. An increase in axial load reduces the column's deformability and ductility and, also, accelerates strength and stiffness degradation with every load cycle. It was mentioned that, the amount of lateral reinforcement to reinforcement configuration and the level of axial load must be considered in the design of confinement reinforcement.

Yun (2003) had an experimental and analytical study on high strength concrete columns under seismic loading. 510 mm square cross sections columns were reinforced with 4 No.29 and 4 No.36 as longitudinal steel reinforcement with a ratio of 2.6% of the column gross sectional area. The studied parameter was the transverse reinforcement details. The authors concluded that the deformability and behavior of the columns were extremely affected by the amount and details of the transverse reinforcement in the plastic hinge region as well as the axial load levels. 6% drift ratio was reached without degradation of load carrying capacity at case of columns with 82% or more of confinement specified in the seismic design provision of the ACI 318 (1995) code when the axial load ratio was 20%. Increasing the applied axial load

level resulted in decreasing the ultimate drift ratio and deformability of the columns. 4% drift ratio was reached in case of 52% of confinement specified in the seismic design provision of the ACI 318-95 code when the axial load ratio was 20%. A micro-analysis was performed with ADINA by constructing three-dimensional finite element models. The results, with all parameters properly prescribed, provided good correlation with the experimental values. The finite element method could provide detailed analytical results of stress and crack distributions and provided insights in stress and crack variations during the stages of loading as well as verification of the experimental results.

Bae and Bayrak (2008) had an experimental and analytical study to estimate the plastic hinge length of reinforced concrete columns. The effect of axial load level and shear span to depth ratio (L/h) were studied. Based on the experimental results, it was concluded that the level of axial load influenced the length of the plastic hinge. Specimens tested under high axial loads developed longer plastic hinge lengths than those tested under low axial loads. The following equation was proposed to estimate the length of the plastic hinges forming in RC columns:

$$\frac{l_p}{h} = \left[0.3\left(\frac{P}{P_o}\right) + 3\left(\frac{A_s}{A_g}\right) - 0.1\right]\left(\frac{L}{h}\right) + 0.25 \geq 0.25 \qquad (2-1)$$

where,

l_p : Plastic hinge length.
h : Overall depth of column.
P : Applied axial load.
P_o : Nominal axial load capacity.
A_s : Area of tension reinforcement.
A_g : Gross area of concrete section.
L : Distance from critical section to point of contraflexure.

Mortezaei and Ronagh (2013) had 1316 inelastic time-history analyses that been performed to predict the nonlinear behavior of RC columns under both far-fault and near-fault ground motions. The axial load level, height over depth ratio, amount of longitudinal reinforcement, and different characteristics of earthquakes effects on column seismic behavior were evaluated

analytically by finite element methods. The results were compared with corresponding experimental data. Based on the results, the following expressions were proposed to be used to estimate plastic hinge length of RC columns subjected to both far-fault and near-fault earthquakes that contain a forward-directivity effect.

For far fault earthquakes:

$$\frac{l_p}{h} = \left[0.4\left(\frac{P}{P_o}\right) + 3\left(\frac{A_s}{A_g}\right) - 0.1\right]\left(\frac{L}{h}\right) + 0.6 \geq 0.6 \qquad (2-2)$$

For near fault earthquakes:

$$\frac{l_p}{h} = \left[0.4\left(\frac{P}{P_o}\right) + 3\left(\frac{A_s}{A_g}\right) - 0.1\right]\left(\frac{L}{h}\right) + 0.45 \geq 0.45 \qquad (2-3)$$

where,

h : Overall depth of column.

P : Applied axial load.

P_0 : Nominal axial load capacity.

A_s : Area of tension reinforcement.

A_g : Gross area of concrete section.

L : Distance from critical section to the point of contraflexure.

Ho (2011) constructed eight 325 × 325 mm square cross-section columns with a height of 1515 mm to study the structural parameters affecting the flexural ductility of high-strength reinforced concrete (HSRC) columns under constant compressive axial load and reversed cyclic displacements. The specimen represented a real column in an RC moment-resisting framed building between the contra-flexure and the maximum bending moment points, which are located around the mid-height and at the face of the beam-column joint respectively. The reinforcement ratio of the longitudinal steel bars varied from 0.9 to 6.1%. The confining steel content within critical region was calculated using the following equation:

$$\rho_s = 1.02\left(\frac{A_g}{A_c}\right)\left(0.2 - 0.16\frac{\rho f_y}{f_c'}\right)\left(\frac{P}{A_g f_c'}\right)^{0.9}\left(\frac{f_c'}{f_{ys}}\right) + 0.008 \qquad (2-4)$$

While that outside the critical region was designed to resist the ultimate shear force only. From the test results, it is evident that ultimate curvature ductility factors obtained for all the column specimens were close to 10, which is considered the standard for limited ductility. The design is thus suitable for HSRC columns of tall buildings in regions having low to moderate seismic risk where the design of fully ductile columns is too generous and/or not necessary.

Gajalakshmi and Helena (2012) studied experimentally the behavior of concrete-filled steel tube columns subjected to lateral cyclic loading. The studied parameters were the diameter-to-thickness ratio of the steel tube and two types of in-fills namely plain cement concrete and steel fiber reinforced concrete. The authors concluded that steel fiber reinforced concrete-filled steel tube (SCFT) columns, exhibited about 1.5 to 2 times the energy absorption capacity of plain cement concrete-filled steel tube, enhanced ductility and reduced damage index compared to concrete-filled steel tube (CFT) columns. The failure pattern of the specimens are found to be governed by diameter of columns-to-thickness ratio of the columns and are independent of the type of in-fill and type of loading pattern.

2.2.3 FRP Reinforced concrete members

2.2.3.1 Columns under axial compression only

Tobbi et al. (2012) performed an experimental study on concrete columns, reinforced longitudinally and transversally with GFRP bars. The specimen cross-section dimensions were 350x350 mm with a height of 1400 mm. Figure 2-6 shows the concrete dimensions and reinforcement details. The specimens tested under concentric load to investigate the behavior of GFRP internally reinforced concrete columns and comparing it with steel control specimen. The studied parameters were the longitudinal reinforcement ratio, transverse reinforcement spacing and ties configurations. The authors concluded that the tie configurations and spacing had a clear influence on GFRP columns in increasing the strength, stiffness and ductility of the confined concrete core. The strength reduction factor 0.85 (at case of steel) can be adopted for GFRP reinforced concrete columns. The GFRP bars could contribute 10% of the columns capacity which reveals the possibility of using GFRP bars in compression members, however, adequate confinement is needed for avoiding the bars local buckling.

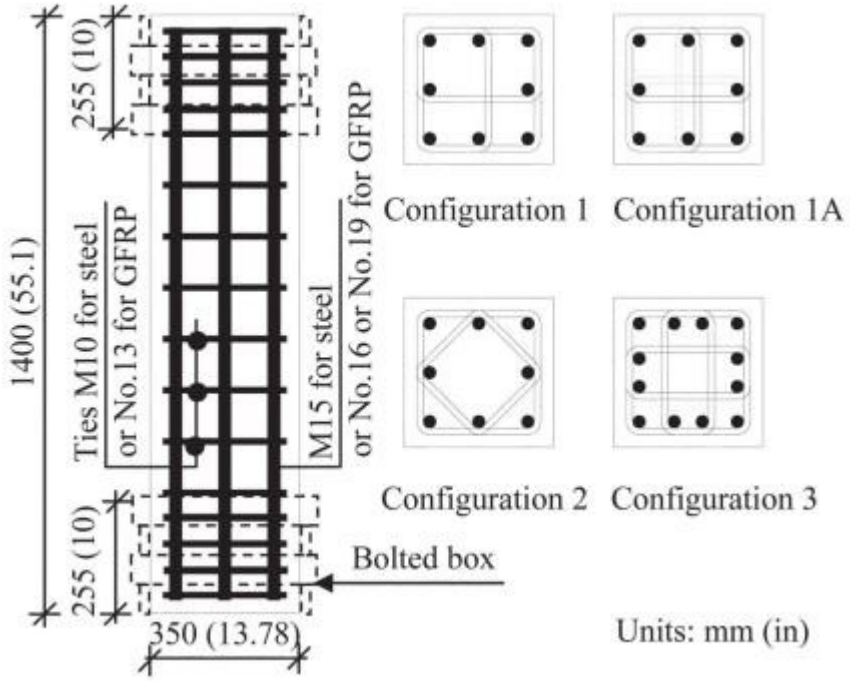

Figure 2-6: Square GFRP-reinforced concrete columns details (Tobbi et al. 2012)

Pantelides et al. (2013) evaluated the GFRP spiral confinement behavior for longitudinal GFRP and steel reinforced concrete columns under axial compression loads. It was concluded that hybrid control and entirely GFRP-reinforced columns achieved 87 and 84% of the axial load capacity of the entirely steel-reinforced control column, respectively. To achieve a similar performance to entirely steel-reinforced columns, hybrid columns must be reinforced with a larger GFRP spiral reinforcement ratio. Entirely GFRP-reinforced columns must be reinforced with a larger reinforcement ratio for both GFRP vertical bars and GFRP spirals.

Wu (1990) reported that the compressive strength of FRP bars were lower than their tensile strength. Accordingly, the compressive strength of GFRP, CFRP and AFRP bars were 55%, 78% and 20% of their tensile strengths, respectively.

2.2.3.2 Columns under eccentric loads

Paramanantham (1993) studied the behavior of FRP reinforced concrete columns under concentric and eccentric loading. Fifteen FRP-reinforced concrete blocks and 16 columns were constructed and tested under concentric and eccentric loading, respectively. The longitudinal and transverse reinforcement were GFRP bar type. The fifteen FRP-reinforced

concrete blocks were tested to investigate the concentric capacity of specimens as affected by tie spacing and bar local buckling. The studied parameter – tie spacing – was chosen as 100, 150, and 200 mm. The authors concluded that no major difference for the concentric capacity due to tie spacing, but it was noticed that small improved strength due to better control for buckling of FRP reinforcement in the case of 100 mm tie spacing. FRP bars contributed to the load carrying corresponding to 0.003 strains. This represented 20-30% of the ultimate strength of FRP reinforcement. The other specimens (16 columns) tested under different axial loading and moment combinations. All the specimens failed in compression crushing mode. The columns behavior was characterized upon the ratios of moment-deflection relationships slopes into three parts, the first and the second parts were linear, but the third part was nonlinear. When the ratio of first to second slope varied between 1.25 and 1.85, the failure was defined as compression failure. When the ratio varied between 2.22 and 2.37, the failure was defined as compression with tensile cracking. When the ratio varied between 5.5 and 6.0, the failure was defined as compression-flexure failure. It was also concluded that the best results were produced using a transverse spacing 100 mm. The maximum tensile stress measured in FRP bars was about 70% of their ultimate tensile strength in direct tension. The experimental results were compared with a moment axial force interaction diagram derived analytically on the basis of the plane section analysis. The comparison showed that the experimental strength values were higher than those computed analytically except for four columns. The compression-controlled portion of interaction diagrams was similar for both FRP and steel reinforced columns but the tension governing portions were different. At last, the researchers developed equations for calculating column capacities under concentric and eccentric axial loads.

For concentric loading, the axial capacity of the column (P_n) can be calculated as:

$$P_n = 0.85 f_c^{'}\left(A_g - A_f\right) + 0.003 E_f A_f \qquad (2-5)$$

For columns under eccentric loading:

$$P_n = C_c + C_f - T_f \qquad (2-6)$$

$$C_c = 0.85 f_c^{'} \beta_1 ab \qquad (2-7)$$

$$C_f = 0.50\, A_f \varepsilon_c^{'} E_{fc} \qquad (2-8)$$

$$T_f = 0.50 A_f \varepsilon_t E_f \qquad (2-9)$$

where,

$f_c^{'}$: Compressive concrete strength.

C_c : Force carried by concrete.

C_f : Force carried by the bars in compression.

T_f : Force carried by the bars in tension.

A_g : Gross cross sectional area.

A_f : Area of FRP reinforcement fibers.

E_f : Tensile modulus of elasticity of FRP bars.

β_1 : Ratio of depth of rectangular compression block to depth to the neutral axis.

A : Depth of equivalent rectangular stress block.

B : Width of compression face of the member.

$\varepsilon_c^{'}$: Compressive strain of FRP bars.

E_{fc} : Compressive modulus of elasticity of FRP bars.

ε_t : Tensile strain of FRP bars.

2.2.3.3 Columns under cyclic lateral load

Similar reduction in strength was reported by Kobayashi and Fujisaki (1995). The researchers conducted materials tests on FRP bars, as well as FRP reinforced columns tests under monotonic and reversed cyclic loading, the FRP bars were CFRP, AFRP and GFRP bars. The FRP bars were embedded in concrete and subjected to compression. The compressive capacity was 30 to 50% for CFRP, 10% for AFRP and 30-40% for GFRP bars of their tensile capacity. The same bars were subjected to incrementally increasing axial tension and compression reversals, AFRP and GFRP bars showed a reduction of 20-50% in their compressive capacity not like the CFRP bars which did not show any significant reduction in the strength. All the bars failed in compression and the tension capacity was not affected by reversing the load. Also 200 mm square cross-section and 650 mm height concrete columns and reinforced with CFRP, AFRP and GFRP hoops were studied. The researchers observed that the strain compatibility was maintained up to the crushing of concrete, the columns reached concentric capacity at 0.25-0.4% compressive strains. The FRP bars continued straining up to 1.00 to

1.8% in compression, beyond the peak column load, before they failed in compression. The researchers suggested that the concentric capacity of FRP reinforced concrete columns could be computed by using the gross area of the column, multiplied by 85% of concrete strength with neglecting the FRP bars contribution. The researchers also reported that under strain gradient, plane section analysis could be employed with failure governed by concrete crushing. The researchers reported also that the column strength and behavior were not affected by FRP compression failure in compression zone but those bars were not expected to resist subsequent tension after load reversing.

Zafra R., G. and Kawashima K. (2009) studied experimentally and analytically the behavior of CFRP sheet-retrofitted RC bridge columns under lateral cyclic loading. It was concluded that the fiber element analysis using constitutive models for concrete confined by both CFRP sheet and tie reinforcement provides good numerical simulation of the experimental results. The failure mode and progress of failure of the columns can be well explained based on the fiber element analysis. As CFRP sheet ratio increases, flexural strength and ductility of CFRP sheet-retrofitted columns also increases. However, as tie reinforcement ratio increases, there is no much difference on the hysteretic response for low tie reinforcement ratios. The hysteretic response of as-built columns can be enhanced by CFRP sheet jacketing which effectively increases lateral confinement, allowing an increase in flexural strength and ductile behavior. Simulation of the 7.5 m tall pier under a large earthquake shows that CFRP sheet retrofit increases the flexural strength of the as-built pier while limiting its displacement.

Sharbatdar (2003) studied experimentally the behavior of full-scale square columns and rectangular beams reinforced with CFRP bars and stirrups under seismic loading. Based on characterization testing, the used CFRP bars had compression strength and modulus of elasticity of 16-21% and approximately 20% of their corresponding tensile properties, respectively. The authors concluded that columns with 30% of the confinement reinforcement required by the CSA S806 (2002) had a brittle behavior shortly after 2.0% lateral drift ratio. Also, those columns showed a 50% drop in flexural capacity at 3.0% drift ratio. On the other hand, columns that had 60% of the confinement reinforcement required by CSA S806 (2002) showed increased deformability with lateral drift ratio up to 3.0% associated with approximately 23% strength degradation. In general, all the columns specimens sustained

lateral drift ratios higher than the limits specified by the national building code of Canada (1995)

Ozbakkaloglu and Saatcioglu (2007) studied the seismic performance of square high-strength concrete columns in FRP stay-in-place formwork. The columns had 270 mm square sections and concrete strengths up to 90 MPa. Figure 2-7 shows the concrete dimensions and reinforcement details. The studied parameters were the introduction of the corner radius, validity of FRP casing for confinement and the presence of internally placed FRP crossties. Results indicated that the deformation capacity of HSC columns can be improved significantly by using FRP casings. The results further indicate that the confinement effectiveness of columns is significantly affected by the corner radius of casings. Additionally, the confinement efficiency can be improved with the use of FRP crossties. The columns developed inelastic drift capacities of up to 11%, demonstrating the usefulness of FRP stay-in-place formwork in improving deformability of HSC columns.

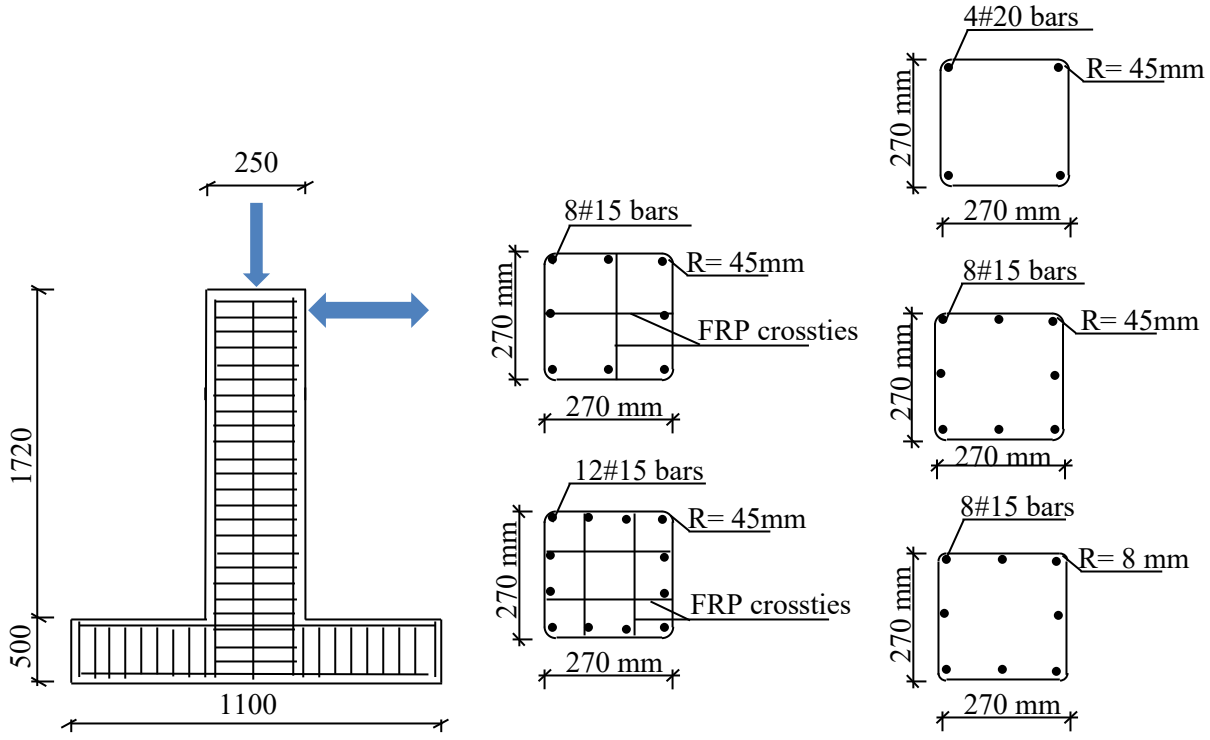

Figure 2-7: Square high strength concrete column details (Ozbakkaloglu and Saatcioglu 2007)

Dong et al. (2012) studied experimentally and analytically the effect of FRP Jacket as external confinement for steel reinforced concrete columns under seismic loading on the plastic hinge length as well as the drift capacity of FRP confined circular concrete columns. The experimental results and the obtained plastic hinge model showed that FRP confinement increased the plastic hinge length at low confinement ratio, however, it had an opposite effect when the confinement ratio is high. The ultimate drift ratio of a column was affected by its axial load level, confinement ratio, and aspect ratio. Confinement at a low level increased the drift capacity of the column. However, after a critical value had been exceeded a further increase in confinement will cause a reduction in the deformation capacity of the column.

Choo et al. (2006) performed an analytical study on short and slender FRP reinforced concrete columns to investigate the seismic behavior of FRP-RC columns and to study the axial-moment-curvatures relations. The authors concluded that unlike steel, FRP-RC columns did not exhibit balance points bound by the reinforcement limits [$(\rho_{min} = 1\%) \leq \rho \leq (\rho_{max} = 8\%)$] defined by the ACI 318 (2005). The FRP-RC columns were tending to brittle tension failure according to this study. Ignoring the contribution of FRP reinforcement in the compression zone may be conservative. However, the ultimate compressive strain of FRP reinforcing bars must be checked to ensure that compressive failure does not occur in FRP bars.

Tavassoli et al. (2015) studied experimentally nine GFRP reinforced circular concrete columns under simulated seismic loading. The specimens were reinforced longitudinally and transversally with GFRP bars and spiral. The specimen diameter and length were 356 mm and 1473 mm respectively as shown in Figure 2.8. The column was tested in away resulted in 1841 mm shear span. The studied parameters were the spiral diameter; spacing and axial load level also two different types of GFRP bars and spiral were used. The authors concluded that the GFRP columns had a stable seismic performance as well as high drift ratios reached 9% in some columns. The confinement level is very effective parameter also it is more critical for high axially loaded columns. Columns with higher axial loads showed more damage and lower level of deformability. The authors concluded that GFRP bars can be successfully used as internal reinforcement in ductile concrete columns.

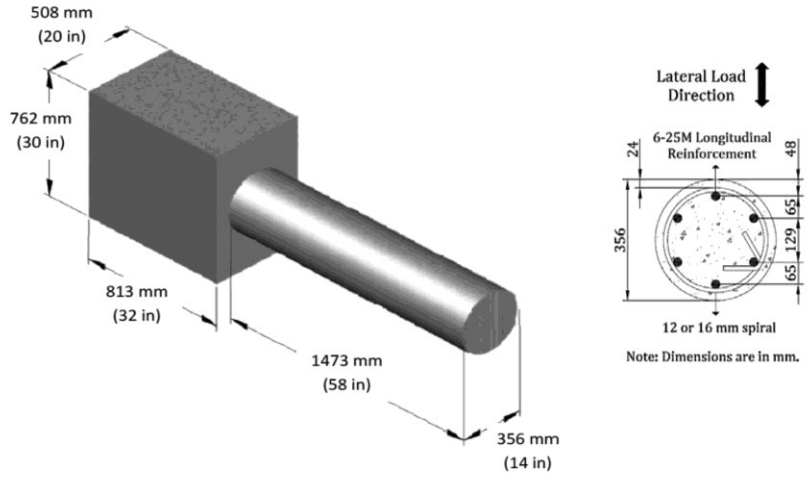

Figure 2.8 – GFRP-reinforced circular concrete column details (Tavassoli et al. 2015)

Ali and El-Salakawy (2016) studied experimentally eight reinforced concrete columns subjected to simulated seismic loads. Seven of the specimens were reinforced with GFRP bars and stirrups while one was reinforced with steel bars and stirrups as a control specimen. The specimen had a 350 mm square cross section and a shear span of 1650 mm as shown in Figure 2.9. The studied parameters were the longitudinal ratio, spacing and the axial load level. The authors concluded that all the columns reached high drift ratio around 8.5%. The dissipated energy of GFRP column was 50% of counter steel one at 4% drift ratio. Increasing the reinforcement ratio resulted in increasing the lateral capacity while decreasing the deformation capacity. Increasing the confinement level for column plays important role in increasing the drift capacity. Increasing the axial load results in rapid deterioration and decreasing the strength and drift capacity.

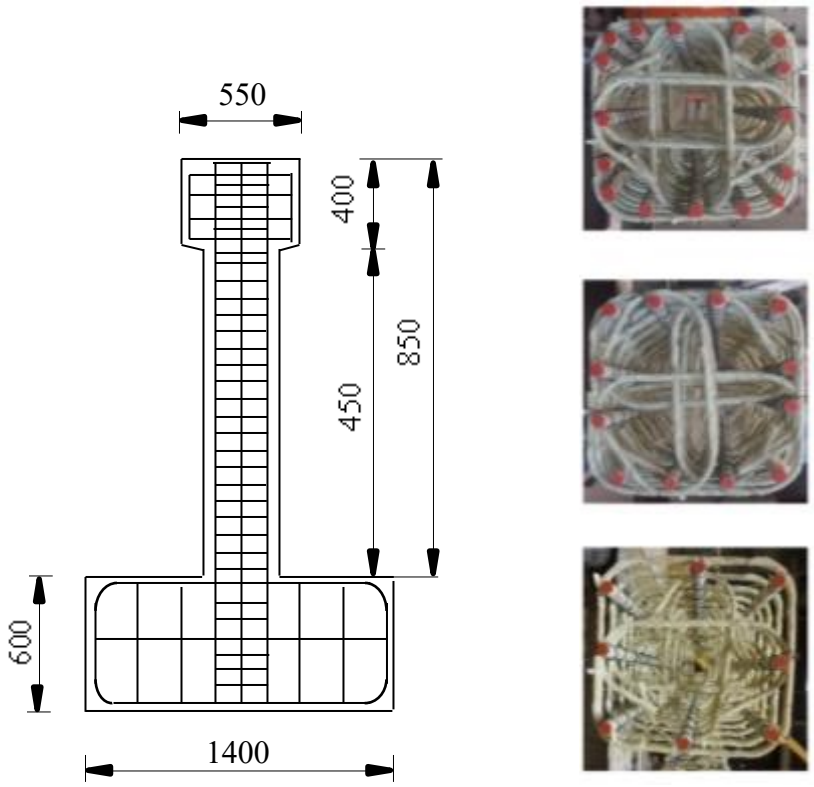

Figure 2.9 – GFRP-reinforced square concrete column details (Ali and El-Salakawy 2016)

2.2.3.4 Beam-column joint under cyclic lateral load

Sharbatdar et al. (2011) constructed and tested three large-scale FRP reinforced concrete joints under cyclic loading. The specimens were T-shape joints consisting of two columns and one beam representing half portion of the first and the second floor of one-bay reinforced concrete frame, or exterior joint of frames with more than one bay. Figure 2-10 shows the concrete dimensions and reinforcement details. The columns subjected to constant axial load meanwhile the beams subjected to reversed cyclic loading. The joint reinforced with CFRP bars as longitudinal reinforcement and CFRP grids as transverse reinforcement. Spacing of CFRP grids and arrangement of longitudinal CFRP bars were the main test parameters. The results indicated that FRP reinforcement can be used effectively in new concrete buildings, the joint drift capacity can be in excess of 3%. FRP bars were capable of resisting the significant compression and tension–compression cycles without any distress. The strength and elastic modulus of FRP bars in compression were approximately equal to 20% of the values in tension. The failure in tension occurred at about 1.0% strain. Also more bars arrangement

provided more confinement for joint which drove to stable and ductile hysteretic relationships without a sudden failure.

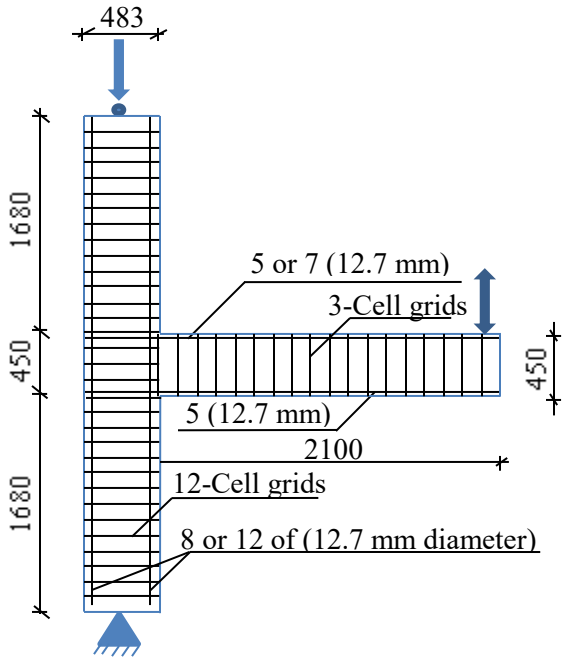

Figure 2-10: Concrete dimensions and reinforcement details (Sharbatdar et al.2011)

Mady et al. (2011) performed an experimental study on full scale exterior T-shaped beam-column joint prototypes, tested under simulated seismic loads. The longitudinal and transversal reinforcement type and ratio are the main investigated parameters. A total of five full-scale beam-column joint prototypes were constructed as follows; the first test specimen (SS) was reinforced with conventional steel bars and stirrups and used as a control specimen; the second specimen (GS) was reinforced with GFRP bars and steel stirrups; the remaining three specimens (GG-1), (GG-2) and (GG-3) were totally reinforced with GFRP bars and stirrups. Each prototype simulated a beam-column connection of an exterior bay in a multistory several bays reinforced concrete moment-resisting plane frame. The span of the considered frame (bay length) is 4700 mm with a story height of 3650 mm. Each specimen represented an exterior connection between assumed point of contra-flexural at mid height of columns and mid span of beams. The beam length was 2350 mm with cross section 350×450 mm, the column length was 3650 mm with cross section 350×500 mm. The authors concluded that the GFRP-reinforced concrete joints could successfully sustain a 4.0% drift ratio without significant damage. This indicates the feasibility of using GFRP bars and stirrups as

reinforcement in the beam-column joints subjected to seismic-type loading. Increasing the beam reinforcement ratio, while satisfying the strong column-weak beam concept, can enhance the ability of the joint to dissipate seismic energy. A length of 24 times the beam bars diameters is enough to transfer the forces in the beam bars to the joint under cyclic loading. After 4.0% lateral drift and unloading, the measured residual strains in the GFRP reinforced joint were negligible compared with steel-reinforced joint which showed larger residual strains. This indicates that, surviving an earthquake event, GFRP-reinforced joints would remain functional with a minimum required amount of repair, if any.

Said and Nehdi (2004) studied the performance of GFRP reinforced beam-column joints under reversal quasi-static cyclic loading. They constructed and tested two specimens, the first specimen was reinforced with GFRP rebars and grids, and the second specimen was reinforced with steel. Both specimens were designed and reinforced to have similar flexural capacity. The authors concluded that the steel reinforced specimen had higher drift ratio and ductility than GFRP reinforced joint. Lower energy dissipation in case of GFRP reinforced beam-column joint was observed. The GFRP-reinforced specimen reached 6% drift ratio. The researchers concluded that design code provisions for the seismic design of RC structures which have been developed for ductile steel reinforcement need to be re-evaluated for FRP-reinforced structures to address their low energy dissipation capacity.

Hasaballa et al. (2009) investigated the Seismic performance of exterior beam–column joints reinforced with glass fiber reinforced polymer bars and stirrups. Four full-scale beam–column joint prototypes were constructed and tested under reversed quasi-static loading. Each prototype simulated a beam–column connection between assumed point of contra-flexural of an exterior bay in a multi-bay, multi-story reinforced concrete moment-resisting plane frame. The span of the considered frame (bay length) is 4700 mm with a story height of 3650 mm. The beam had 350×450 mm cross section, and the column had 350×350 mm cross section. One test prototype, S0, totally reinforced with steel, is used as a control specimen. Two prototypes, G2 and G3, were reinforced with straight longitudinal GFRP bars and stirrups. Specimen G1 was reinforced with longitudinal GFRP bent bars and steel stirrups. Specimen G3 had an additional 200 mm long beam stub. The steel and GFRP specimens were designed to have a similar ultimate capacity. The specimens were tested under seismic loading. The test

parameters were the type of flexural and shear reinforcement, and the beam reinforcement detailing. The authors concluded that GFRP bars and stirrups can be used as longitudinal and transverse reinforcements for beam-column joint under seismic loading, also GFRP reinforcement are capable of resisting tension–compression cycles with no strength degradation. The results showed that GFRP-reinforced joints can be designed to satisfy both strength and ductility (deformability) requirements of earthquake-resistant structures. The steel reinforced specimen was able to dissipate energy about 2 to 3 times that of the GFRP specimens. The residual strains in the GFRP flexural reinforcement after the 4.0% drift ratio were much lower compared with steel specimen, thus requiring minimum amount of repair after surviving a seismic loading event, if any which is considered advantage for GFRP reinforced concrete structures. With taking precautions for bond-slip failure, the GFRP reinforced joint can reach 5.0% drift capacity under reversed cyclic loading. This drift capacity is more than the 2.5% required by the National Building Code of Canada NBCC (2005).

2.2.3.5 Structural walls under cyclic lateral load

Yamakawa and Fujisaki (1995) investigated the seismic behavior of structural walls reinforced by CFRP (carbon fibers reinforced plastics) grids. They constructed and tested thirteen structural walls. Seven specimens were tested under reversed cyclic loading and constant compressive force simultaneously. The other six specimens have been exposed at the coast in Okinawa since December 1992. All the test specimens were about one-third scale and the dimensions were 800×950×80 mm, rigid edge beams were attached to the top and the bottom of the wall panel. CFRP grids with 100 mm meshes were arranged by double layered reinforcement. The researchers concluded that it is difficult to expect superior seismic behavior for CFRP grids reinforced structural walls in comparison with ordinary steel reinforced structural walls. The seismic behavior of CFRP structural walls may be improved if the steel reinforcement is partially arranged with CFRP bars and stirrups; however large deformations and ductility may not be expected.

Mohamed et al. (2014) constructed four large scale shear walls, three specimens were reinforced with GFRP bars and forth additional one reinforced with steel as control specimen. All the walls length was 3500 mm with thickness 200 mm and different web length gaining

aspect ratios ranged between 2 and 4. Figure 2-11 shows the concrete dimensions and reinforcement details. The specimens tested under reversed lateral cyclic loading to investigate the seismic behavior of mid-rise GFRP Reinforced shear walls. The authors concluded that properly designed and detailed GFRP-reinforced walls could reach their flexural capacities with no strength degradation, and the failure behavior could be effectively controlled. Acceptable level of energy dissipation was achieved and drift ratio was gained, the GFRP and steel walls reached over 3% and 2.6% respectively.

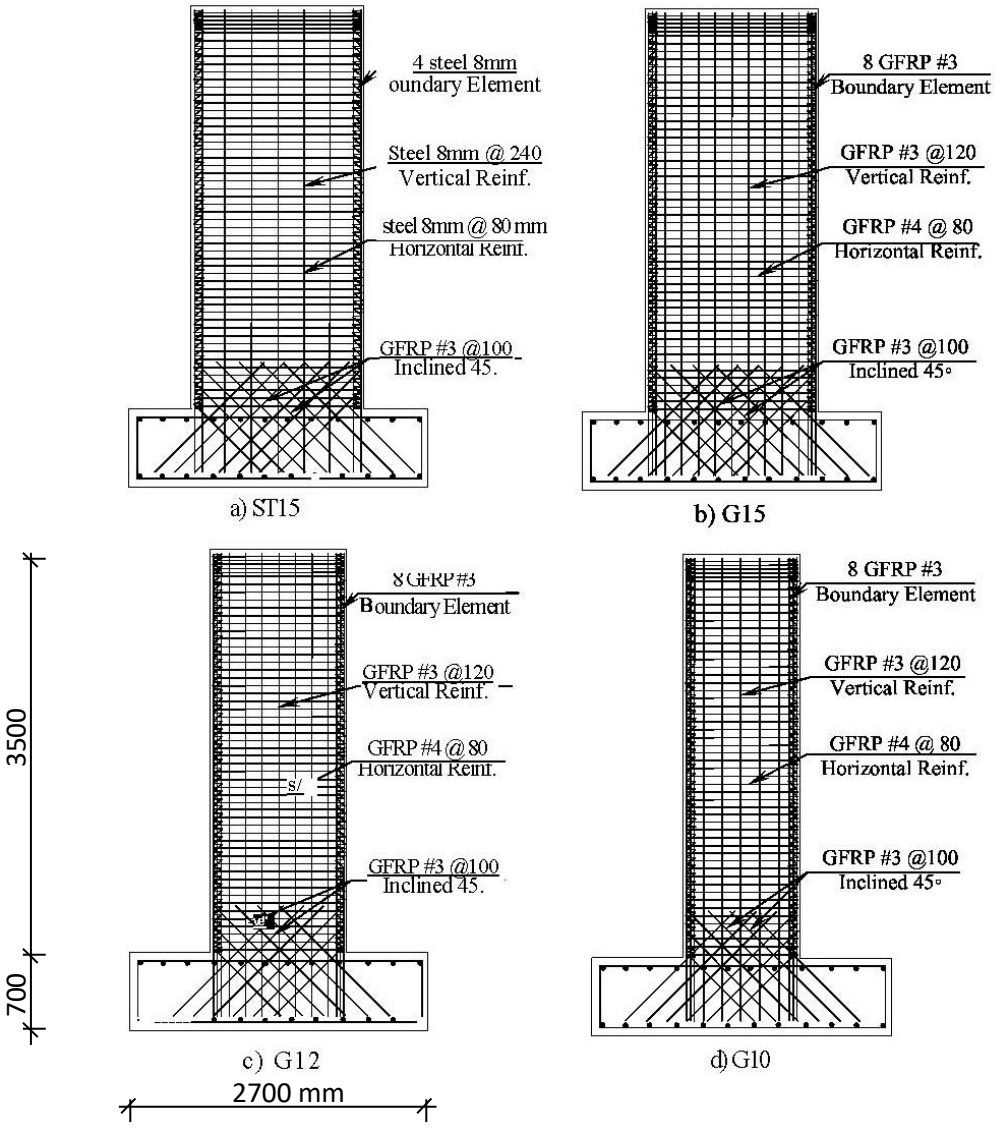

Figure 2-11: Concrete dimensions and reinforcement details (Mohamed et al.2014)

2.2.3.6 FRP-Reinforced concrete frames under simulated seismic loading

Fukuyama and Masude (1995) studied experimentally and analytically the seismic performance of a half-scale three-story FRP reinforced concrete frame. The frame had two 3500 mm spans and 1800 mm story height. The frame reinforced with Aramid FRP reinforcement in both longitudinal and transverse direction. The columns had a 350x350 mm cross-section with 20 longitudinal bars, each having 90 mm^2 cross sectional areas. The beams had a 200×400 mm cross-section with total 18 longitudinal bars, each 90 mm^2 cross sectional area. The reinforcement ratio of the beams was 0.64% and 0.48% at the bottom and the top, respectively. A reinforcement ratio of 1.47% was kept constant for the columns in all floors. No hooks or lap splices for main reinforcement were used. The beam bars development length was 200 mm in the beam stubs. Figure 2-12 shows the concrete dimensions and reinforcement details. The objective of that study was to set a seismic design philosophy of such structures under seismic loading. The structural behavior of FRP-reinforced concrete frames was compared with the conventional steel-reinforced ones. Spiral shear reinforcement was provided to all members to avoid shear failure. The frame subjected to reversed lateral load at the third story mid-height level. The elasticity modulus for beams, columns and slabs AFRP reinforcement was 67000 MPa. The bars were coated with silica sand to improve their bond characteristics. The researchers observed initial cracking near the column base at 0.5% lateral drift. These cracks were flexural cracks. Behavior of the specimen can be identified with three parts, part 1, up to a drift ratio of 0.50%, represents the elastic range before cracking. Part 2, between drift ratios of 0.50% to 2.0%, represent a stable plastic behavior due to growth of cracking in members. Part 3, drift ratios greater than 2.0%, represents unstable performance with major reduction in stiffness due to crushing of concrete. Non-linear analysis was also performed for steel specimen and FRP one in order to compare the results. The comparison between the results of using the FRP and steel reinforcement indicated that at a specific level of drift, the FRP-reinforced frame is stronger than steel reinforced frame (higher strength capacity). The researchers reported that residual deformations in case of FRP-reinforced frame were small, which would result in minimum rehabilitation needs. It was reported that lateral drift under ultimate limit-state and maximum crack width under serviceability limit-state controlled the design. The researchers concluded that FRP reinforced frames may be designed and constructed without much difficulty but additional researches were needed to establish

many aspects of these structures. Also, it would be better to use densely populated small diameter bars.

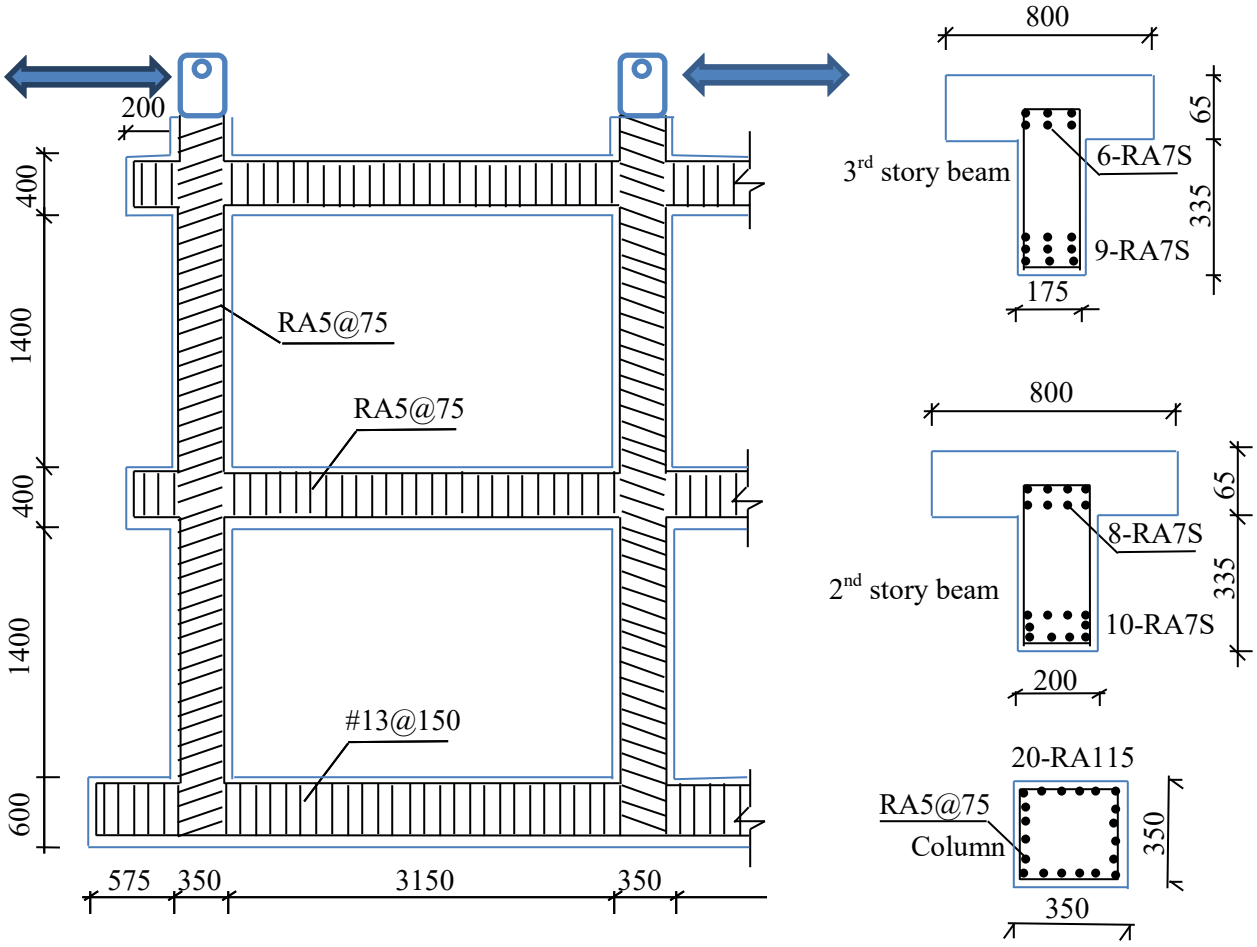

Figure 2-12: Concrete dimensions and reinforcement details (Fukuyama and Masude 1995)

Fisher and Li (2003) adopted a new approach to avoid the formation of plastic hinges at the base of the first story columns. They constructed four small-scale one-bay frames. The beam cross section was 100 × 150 mm, with 660 mm length while of the column cross section was 100 × 125 mm with 635 mm height. The beam in all specimens was reinforced with steel bars while the column was reinforced with steel or FRP bars. The reason of this combination is to utilize the relatively large flexural capacity and large deformations of FRP materials before failure to replace yielding (ductility) of steel bars. The first frame was reinforced with steel bars as a control specimen. While in the second, third, and fourth frame, the column was

reinforced with aramid FRP bars (AFRP), carbon FRP tendons (CFRP) and carbon FRP bars respectively. Reversal lateral displacements were applied to the frame simulating seismic loading. Results for the steel specimen exhibited a good range of ductility, and had an elastic plastic behavior till failure at 5.0 % drift ratio. For FRP reinforced specimen, the cracks started in the column till 1.0 % drift ratio then a plastic hinge appeared in at the beam at the range of 1.0 to 2.0 % drift ratio. FRP reinforced specimens showed increasing strength with higher drift ratios till 5.0% drift ratio, however they had lower stiffness compared with steel-reinforced specimen. This is attributed to the lower modulus of elasticity of FRP materials. The authors mentioned that FRP reinforced frames had a residual displacement about 50% of that reinforced with steel which make it possible for further rehabilitation after surviving an earthquake event. The steel reinforced specimen dissipated an amount of energy about 30 to 65% higher than FRP-reinforced specimens at 2.5 % drift ratio.

2.4 Summary of the Literature Review

The steel reinforcement enables the well-designed structural member to have the needed strength and much ductility. The deterioration case of steel reinforced concrete structural members due to corrosion leads structures owners, engineers and designers to search for an alternative for steel reinforcement in corrosive environments. FRP materials have many advantages such as high corrosion resistance; high strength to weight ratio; high fatigue strength; and low relaxation. FRP bars, however, show linear elastic stress–strain characteristics up to failure without any ductility, and therefore, due to the lack of experimental data, the current ACI 440.1R (2015) design guidelines do not recommend the use of FRP bars as longitudinal reinforcement in compression members, while CSA S806 (2012) states that the compressive contribution of FRP longitudinal reinforcement is negligible.

The linear elastic response of stress-strain curve of FRP bars raises concerns about the applicability of using FRP reinforcement as main reinforcement in earthquake resistant structures in which the ductility is a main demand. From the reported review, the authors found limited studies on GFRP-RC columns under quasi-static reversed cyclic loading

simulating seismic loading. Thus there is a need to investigate the seismic performance of GFRP-reinforced concrete columns.

CHAPTER 3: EXPERIMENTAL PROGRAM

3.1 Introduction

Eleven columns with their stub bases were constructed and tested under quasi static cyclic lateral loading, simulating seismic loads. Nine columns were entirely reinforced with glass fiber-reinforced-polymer (GFRP) in addition to two steel-reinforced columns, which serve as control specimens with similar axial stiffness. This chapter presents the details of the test specimens, the applied design philosophy, preparations, instrumentation, test setup, and loading procedures.

3.2 Design Philosophy of FRP Reinforced Concrete Elements

3.2.1 General

The specimens were designed according to the available design codes. GFRP-RC columns were designed according to CSA S806-12, while the two steel reinforced concrete columns were designed to have similar axial stiffness and according to CSA A23.3 (2014) as possible. Moreover, the assumptions and the recommendations of ACI 318 (2011); ACI 440.1R (2015); ISIS Canada (2007) in addition to previous researches were taken into account as possible in establishing the current study. The dimensions of the columns and amount of reinforcement are determined to guarantee a dominant flexural behavior.

3.2.2 Column Design

3.2.2.1 Design for Combined Flexural and Axial Capacity

According to CSA S806 (2012) - Clause 8.4.1, ACI 440.1R (2015) - Clause 8.1.1, and design manual ISIS (2007) Clause 6.2, CSA A23.3 (2014), Computations of the strength of cross sections should be performed based on the following assumptions:

- The tensile strength of concrete shall be neglected in the calculation of the factored flexural resistance of reinforced concrete members.
- The strain in concrete and FRP at any level is proportional to the distance from the neutral axis (plane section before loading remains plane after loading).
- The stress-strain relationship for FRP is linear up to failure.
- Reasonable bond exists between the concrete and the FRP reinforcement.

Following the provisions of CSA S806 (2012) - Clause 8.2.1, all FRP reinforced concrete sections shall be designed in such a way that failure of the section is initiated by crushing of the concrete in the compression zone. The concrete crushing failure mode is more desirable for flexural members reinforced with FRP bars. By experiencing concrete crushing, a flexural member does exhibit some plastic behavior before failure. To avoid the brittle failure due to rupture of FRP bars, the over reinforced section should be followed.

According to CSA S806 (2012) and ISIS (2007) for over-reinforced concrete section, the ultimate strain in the extreme concrete compression fiber is assumed to be 0.0035, the compressive stress of concrete ($\alpha_1\phi_c f_c'$), is assumed to be uniformly distributed as a rectangular stress block within a distance β_1c, measured from the maximum compressive fiber.
Where c is the distance from the extreme compression fiber to neutral axis, ϕ_c (taken = 1.00) is the material resistance factor for concrete, f_c' is the compression strength for concrete, $\propto_1$and $\beta_1$are the concrete rectangular stress block coefficients, can be determined according to ISIS (2007) and CSA S806 (2012) - Clause 8.4.1.5 as follows:

$$\propto_1 = 0.85 - 0.0015 f_c' \quad \geq 0.67 \qquad (3-1)$$

$$\beta_1 = 0.97 - 0.0025 f_c' \quad \geq 0.67 \qquad (3-2)$$

In order to achieve and ensure compression concrete failure the following equation should be applied

$$\rho_{frp} > \rho_{frpb} \qquad (3-3)$$

where ρ_{frp} is the actual reinforcement ratio, is equal

$$\rho_{frp} = \frac{A_{frp}}{bd} \qquad (3-4)$$

ρ_{frpb} is the balanced reinforcement ratio which can be computed as follows:

$$\rho_{frpb} = \alpha_1\beta_1 \frac{\emptyset_c}{\emptyset_f} \frac{f_c'}{f_{frpu}} \left(\frac{\varepsilon_{cu}}{\varepsilon_{cu} + \varepsilon_{frpu}} \right) \qquad (3-5)$$

where,

f_{frpu} is the ultimate tensile strength of FRP (MPa), ε_{cu} is the ultimate strain in concrete in compression (0.0035), ε_{frpu} is the strain in FRP in tension in extreme layer, $\emptyset_f$ (taken = 1.00) is the material resistance factor for FRP reinforcement.

As long as the section is over-reinforced, crushing of concrete occurs prior to rupture of the FRP bars and in this case the stress of FRP bars at crushing concrete failure f_{frp} can be calculated from the following equation.

$$f_{frp} = 0.5E_{frp}\varepsilon_{cu}\left[\left(1+\frac{4\alpha_1\beta_1 f_c'}{\rho_{frp}E_{frp}\varepsilon_{cu}}\right)^{1/2}-1\right] \qquad (3-6)$$

where, E_{frp} is the tensile modulus of elasticity for FRP bars.

Also the moment of resistance for the section can be calculated from the following equation.

$$M_r = A_{frp}f_{frp}\emptyset_f\left(d-\frac{\beta_1 c}{2}\right) \qquad (3-7)$$

According to CSA S806 (2012) - Clause 8.4.3.7, the area of longitudinal bars in compression members shall be not less than 0.01 times the gross area, Ag, of the section. CSA S806 (2012) - Clause 8.4.3.10, the minimum number of longitudinal reinforcing bars in compression members shall be four for bars within rectangular and circular ties, three for bars within triangular ties, and six for bars enclosed by spirals.

According to ACI 318 (2011) - Clause 7.6.3, in spirally or tied reinforced compression members, clear distance between longitudinal bars shall be not less than 1.5 d_b (23.7 mm) nor less 1-1/2 in (38.1mm). ACI 318 (2011) - Clause 10.9.1, area of the longitudinal reinforcement of compression members shall be not less than $0.01A_g$ or more than $0.08A_g$ and in R10.9.1, the percentage of the reinforcement in columns should usually not exceed 4% if the column bars are required to be lap spliced. In Clause 10.9.2 of ACI 318 (2011), the minimum number of longitudinal reinforcing bars in compression members shall be 4 for bars within rectangular or circular ties, 3 for bars within triangular ties, and 6 for bars enclosed by spirals

According to CSA A23.3 (2014) - Clause 10.9.1, the area of longitudinal bars for compression members shall be not less than 0.01 times the gross area, A_g, of the section. CSA A23.3 (2014) - Clause 10.9.2, the area of longitudinal bars for compression members, including regions

containing lap splices, shall not exceed 0.08 times the gross area of the section. CSA A23.3 (2014) - Clause 10.9.3, The minimum number of longitudinal reinforcing bars in compression members shall be four for bars within rectangular or circular ties, three for bars within triangular ties, and six for bars enclosed by spirals.

According to CSA S806 (2012) - Clause 8.4.3.13, FRP spirals for compression members shall conform to the following:

1. Spiral reinforcement shall have a minimum diameter of 6 mm.
2. The pitch or distance between turns of the spirals shall not exceed 1/6 of the core diameter.
3. The clear spacing between successive turns of a spiral shall not exceed 75 mm nor be less than 25 mm.
4. The volumetric ratio of spiral reinforcement shall be not less than the value given by

$$\rho_{fs} = \frac{f_c'}{f_{fh}}\left[\frac{A_g}{A_c} - 1\right]\left(\frac{P}{P_o}\right) \qquad (3-8)$$

where,

$\frac{P}{P_o} \geq 0.2$

$\frac{A_g}{A_c} \geq 0.3$

ρ_{fs} : Volumetric ratio of spiral reinforcement.

A_g : Gross area of the section.

A_c : Cross section area of the core.

P : Applied concentrated load.

P_o : Nominal unconfined axial load capacity of the column.

f_c' : Specified compressive strength of concrete.

f_{fh} : The least stress of the stress corresponding to a strain of $0.006E_{frp}$ in the FRP, or the stress corresponding to the failure of corners, hooks, bends, and laps.

According to CSA S806 (2012) - Clause 8.4.3.14, the spacing of FRP ties shall not exceed the least of the following dimensions:

1. 16 times the diameter of the smallest longitudinal bars or the smallest bar in a bundle;
2. 48 times the minimum cross-sectional dimension (or diameter) of FRP tie or grid;
3. the least dimension of the compression member; or
4. 300 mm in compression members containing bundled bars.

For specified concrete compressive strength in excess of 50 MPa, the tie or grid spacing determined above shall be multiplied by 0.75.

According to CSA S806 (2012) - Clause 8.4.3.15 all non-prestressed bars for tied compression members shall be enclosed by FRP ties having a minimum cross-sectional dimension (or diameter) of at least 30% of the diameter of the largest longitudinal bar when these are No. 30 or smaller, and a minimum cross-sectional dimension (or diameter) of at least 10 mm for No. 35, No. 45, No. 55, and bundled longitudinal bars. According to CSA S806 (2012) - Clause 8.4.6, the spacing of transverse reinforcement, s, placed perpendicular to the axis of the member shall not exceed $0.6d_v \cot\theta$ or 400 mm. According to CSA S806 (2012) - Clause 12.7.4.4, the first hoop shall be located not more than 50 mm from the face of a supporting member. The maximum spacing of the hoops shall not exceed

1. *d*/4
2. six times the diameter of the smallest longitudinal bars;
3. 24 times the cross-sectional dimension of the hoop FRP; or
4. 300 mm.

According to ACI 318 (2011) - Clauses 7.10.4.2 and 7.10.4.3, size of spirals shall not be less than $\frac{3}{8}$ in with clear spacing between spirals shall not exceed 3 in and not less than 1 in. According to ACI 318 (2011) - Clause 7.10.5.2, vertical spacing of ties shall not exceed the following:

1. 16 longitudinal bar diameters.
2. 48 tie bar or wire diameters.
3. Least dimension of the compression member.

According to CSA A23.3 (2014) - Clause 10.9.4, the ratio of spiral reinforcement shall be not less than the value given by

$$\rho_s = 0.45\left[\frac{A_g}{A_c} - 1\right]\frac{f_c'}{f_y} \qquad (3-9)$$

where, f_y : is the specified yield strength of spiral reinforcement (not to be taken more than 500 MPa).

3.2.2.2 Design for confinement

According to CSA S806 (2012) - Clause 12.7.3.3, the required area of the transverse FRP reinforcement for moment resisting frames members could be calculated as follows:

$$A_{sh} = 14\, sh_c \frac{f_c^{'}}{f_{fh}}\left[\frac{A_g}{A_c} - 1\right]\frac{P}{P_o}\frac{\delta}{\sqrt{K_c}} \qquad (3-10)$$

Where A_{sh} is the transverse FRP reinforcement area, P/Po is the applied axial load to axial capacity ≥ 0.2, A_g is the cross sectional area, A_c is the confined concrete core. $\left(\frac{A_g}{A_c} - 1\right) \geq 0.3$. f_{fh}= 0.006 E_f or $Ø_f f_{Fu}$, whichever is less, K_c = 1.0 for circular spirals and circular hoops, $K_c = 0.15\sqrt{\frac{h_c}{s}\frac{h_c}{s_l}}$ for rectilinear transverse reinforcement, hc is the confined core height, s is the spacing of transverse reinforcement, s_l is the spacing of the tie legs and δ is the drift ratio which is not less than 0.025 and 0.04 for moderate ductile and ductile moment resisting frame respectively. The presented GFRP columns were designed to provide 2.5% or 4% drift ratio to satisfy the moderate ductile and ductile moment resisting frames respectively except the columns G8N13-C1-100 and G12N13-C3-100 which do not follow Eq. 3-10, however were constructed for comparison.

Also according to CSA S806-12, Clause 12.7.3.4, the transverse reinforcement shall be spaced at distance not exceeding the least of the following:

1. one-quarter of the minimum member dimension;
2. 150 mm; or
3. 6 times the diameter of the smallest longitudinal bar.

3.2.2.3 Design for Anchorage length

The bars development length (l_d) required to prevent the premature anchorage failure calculated based on CSA S806 (2012) – Clause 9.3.2, as follows

$$l_d = 1.15[K_1K_2K_3K_4K_5/d_{cs}]\left(f_f/\sqrt{f_c'}\right)A_b \qquad (3-11)$$

but d_{cs} shall not be greater than $2.5d_b$ and $\sqrt{f_c'}$ shall not be greater than 5 MPa.

where,

K_1 : Bar location factor.

K_2 : Concrete density factor.

K_3 : Bar size factor.

K_4 : Bar fiber factor.

K_5 : Bar surface profile factor.

d_{cs} : Smaller of;

1- the distance from the closest concrete surface to the center of the bar being developed; or

2- two-thirds of the center-to-center spacing of the bars being developed

A_b : Area of an individual bar.

f_c' : Specified compressive strength of concrete.

Moreover, an embedded length of 24 times bar diameter, $24d_b$, is adequate to prevent slippage of the longitudinal bars as reported by Mady et al. 2011.

3.3 Details of Column specimens

Eleven column specimens were constructed and tested to failure through this research study. The specimens are representing part of a first-story building column between the footing and point of inflection. The columns were tested under a constant compression axial load and incrementally increasing lateral deformation reversals, simulating seismic loading. The columns height is 1850 mm with square cross-section 400×400 mm. The columns specimens are chosen to represent a dominant flexural behavior with shear span 1650 mm. The column base was 600 mm height, 1200 mm width, and 1200 mm length and heavily reinforced with 20M Grade 60 deformed steel bar. Figure 3.1 shows the concrete dimensions of the column specimen and the footing.

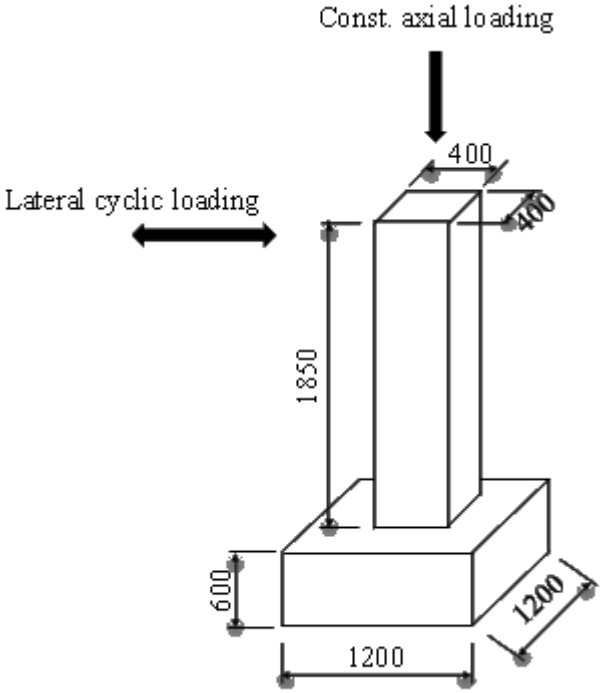

Figure. 3.1- Specimen concrete dimensions.(All dimensions in mm)

The variable parameters under study in this research are: column longitudinal reinforcement ratio, spacing of transverse reinforcement, ties configurations and axial load level. From the reported review and Eq. 3-10 from CSA S806-12, it is clear that the confinement played essential role in enhancing the deformability of the columns. This confinement is represented by two selected studied parameters which are tie configuration and spacing. Also, it is

expected that the longitudinal reinforcement ratio will affect on the confinement of the concrete column core. As the axial load value depends on the building floors number, three different axial load levels were chosen to cover range from 20% to 40% of the axial capacity of the column.

Figure 3.2 shows the variables parameters under studying. The reinforcement details were according to CSA S806 (2012), ACI 440.1R (2015), CSA A23.3 (2014), and ACI 318 (2011). The specimens are identified by reinforcement type (ST for steel and G for GFRP, respectively), number of longitudinal bars (8 and 12), longitudinal-bar diameter (N10 for steel and N13 and N19 for GFRP), tie configuration (C1, C2, C3, and C4), spacing (80, 100, and 150 mm). In addition, the numbers 30 and 40 identify the two columns subjected to axial load equal to 30% and 40% of the axial capacity which is calculated as $Øf_c^{'}A_{gross}$; the other columns were subjected to axial load equal to 20% of the axial capacity. Also, the name tag for the specimens is explained in Figure 3.3.

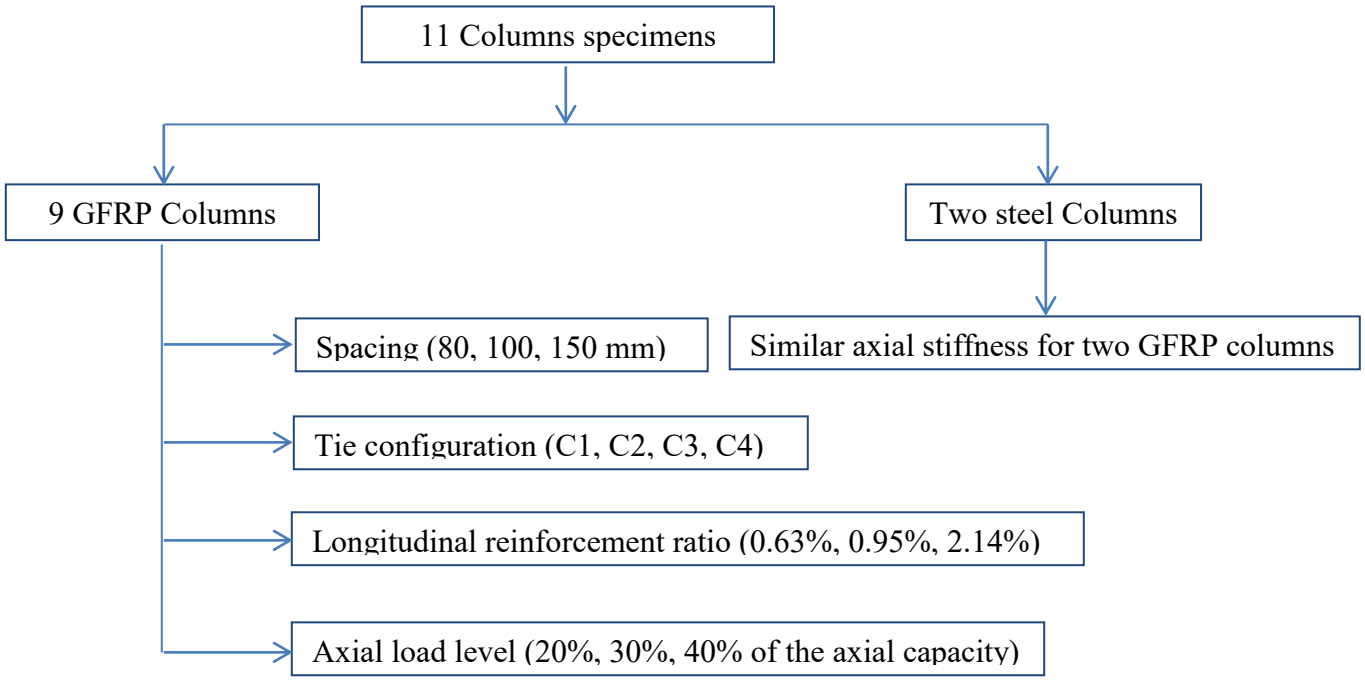

Figure. 3.2 - Flow chart illustrating the studied parameters

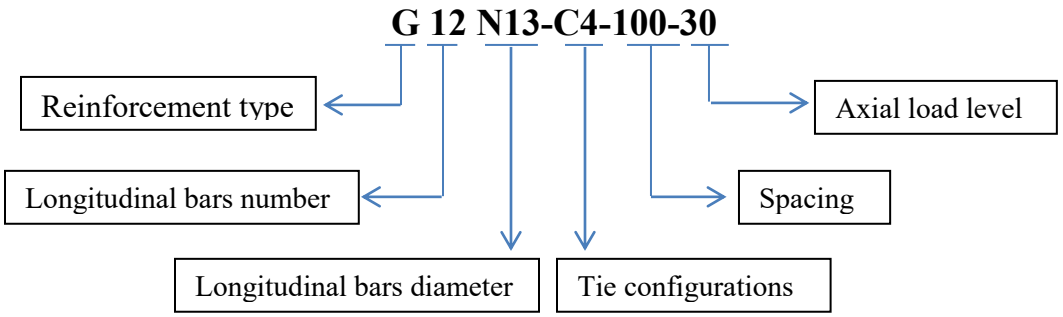

Figure 3.3 - Identification key

Three longitudinal reinforcement ratios are selected 0.63%, 0.95% and 2.14% of the gross cross section area. Eight and twelve longitudinal bars arrangement are chosen to represent the percentages of 0.63% and 0.95% respectively, and are represented by columns G8N13-C1-100 and G12N13-C3-100 respectively. GFRP #4 (diameter 12.7 mm) bars are used for longitudinal reinforcement of the columns. Figure 3.4 shows the concrete dimensions and reinforcement details for these two specimens. Also the percentages of 0.95% and 2.14% are represented by columns G12N13-C4-100 and G12N19-C4-100 respectively. Twelve longitudinal bars arrangement are chosen to represent these percentages. GFRP #4 (diameter 12.7 mm) bars are used for longitudinal reinforcement of the column G12N13-C4-100 while GFRP #6 (diameter 19.05 mm) is used for the longitudinal reinforcement for G12N19-C4-100. Figure 3.5 shows the concrete dimensions and reinforcement details for these two specimens. GFRP #3 is used for the transverse ties and rectilinear spiral for all specimens G8N13-C1-100, G12N13-C3-100, G12N13-C4-100 and G12N19-C4-100. All the specimens are reinforced with glass-FRP V-ROD. The longitudinal bars extended into the footing, which has a depth of 600 mm. The length of longitudinal bars inside the footing is 550 mm. Development lengths comply with the CSA S806 (2012) and Mady et al. 2011. Clear concrete cover is 25 mm in all cases, measured from the face of the column to the outer surface of the transverse reinforcement. Transverse reinforcement spacing is 100 mm for these four specimens.

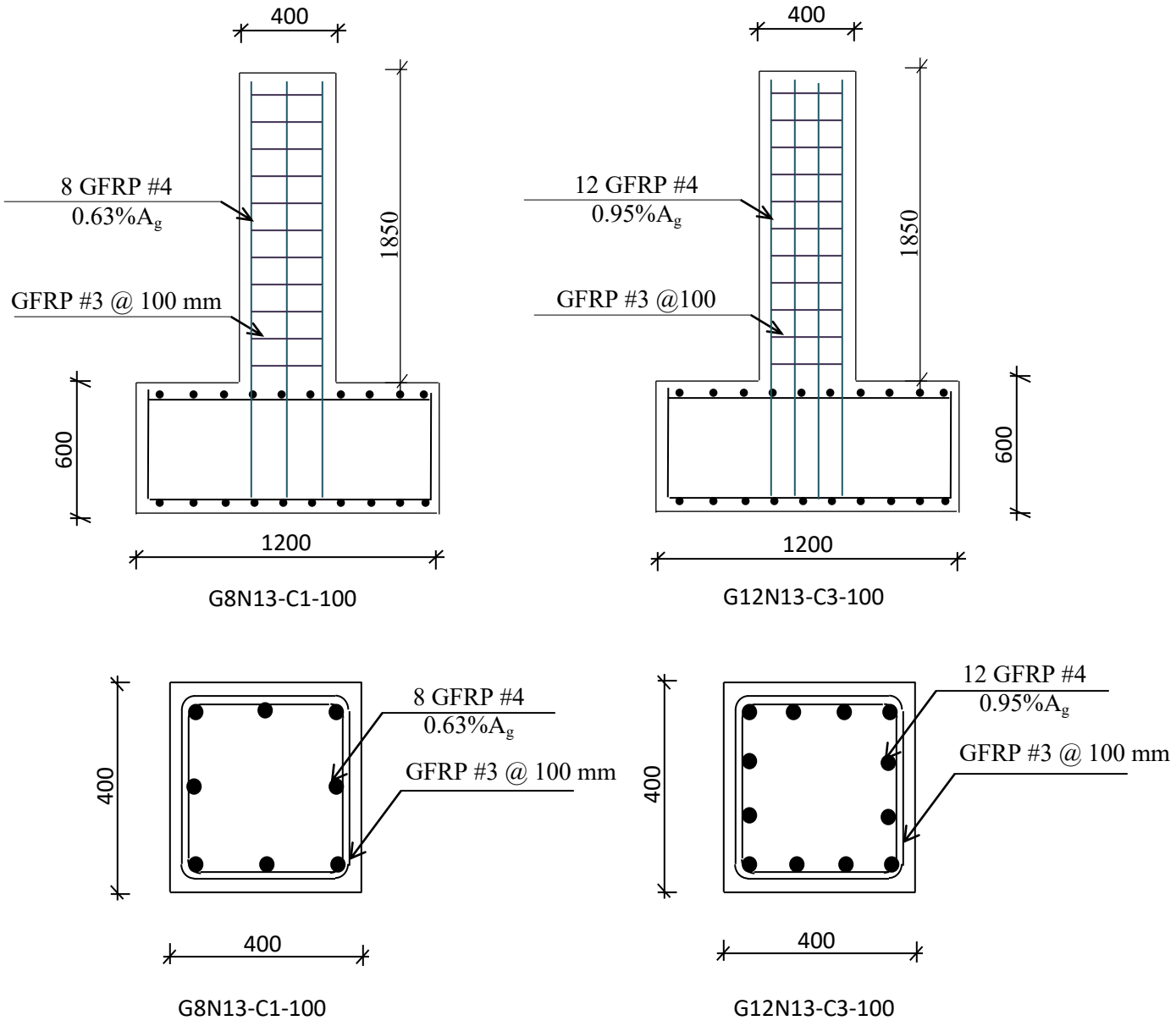

Figure 3.4 Concrete dimensions and the reinforcement details (dimensions in mm)

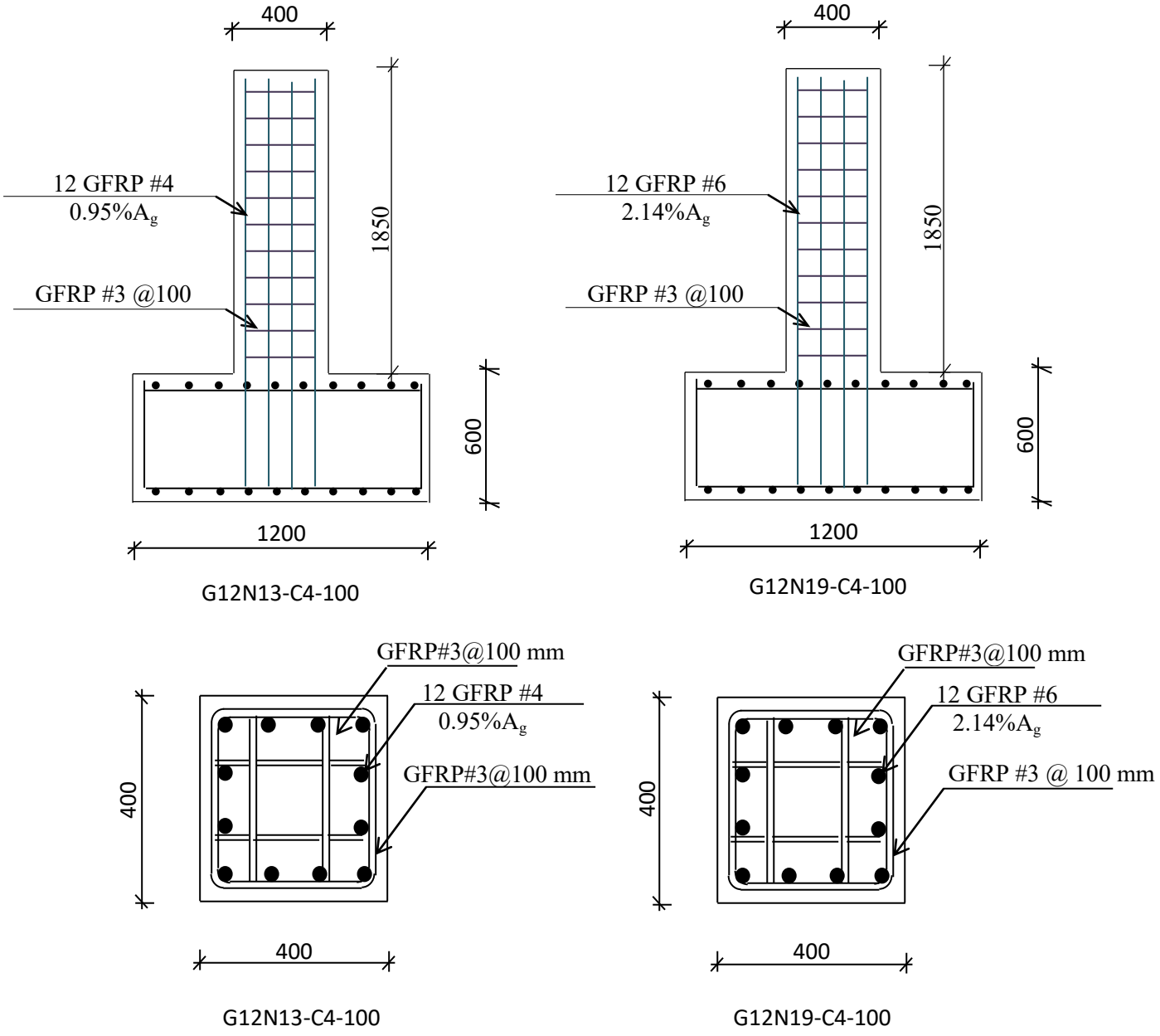

Figure 3.5 - Concrete dimensions and reinforcement details (dimensions in mm)

To study the effect of FRP transverse reinforcement spacing, based on the previous recommendations and provisions of the design codes, three spacing for the transversal reinforcement 80, 100, 150 mm are selected. Figure 3.6 shows the different spacing details.

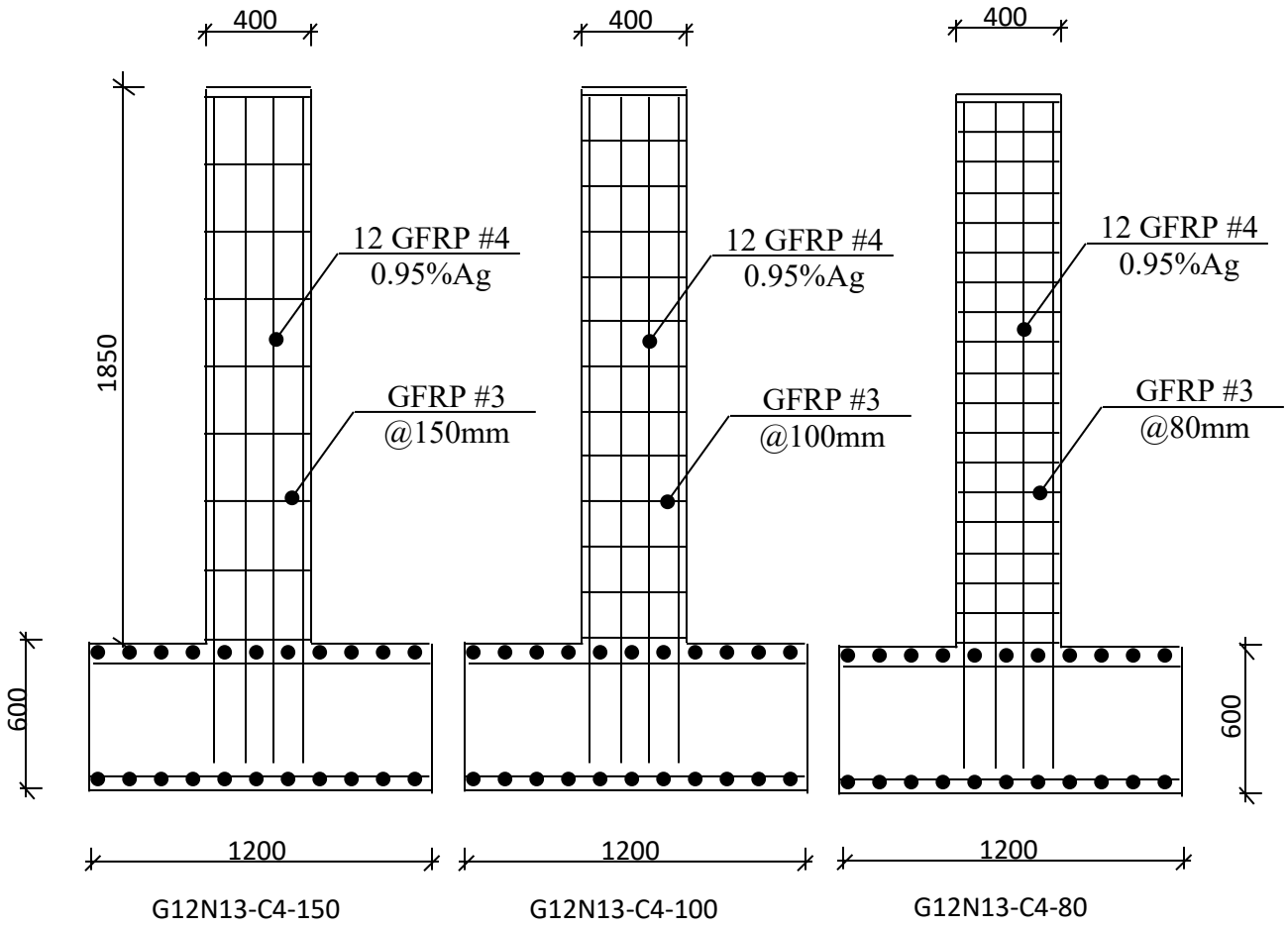

Figure 3.6 - Spacing details (dimensions in mm)

To study the effect of ties configurations, four different configurations were selected based on Equation 3-10 (CSA S806-12, clause 12.7.3.3). C1, C2, C3 and C4 represent cross-section without ties, with single cross tie and with internal closed stirrups as shown in Figure 3.7 were selected.

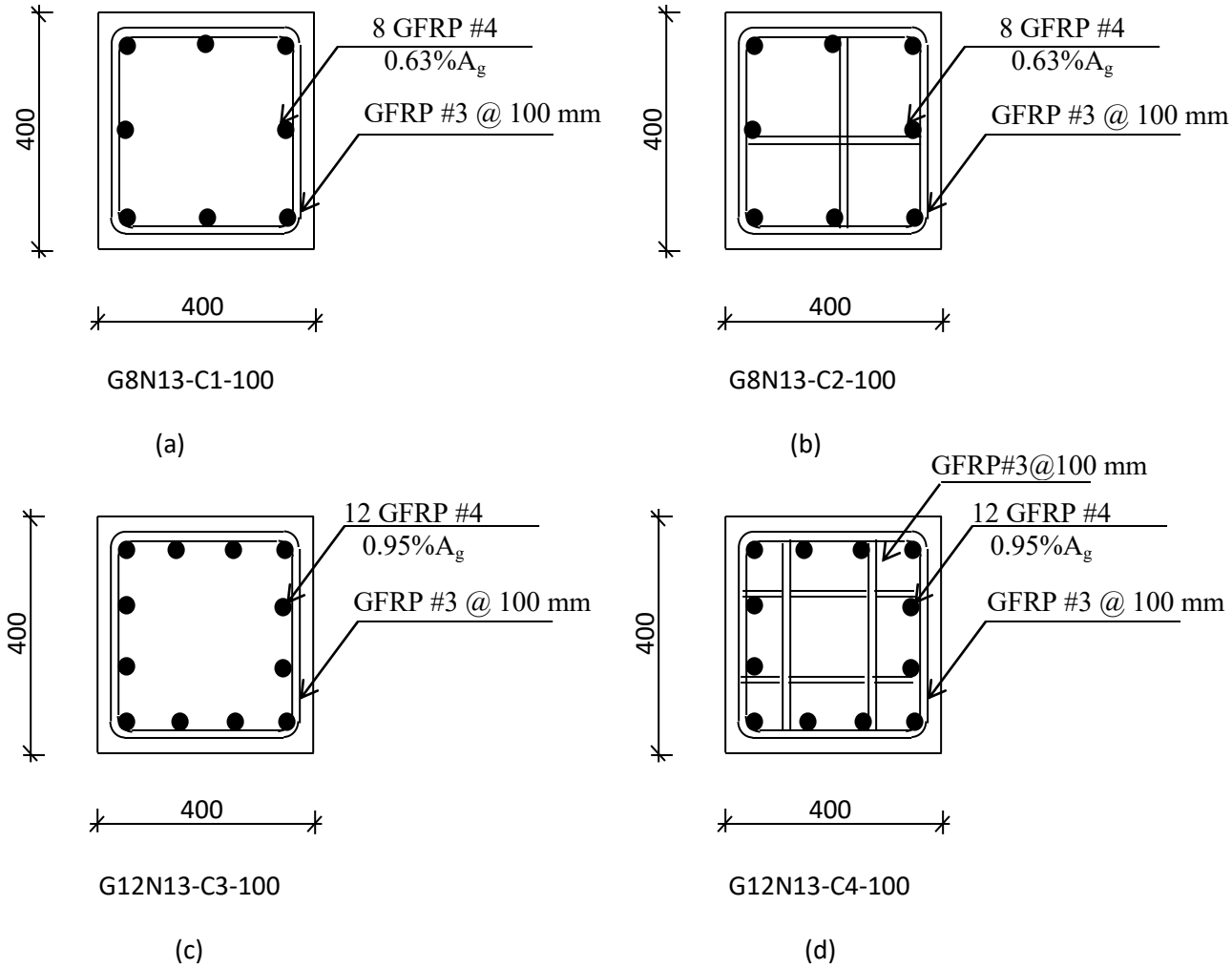

Figure 3.7 - Configuration details (dimensions in mm)

To compare the behavior of GFRP reinforced concrete columns with steel reinforced concrete columns, two steel columns with similar axial stiffness serve as control specimens, were tested, the first specimen ST8N10-C1-100, with axial stiffness E_sA_s=111000 kN and it will be compared with specimen G12N13-C3-100 with axial stiffness EA=106000 kN, while the second specimen G12N19-C4-100, EA=208000 kN, will be compared with specimen ST12N10-C4-100 with axial stiffness E_sA_s=170000 kN. The first steel specimen reinforced with 8 bars of 9.5 mm diameter (8#3) for the longitudinal reinforcement. The transverse

reinforcement diameter is 8 mm and spaced 100 mm, the same for the second steel specimen except that the number of the longitudinal bars are twelve (12#3). Figure 3.8 and Figure 3.9 show the elevation and cross section details respectively for the steel and GFRP reinforced concrete columns.

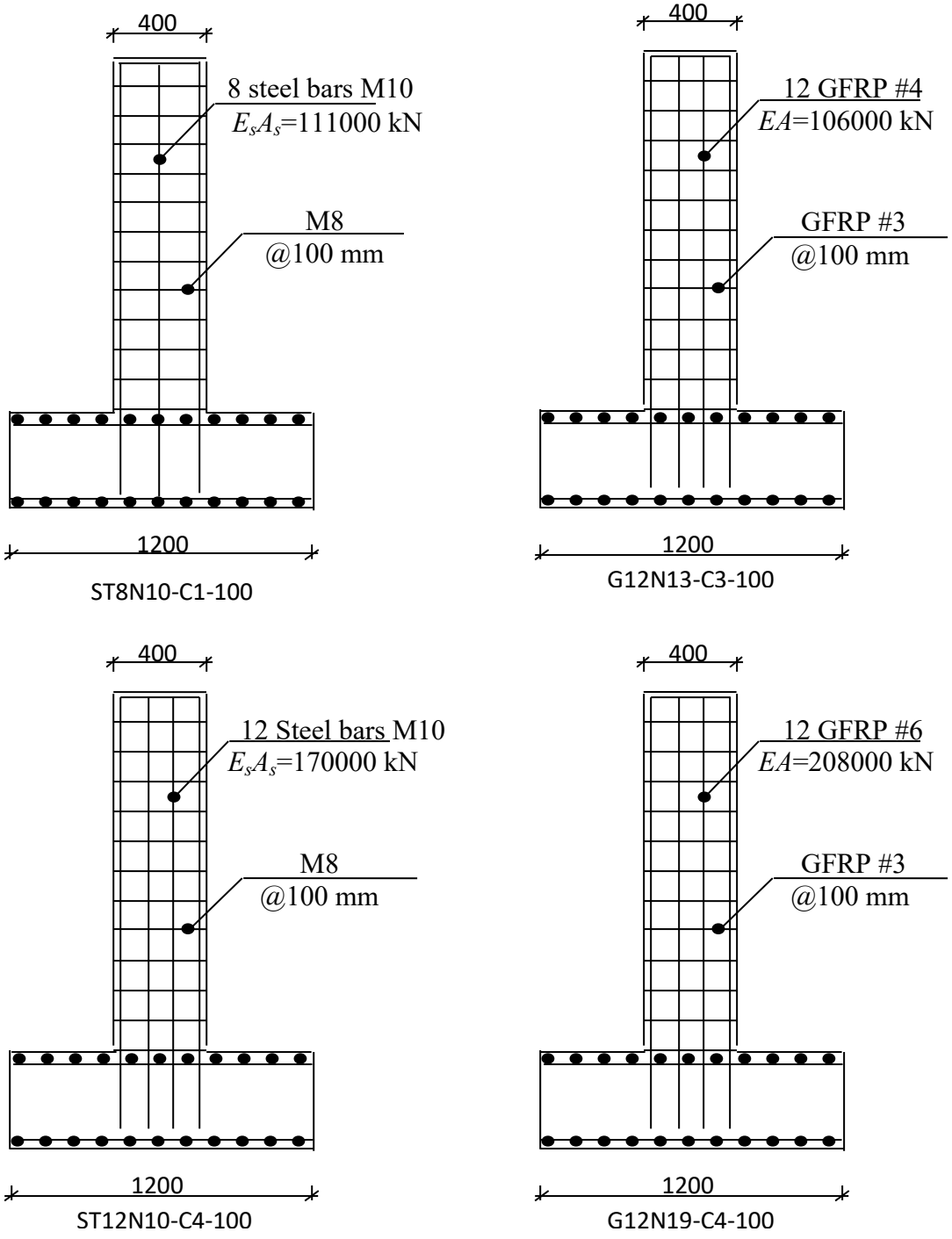

Figure 3.8 - Elevation details (dimensions in mm)

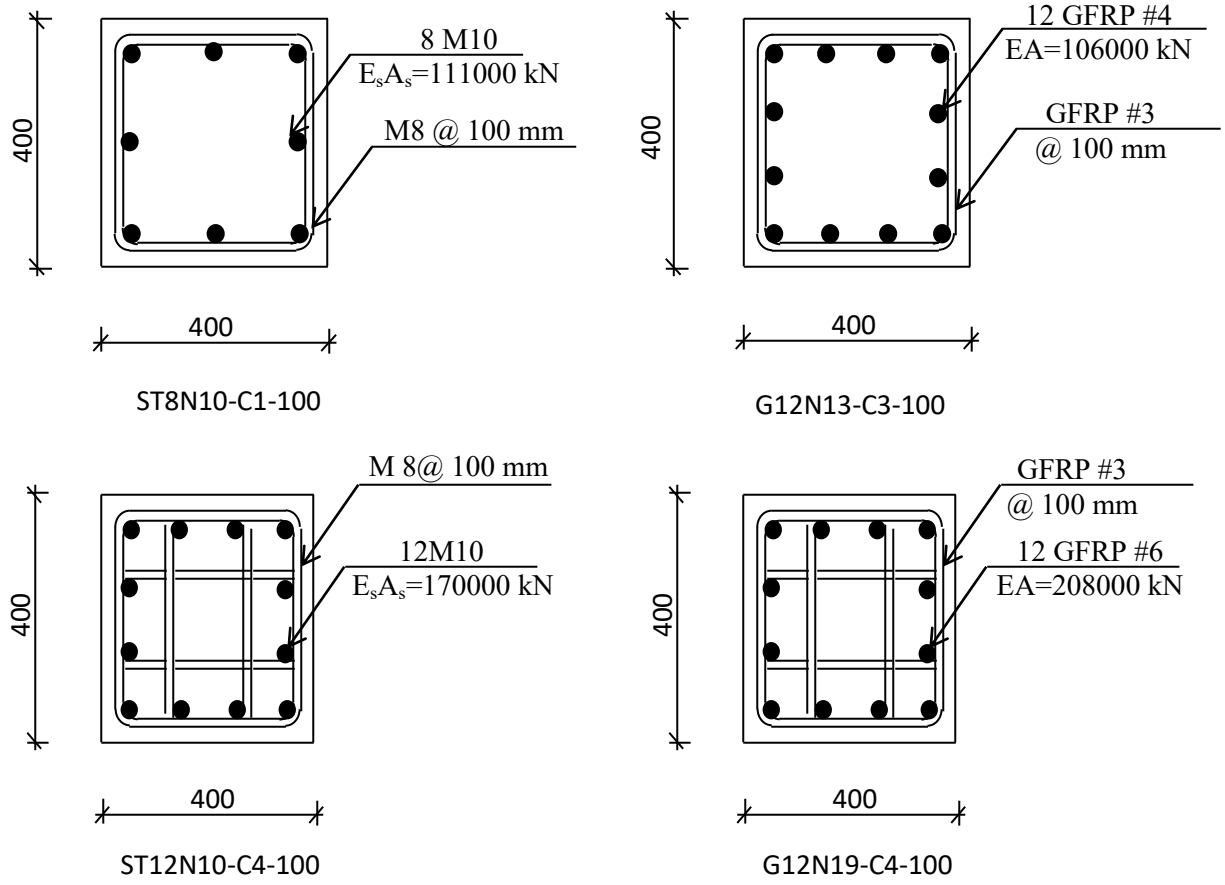

Figure 3.9 - Cross-section details (dimensions in mm)

To study the axial load level effect, specimens G12N13-C4-100, G12N13-C4-100-30 and G12N13-C4-100-40 were subjected to an axial load level equivalent to 20%, 30% and 40% of the axial capacity respectively, same reinforcement details and concrete dimensions for these specimens are provided and shown in Figure 3.7 and 3.8. Figure 3.10 shows reinforcement cages, configurations, rectilinear spiral and cross ties. Table 3.1 lists the test matrix and specimens details of the experimental program for investigating the behavior of GFRP reinforced concrete columns under quasi-static cyclic loading.

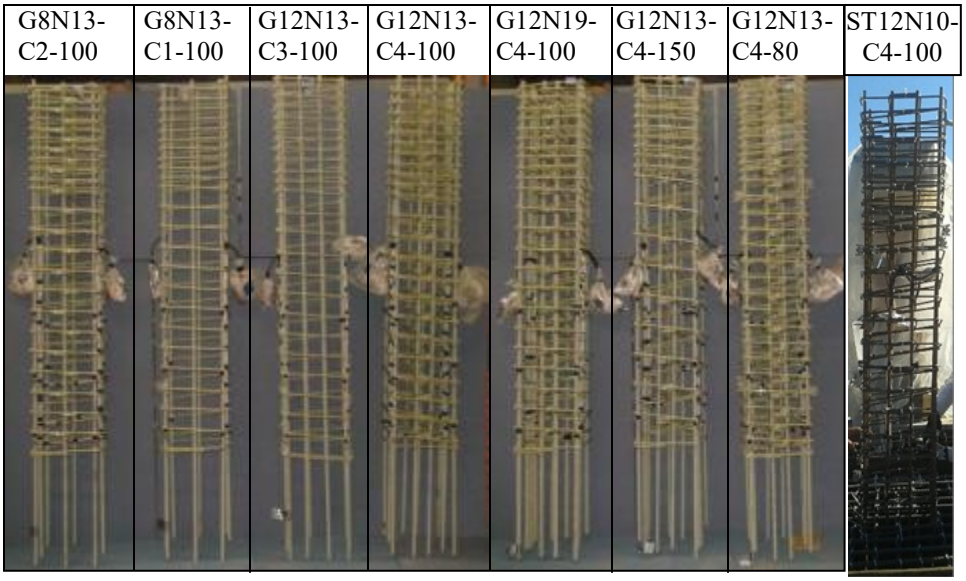

(a) Cage reinforcement

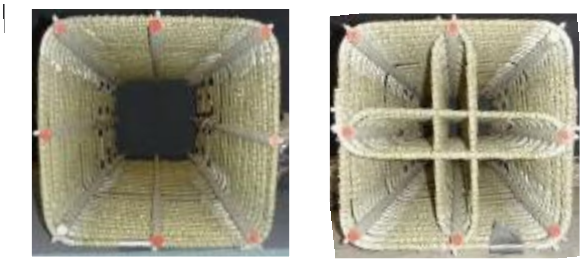

Configuration C1 Configuration C2

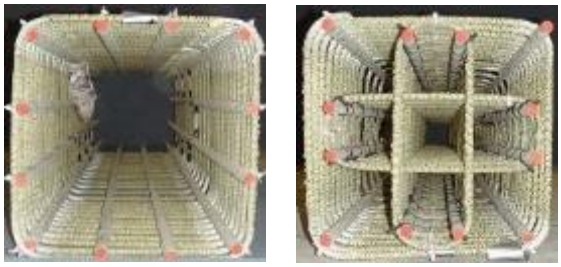

Configuration C3 Configuration C4

(b) Configurations

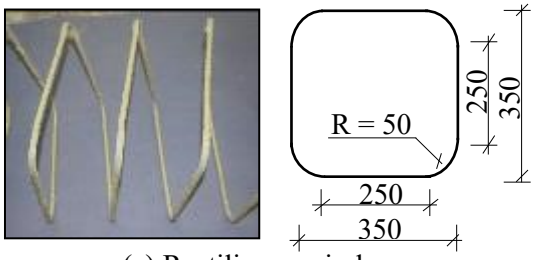

(c) Rectilinear spiral

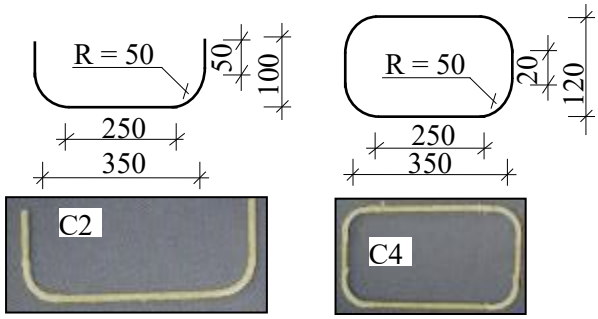

One-leg C-shaped Rectilinear closed stirrup

(d) Cross ties

Figure 3.10 - reinforcement details

Table 3.1: Test matrix and specimens details

Specimen	Bar and stirrups type	Long. Bars	Configuration	Spacing (mm)	ρ_l%	Transverse reinforcement				Axial load percentage	*Actual* f_c'*(MPa)*	*EA*
						ρ_v %	A_{sh} act	Ash req for drift				
								>2.5%	>4%			
ST8N10-C1-100	steel	8 # 3	C1	100	0.35	0.25	---	---	---	20%	44	111
ST12N10-C4-100	steel	12 # 3	C4	100	0.53	0.5	---	---	---	20%	34	170
G8N13-C1-100	GFRP	8 # 4	C1	100	0.63	0.36	142.6	168.6	269.8	20%	37	71
G8N13-C2-100	GFRP	8 # 4	C2	100	0.63	0.53	213.9	141.8	226.9	20%	37	71
G12N13-C3-100	GFRP	12 # 4	C3	100	0.95	0.36	142.6	179.0	286.4	20%	39	106
G12N13-C4-100	GFRP	12 # 4	C4	100	0.95	0.71	285.2	136.1	217.8	20%	39	106
G12N13-C4-80	GFRP	12 # 4	C4	80	0.95	0.89	285.2	106.8	170.8	20%	32	106
G12N13-C4-150	GFRP	12 # 4	C4	150	0.95	0.48	285.2	233.1	373.0	20%	33	106
G12N19-C4-100	GFRP	12 # 6	C4	100	2.14	0.71	285.2	148.4	237.4	20%	43	208
G12N13-C4-100-30	GFRP	12 # 4	C4	100	0.95	0.71	285.2	165.6	265.0	30%	41	106
G12N13-C4-100-40	GFRP	12 # 4	C4	100	0.95	0.71	285.2	231.2	369.9	40%	41	106

f_c': concrete compressive strength (MPa); ρ_l: longitudinal-reinforcement ratio; ρ_v: transverse-reinforcement ratio; $A_{sh\ act}$: actual provided transverse reinforcement (mm^2); $A_{sh\ req}$: required transverse reinforcement according to Eq. 3-10 to achieve either 2.5% or 4% drift (mm^2); s:spacing of transverse reinforcement (mm); and $P/f_c'A_g$: axial-load level; EA: axial stiffness; E: longitudinal-bar modulus of elasticity; A: longitudinal-bar area.

3.4 Materials properties

Three materials are used in fabricating the test specimens, these materials are the concrete, steel (for control specimens), and Glass-FRP (for the longitudinal and transverse reinforcement).

3.4.1 Concrete

The concrete produced by using ready mix normal weight concrete with a target compressive strength 40 MPa and 50 MPa after 28 days for the columns and bases, respectively. The actual compressive strength is determined based on the average values from testing three cylinders from each batch at the day of specimen testing, and are listed in Table 3.1.

3.4.2 Reinforcement

The used GFRP reinforcing bars were three diameters of high-modulus sand-coated bars #3 (9.5 mm) for the transverse reinforcement and ties, #4 (12.7 mm) and #6 (19.05 mm) for the longitudinal reinforcement bars.

The used steel reinforcing bars for the columns were two diameters: #2 (8 mm) of grade 60 for the transverse reinforcement and #3 (9.5 mm) of grade 60 for the longitudinal reinforcement. Table 3.2 lists the material properties of the reinforcing bars and stirrups. The longitudinal tensile properties of the GFRP bars were determined by testing five specimens according to ASTM D7205 (2011), in the case of the straight bars, and test method B.5 in ACI 440.3R (2004), in the case of the bent bars. The steel-bar properties herein were provided by the manufacturer

Table 3.2 the material properties of the reinforcing bars and stirrups.

Bar	d_b (mm)	A_f (mm^2)	A (mm^2)	E_f (GPa)	F_{fu} (MPa)	ε_{fu}(%)	Notes
GFRP #4 (N13)	12.7	126.7	143	69.6	1392	2	
GFRP #6 (N19)	19.05	285	317	60.5	1125	1.82	
Steel #2 (N8)	8	50	-	200	f_y=400	ε_y=0.2	
Steel #3 (N10)	9.5	71.3	-	200	f_y=420	ε_y=0.2	
GFRP #3 (N10)	9.5	71.3	84	52	962	1.85	Straight portion
				-	500	-	Bent portion

where,

d_b : Bar nominal diameter.
A_f : Nominal cross-sectional area.
E_f : GFRP modulus of elasticity.
F_{fu} : GFRP tensile strength.
ε_{fu} : GFRP ultimate strain.
f_y : Steel yielding strength.
ε_y : Steel yielding strain.
A Immersed area

3.5 Cages preparation and specimens casting

The cages preparation and specimens casting were done through many steps as follows:

- Preparation of bases formworks and assembly cages of heavily reinforced steel base as shown in Figure 3.11

Figure 3.11 - Base formwork and cages

- Preparing the columns cages and instrumentations as shown in Figure 3.12.

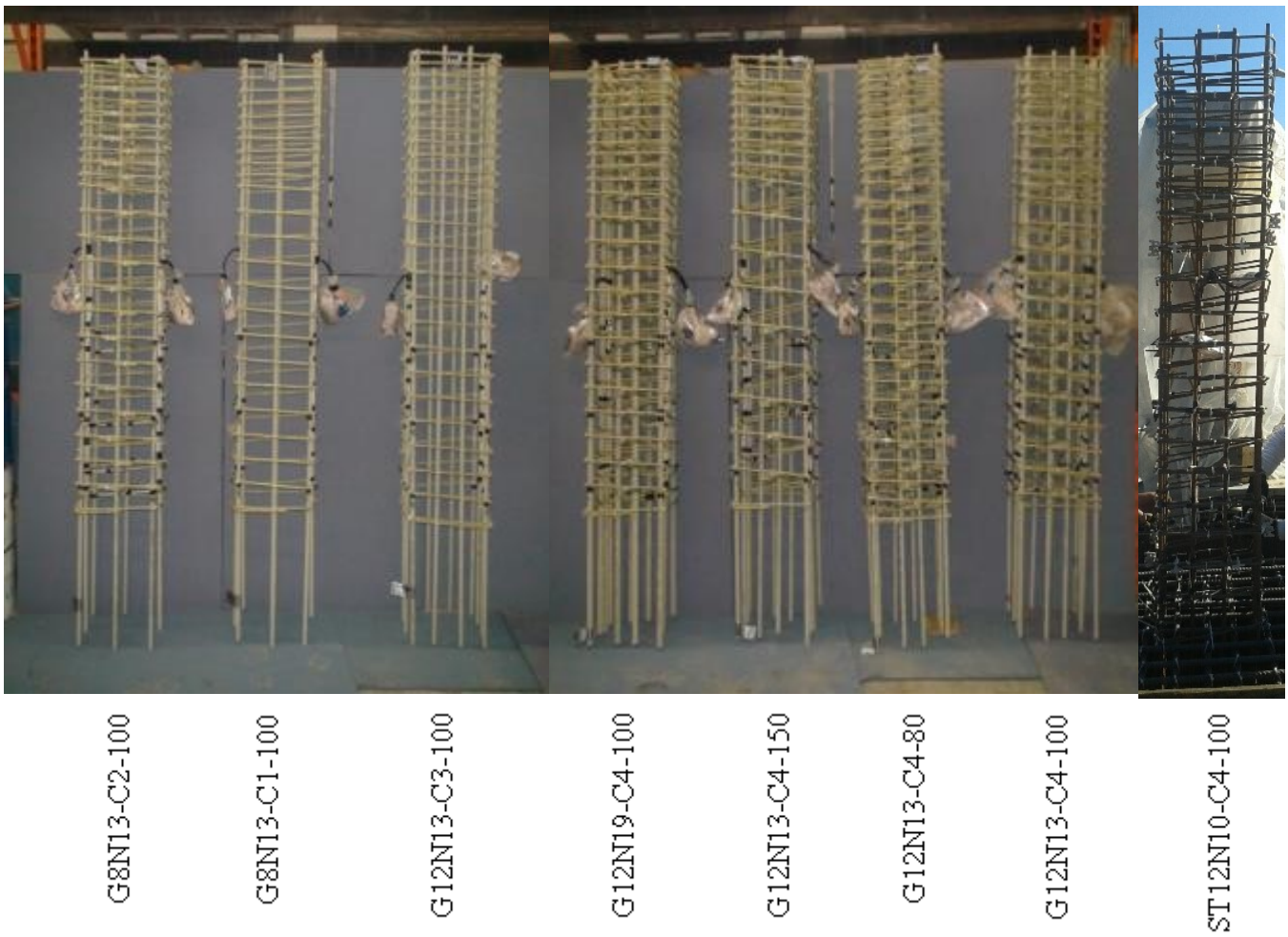

Figure 3.12 - Instrumented Columns cages

- Centralizing the column cage into the base as shown in Figure 3.13

Figure 3.13 - Column cage into the base

- Aligning the columns formworks as shown in Figure 3.14

Figure 3.14 - Align the columns formworks

- Casting the base and preparing for the columns casting as shown in Figure 3.15

Figure 3.15 - Casting the base

- Casting the columns process as shown in Figure 3.16.

Figure 3.16 - Ready mix concrete and pump truck

- Pouring concrete into columns' formworks as shown in Figure 3.17.

Figure 3.17 - Pouring concrete into columns' formworks

- Curing columns as shown in Figure 3.18

Figure 3.18 - Cured columns ready for testing

3.6 Instrumentation

A series of LVDTs and strain gauges were installed to measure deformation and strain at different levels to cover the virtual plastic hinge as shown in Figure 3.19. The four corner bars, stirrups and ties are instrumented with strain gauges at distance 50, 350 and 650 mm above the column base-footing interface. Four LVDTs (H1, H2, H3 and H4) were instrumented horizontally at different levels of the column to measure the lateral displacement of column. Six LVDTs (V1,V2,V3,V4,V5 and V6) are placed in pairs, one on each side, perpendicular to the direction of loading to measure the curvature at distance 100, 400 and 700 above the column base-footing interface. Two LVDTs were installed at the position of the first two cracks to measure crack width during testing. Two other LVDTs (S1 and S2) are used to check the sliding (if any) between the column base and the footing and also between the footing and the laboratory floor. Figure 3.20 illustrates the location of strain gauges.

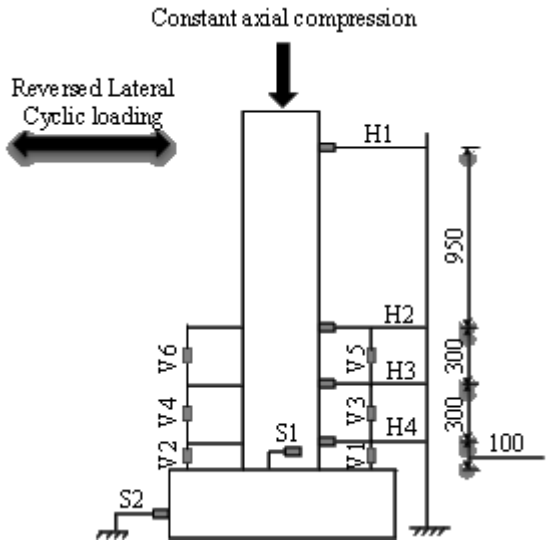

Figure 3.19 - LVDT instrumentation

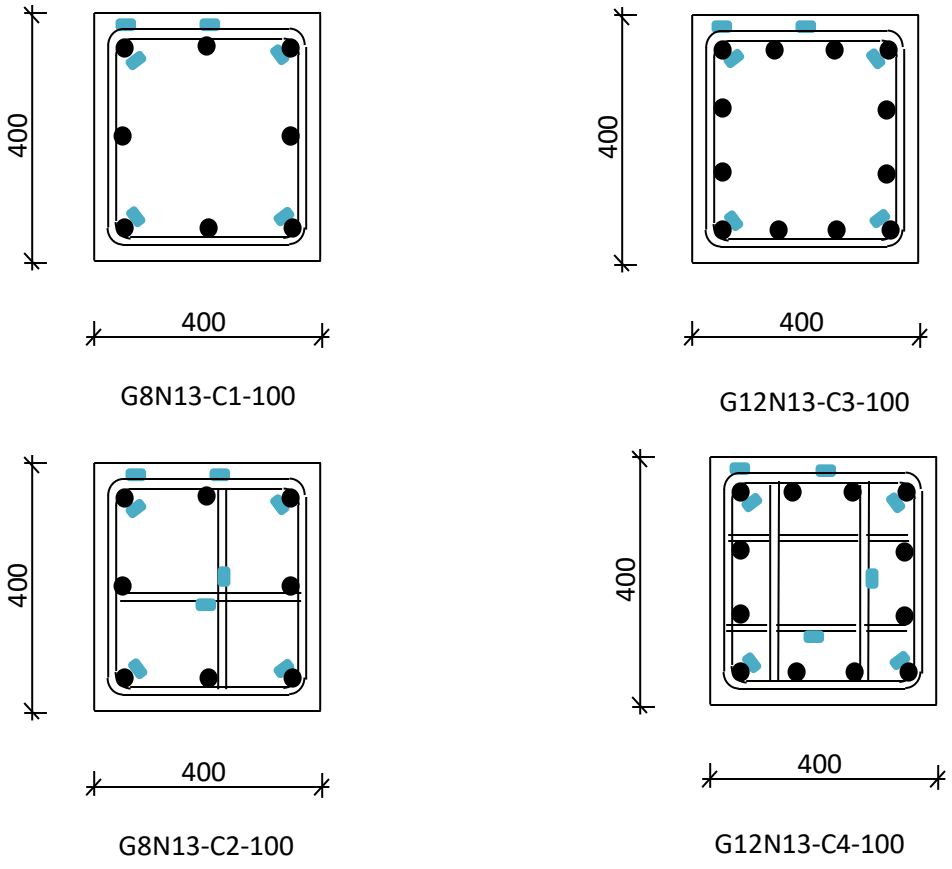

Figure 3.20 - Strain gauge instrumentation

3.7 Test set-up

Figure 3.21 shows the test setup. The column specimen was tested in an upright position. A specially fabricated steel load-transfer assembly was used to transfer both axial and lateral loads to the column specimen. An axial load of 20% or 30% or 40% of the axial capacity of the column was applied at the top of the column and was maintained constant throughout the duration of each test.

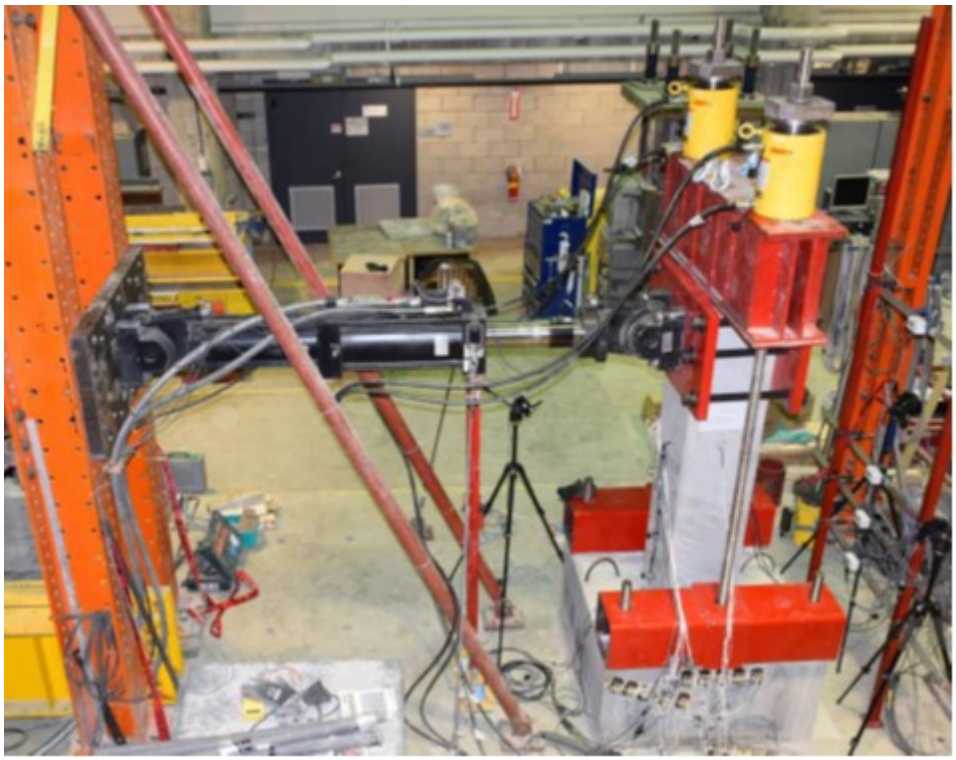

Figure 3.21 - Test set-up

Building the test set-up of the column required following many steps as following:

- Fixing the column base to the laboratory floor using two steel beams and four 66 mm-diameter Dywidag bars (high strength steel bars) to preventing the uplifting and the sliding of the specimen during the testing.
- Fixing the column top steel beam with two plates using six high strength threaded bars of diameter 40 mm.
- Applying the axial load through two hydraulic jacks and using the steel beam which is on the column top and two high strength 66 mm Dywidag steel bars placed on both sides of the column. The two steel bars connected from top to the column top steel beam meanwhile the lower sides were hinged to the steel beam which were used to fix the column base to the floor.

After reaching the desired axial load, the loading was maintained constant during the experiment.

- Applying the lateral loading using a hydraulic actuator with a capacity of 500 kN, the actuator was fixed to a supporting steel frame and connected to the steel beam on the column top.

3.8 Loading procedures

After fixing the column specimen, connecting the hydraulic jacks and the actuator. The axial load was applied slowly to the 20% or 30% or 40% of the axial capacity of the column. After reaching the desired value of the axial load, it was maintained constant through all the experiment. A typical procedure of applying cyclic loading until failure was used. Displacement control was used throughout the test. Similar loading procedure was followed in Sharbatdar and Saatcioglu (2009), Mohamed et al. (2014) and Tavassoli et al. (2015). The columns were cycled twice at each displacement level with increments of ±4.125 mm up to ±16.5 mm, followed by increments of ±8.25 mm up to ±33 mm, and then increments of ±16.5 mm to failure with loading rate 1.3 mm/minute. Hinged connections at the tips of both the horizontal actuator and vertical hydraulic jacks prevented any substantial restraint of rotation of the top of the column, thus ensuring cantilever behavior. A typical loading history is shown in Figure 3-22.

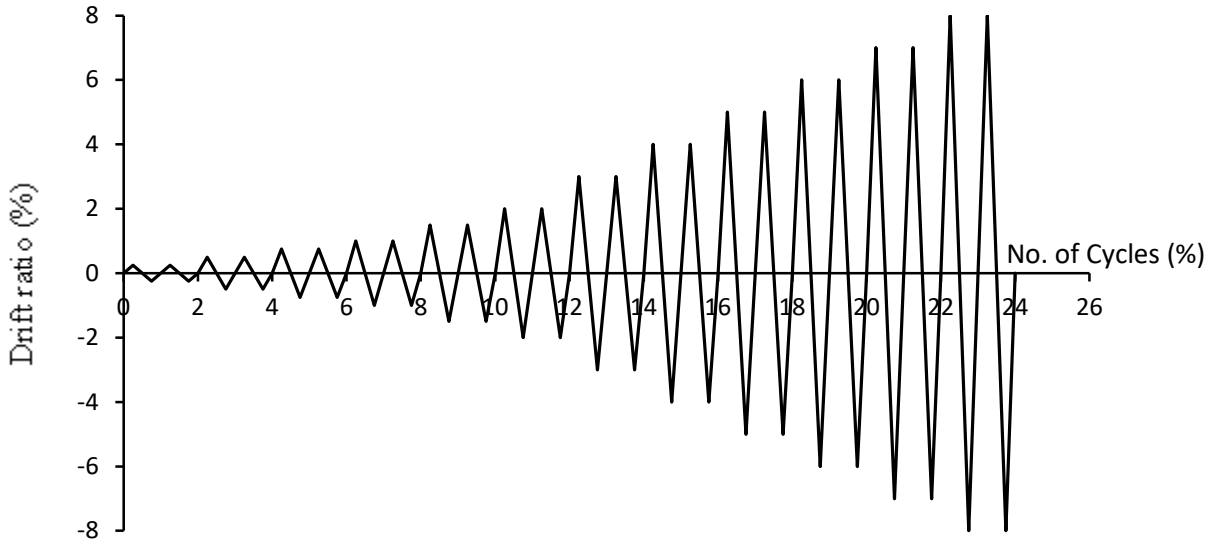

Figure 3.22 - Loading history of testing program

Chapter 4

Experimental Results and Analysis

Foreword

Authors and Affiliation

- Mohammed Gaber Elshamandy: Ph.D. candidate, Department of Civil Engineering, University of Sherbrooke, Sherbrooke, Quebec, Canada, J1K 2R1, Phone: 819-821-8000, ext.65270; Fax: 819-821-7974, E-mail: Mohammed.Mohammed@USherbrooke.ca.
- Ahmed Sabry Farghaly: Postdoctoral fellow, Department of Civil Engineering, University of Sherbrooke, Sherbrooke, Quebec, Canada, J1K 2R1, Phone: 819-821-8000, ext. 62967; Fax: 819-821-7974, E-mail: Ahmed.Farghaly@USherbrooke.ca.
- Brahim Benmokrane: Professor of Civil Engineering and NSERC Research Chair in FRP Reinforcement for Concrete Infrastructure and Tier-1 Canada Research Chair in Advanced Composite Materials for Civil Structures in Department of Civil Engineering, University of Sherbrooke, Quebec, Canada, J1K 2R1, Phone: 819-821-7758, Fax: 819-821-7974, E-mail: Brahim.Benmokrane@USherbrooke.ca.

Journal title: ACI Structural Journal

Acceptation state: submitted April 14, 2016.

Reference: Elshamandy, M. G., Farghaly, A. S., and Benmokrane, B., 2016, “Experimental Behavior of GFRP-Reinforced Concrete Columns under Lateral Cyclic Load,” ACI Structural Journal.

4.1 Abstract

The present study addresses the feasibility of reinforced-concrete columns totally reinforced with glass-fiber-reinforced-polymer (GFRP) bars achieving reasonable strength and drift requirements specified in various codes. Eleven full-scale concrete columns-two reinforced with steel bars (as reference specimens) and nine totally reinforced with GFRP bars-were constructed and tested to failure under quasi-static reversed cyclic lateral loading and simultaneously subjected to compression axial load. The reported test results clearly show that properly designed and detailed GFRP-reinforced concrete columns could reach high deformation levels with no strength degradation. The results also show that the achieved drift satisfies the limitation in most building codes. Acceptable levels of energy dissipation and ductility parameters, compared to the steel-reinforced columns, were observed. The promising results can provide impetus for constructing concrete columns reinforced with GFRP and constitute a step toward using GFRP reinforcement in such lateral-resisting systems.

Keywords: GFRP bars, concrete columns, hysteretic response, ductility parameters, energy dissipation.

4.2 Introduction

The use of fiber-reinforced polymers (FRPs) as a construction material has increased in recent years, primarily because of their noncorrodible nature and high tensile strength. FRP bars have high strength-to-weight ratios, favorable fatigue strength, electromagnetic transparency, and low relaxation characteristics in comparison to steel reinforcement (ACI 440 2007; *fib* Task Group 9.3 2007), delivering an acceptable level of performance and offering a structurally sound alternative in most applications such as beams and bridge deck slabs (Kassem et al. 2011; Bakis et al. 2002; El-Salakawy et al. 2005).

Columns figure among the structural elements that can be exposed to severe environmental conditions. The principle application of FRPs in columns has been as glass and carbon sheets for confinement and rehabilitation purposes. Recent studies conducted by Alsayed et al. (1999), Choo et al. (2006), De Luca et al. (2010), Tobbi et al. (2012), Zadeh and Nanni (2013), and Afifi et al. (2014) showed the feasibility of using FRP exclusively to reinforce columns subjected to concentric compression axial load. In lateral-resisting system, it is important to ensure adequate stiffness and acceptable levels of dissipated energy and deformability for resisting lateral loads induced by wind or earthquakes. FRP bars, however, show linear elastic stress–strain characteristics up to failure without any ductility, and therefore, due to the lack of experimental data, the current ACI 440.1R (2015) design guidelines do not recommend the use of FRP bars as longitudinal reinforcement in compression members, while CSA S806 (2012) states that the compressive contribution of FRP longitudinal reinforcement is negligible.

Little research has been conducted on lateral-resisting systems reinforced solely with FRP bars. For example, Mohamed et al. (2014) studied glass-FRP-reinforced shear walls and concluded that properly designed and detailed GFRP-reinforced shear walls could reach their flexural capacities with no strength degradation and that the failure behavior could be effectively controlled. Mady et al. (2011) studied the seismic behavior of beam–column joints totally reinforced with GFRP bars and stirrups and concluded that the GFRP-reinforced joints could successfully sustain a 4.0% drift ratio without incurring significant damage.

In particular, the research of laterally loaded FRP-reinforced columns (Choo et al. 2006, Sharbatdar and Saatcioglu 2009, Tavassoli et al. 2015, and Ali and El-Salakawy 2016) shows a stable response and high drift ratios with acceptable levels of energy dissipation, thereby

confirming the effectiveness of the FRP transverse reinforcement. This played a major role in enhancing the confinement of the concrete core, which delays concrete crushing.

The main objective of this study is to demonstrate the feasibility of using GFRP bars in longitudinally and transversely reinforced concrete columns subjected to combined axial and cyclic lateral loads. The objective relies on a comprehensive experimental program involving full-scale GFRP-reinforced columns with different detailing configurations, longitudinal reinforcement ratios, transverse volumetric ratios, and axial load levels.

4.3 Research Significance

Experimental research is needed to verify the applicability of concrete columns reinforced with longitudinal and transverse GFRP bars under different stress conditions, particularly simulated seismic load. This poses serious concerns about their feasibility in earthquake-resistant structures, in which seismic energy is expected to be dissipated by inelasticity in members. Full-scale GFRP-reinforced concrete columns were experimentally investigated to determine the behavior of these columns and assess their significance from a seismic-performance perspective based on the dissipated energy and ductility levels attained. This study is expected to set the path for further research to investigate the possibility of using GFRP bars and stirrups as main reinforcement in earthquake-resistant structures.

4.4 Experimental Program

4.4.1 Test Specimen Design

The GFRP reinforced columns were designed and analyzed according to the recommendations and limitations of CSA S806 (2012). While the steel reinforced concrete columns were designed to have similar axial stiffness and according to A23.3 (2014) as possible. The nominal moment were calculated based on plane sectional analysis, taking into account the effect of applied axial load through the moment–axial load interaction diagram for the adopted axial load levels. To satisfy the shear-capacity requirements for the specimens, transverse reinforcement (rectilinear spirals and cross ties) was provided at the maximum allowed spacing, namely, the least of (1) 16 times the diameter of the smallest longitudinal bars; (2) 48 times the minimum cross-sectional diameter of the GFRP tie; (3) the least dimension of the compression member; or (4) 300 mm. This was done for the stability of the longitudinal bars.

4.4.2 Test Specimens

The experimental program consisted of eleven square reinforced-concrete columns measuring 400×400×1850 mm connected to a massive stub 1200×1200×600 and cast vertically. The transverse load was applied at the tip of the specimen 1.65 m from the base of the column with a displacement-controlled hydraulic actuator. The specimens represent a column 3.7 m in height in a typical building with the point of contraflexure located at column mid-height. **Figure 4.1** shows the concrete dimensions and reinforcement details of test specimens.

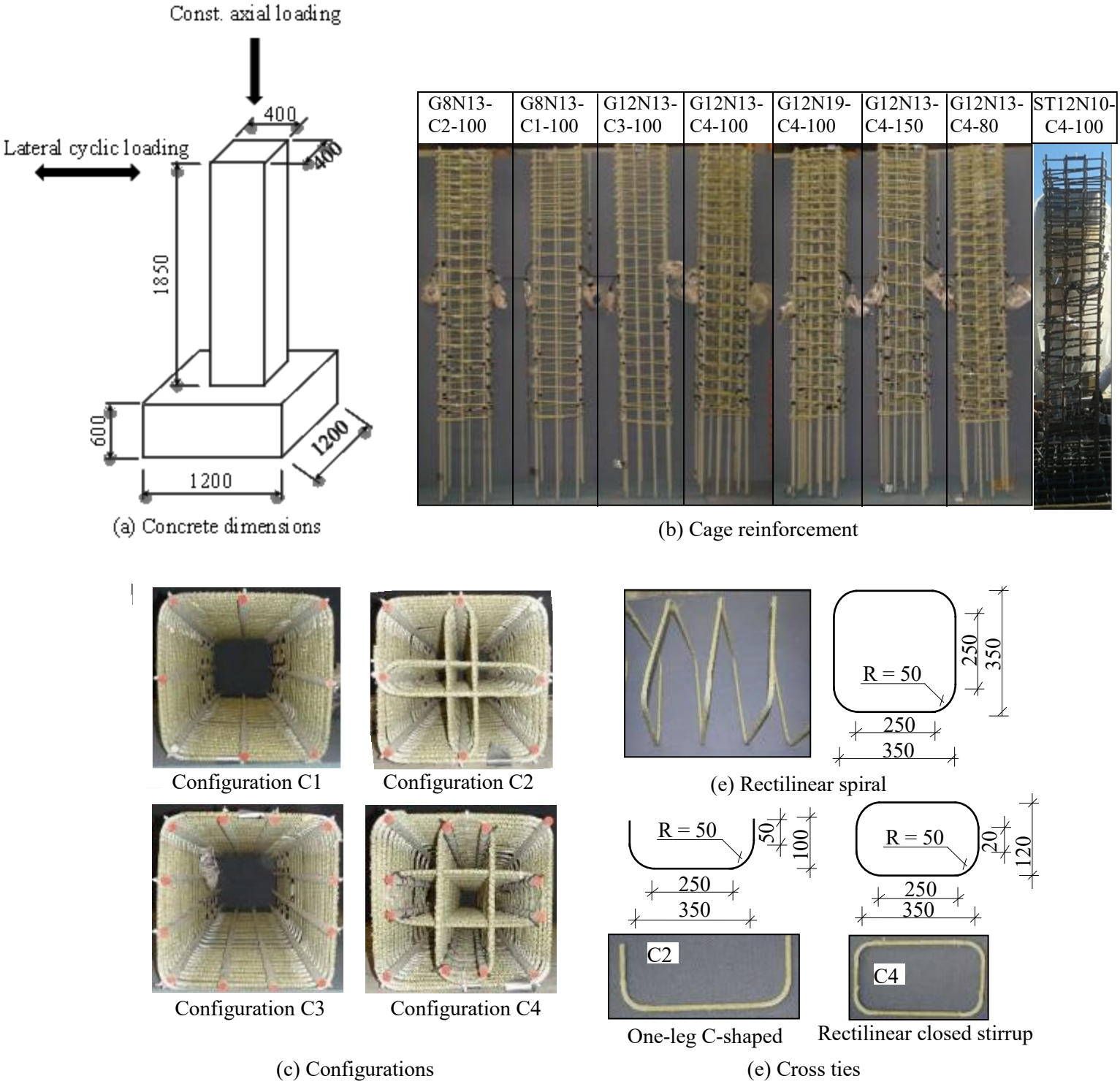

Figure 4.1–Test-specimen details

The main variables investigated were (1) configuration of reinforcement details; (2) axial-load level; (3) the volumetric transverse reinforcement ratio depending on spacing; and (4) the longitudinal reinforcement ratio. **Figure 4.1b** shows the cage reinforcement of the test specimens. The axial-load level is defined as the index $P/f_c'A_g$, where P is the constant axially applied compression load, f_c' is the concrete compressive strength, and A_g is the gross cross-sectional area of the column. Three targeted axial-load levels of 20%, 30%, and 40% were chosen. Four different configurations were adopted to study the effect of the number of longitudinal bars and transverse cross ties on the performance of the laterally loaded columns (**Figure 4.1c**). **Figure 4.1d** shows the rectilinear spiral used for the outer transverse reinforcement. Two shapes of cross ties were used as inner transverse reinforcement; one-leg C-shaped cross tie and rectilinear closed stirrup cross tie, as shown in **Figure 4.1e**.

The specimens are identified by reinforcement type (ST for steel and G for GFRP, respectively), number of longitudinal bars (8 and 12), longitudinal-bar diameter (N10 and N8 for steel and N13 and N19 for GFRP), tie configuration (C1, C2, C3, and C4), spacing (80, 100, and 150 mm). In addition, the numbers 30 and 40 identify the two columns subjected to 30% and 40% of axial load; the other columns were subjected to 20% axial load. It should be noted that, although a spacing of 100 mm and 150 mm as well as configuration C1 and C3 do not satisfy CSA S806-12 requirements and limitations, we chose them intentionally to meet the research goal of examining the deformability performance of GFRP-reinforced columns. **Table 4.1** provides the test matrix and reinforcement details of the test specimens.

Table 4.1- Test-specimens details

Specimen	Bar and stirrups type	Long. Bars	Configuration	Spacing (mm)	ρ_l %	Transverse reinforcement				Axial load percentage	*Actual* f_c'*(MPa)*	*EA*
						ρ_v %	A_{sh} act	Ash req for drift				
								>2.5%	>4%			
ST8N10-C1-100	steel	8 # 3	C1	100	0.35	0.25	---	---	---	20%	44	111
ST12N10-C4-100	steel	12 # 3	C4	100	0.53	0.5	---	---	---	20%	34	170
G8N13-C1-100	GFRP	8 # 4	C1	100	0.63	0.36	142.6	168.6	269.8	20%	37	71
G8N13-C2-100	GFRP	8 # 4	C2	100	0.63	0.53	213.9	141.8	226.9	20%	37	71
G12N13-C3-100	GFRP	12 # 4	C3	100	0.95	0.36	142.6	179.0	286.4	20%	39	106
G12N13-C4-100	GFRP	12 # 4	C4	100	0.95	0.71	285.2	136.1	217.8	20%	39	106
G12N13-C4-80	GFRP	12 # 4	C4	80	0.95	0.89	285.2	106.8	170.8	20%	32	106
G12N13-C4-150	GFRP	12 # 4	C4	150	0.95	0.48	285.2	233.1	373.0	20%	33	106
G12N19-C4-100	GFRP	12 # 6	C4	100	2.14	0.71	285.2	148.4	237.4	20%	43	208
G12N13-C4-100-30	GFRP	12 # 4	C4	100	0.95	0.71	285.2	165.6	265.0	30%	41	106
G12N13-C4-100-40	GFRP	12 # 4	C4	100	0.95	0.71	285.2	231.2	369.9	40%	41	106

f_c': concrete compressive strength (MPa); ρ_l: longitudinal-reinforcement ratio; ρ_v: transverse-reinforcement ratio; $A_{sh\ act}$: actual provided transverse reinforcement (mm^2); $A_{sh\ req}$: required transverse reinforcement according to Eq. 3-10 to achieve either 2.5% or 4% drift (mm^2); s:spacing of transverse reinforcement (mm); and $P/f_c'A_g$: axial-load level; EA: axial stiffness; E: longitudinal-bar modulus of elasticity; A: longitudinal-bar area.

4.4.3 Material Properties

All specimens were constructed with normal-weight, ready-mixed concrete having a target nominal compressive strength f_c' = 40 MPa. **Table 4.1** gives the actual concrete compressive strength based on the average values from tests performed on at least three 100×200 mm cylinders for each concrete batch on the column's day of testing. N10 and N8 grade 60 steel bars were used in the steel-reinforced columns as longitudinal and transverse reinforcement, respectively. The GFRP reinforcing bars in the GFRP-reinforced columns were three diameters of Grade III sand-coated bars (CSA S807 2015): N13 and N19 as longitudinal bars and N10 as transverse reinforcement (rectilinear spirals and cross ties). The longitudinal tensile properties of the GFRP bars were determined by testing five specimens according to ASTM D7205 (2011), in the case of the straight bars, and test method B.5 in ACI 440.3R (2004), in the case of the bent bars. The steel-bar properties herein were provided by the manufacturer. **Table 4.2** lists the material properties of the reinforcing bars.

Table 4.2 – Reinforcement material properties

Bar	d_b (mm)	A_f (mm^2)	A (mm^2)	E_f (GPa)	F_{fu} (MPa)	ε_{fu}(%)	Notes
GFRP #4 (N13)	12.7	126.7	143	69.6	1392	2	
GFRP #6 (N19)	19.05	285	317	60.5	1125	1.82	
Steel #2 (N8)	8	50	-	200	f_y=400	ε_y=0.2	
Steel #3 (N10)	9.5	71.3	-	200	f_y=420	ε_y=0.2	
GFRP #3 (N10)	9.5	71.3	84	52	962	1.85	Straight portion
				-	500	-	Bent portion

Where,

d_b : Bar nominal diameter.
A_f : Nominal cross-sectional area.
E_f : GFRP modulus of elasticity.
F_{fu} : GFRP tensile strength.
ε_{fu} : GFRP ultimate strain.
f_y : Steel yielding strength.
ε_y : Steel yielding strain.
A Immersed area

4.4.4 Instrumentation

Electrical strain gauges and linear variable differential transducers (LVDTs) were used to measure strain and displacement, as shown in **Figure 4.2**. Thirty electrical strain gauges were mounted on the longitudinal and transverse reinforcement at three different levels above the stub. Concrete strain and curvature were calculated using three sets of LVDTs that were placed in each of the loading sides of the columns within the plastic-hinge region. Four LVDTs were mounted to capture the lateral deformation at different column heights. Two addition LVDTs were used to monitor the unlikely possibility of sliding at the column–stub connection and between the stub and rigid floor.

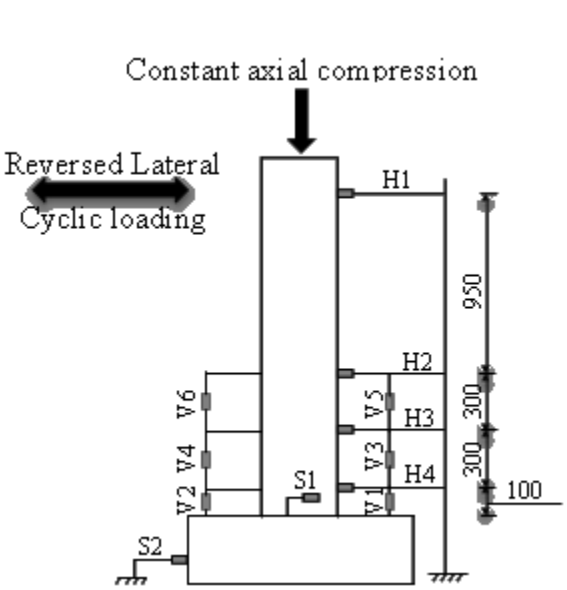

(a) LVDT instrumentation

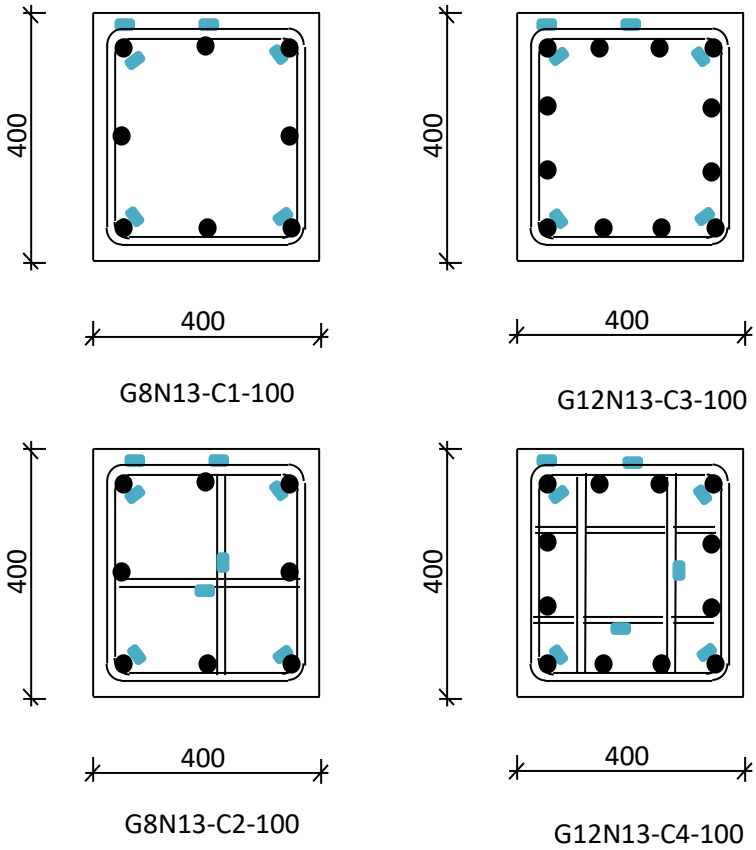

(b) Strain gauges instrumentation

Figure 4.2- Instrumentation of test specimens

4.4.5 Test Setup and Loading Procedure

Figure 4.3 shows the test setup. The axial load was applied at the top of the column, where the axial stress was maintained constant throughout the test. Cyclic lateral displacements at a rate of 1.3 mm/min were applied to the columns with a 500 kN MTS actuator mounted horizontally to a steel reaction frame. As the loading history was not a test variable, a typical procedure of applying quasi-static reversed cyclic loading until failure was used (**Figure 4.4**).

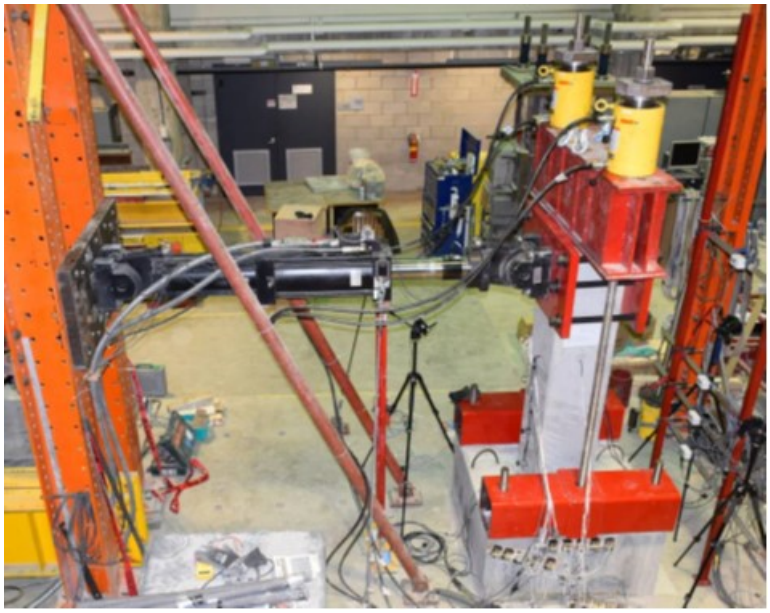

Figure 4.3- Test setup

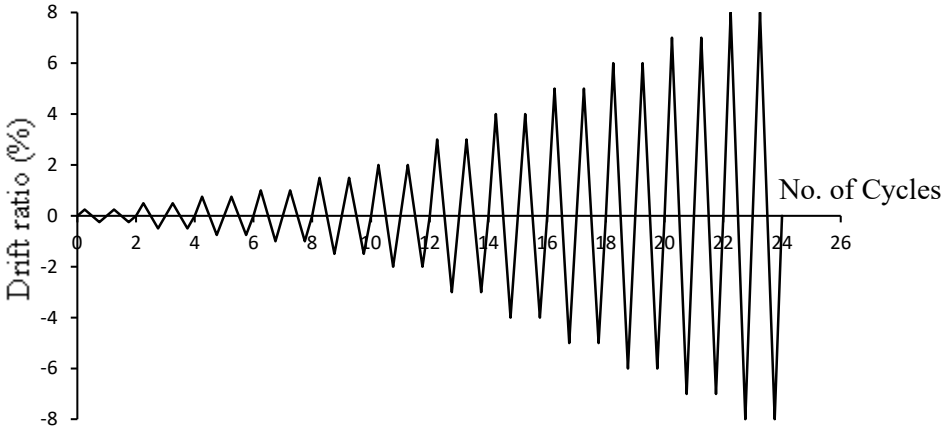

Figure 4.4- Loading history

4.5 Experimental Results

4.5.1 General Behavior and Response

The hysteretic response is a main curve for structural members under simulated seismic loading, illustrating the general behavior of the specimens and achieved drifts. **Figure 4.5** provides the lateral load versus tip drift for all the specimens. The second excursion loading path followed the first excursion but with less stiffness. The second excursion in each chosen lateral drift was eliminated for clarity. **Figure 4.5** illustrates occurrences of special events such as the yielding of longitudinal steel bars, spalling of concrete cover, interlaminar degradation of longitudinal GFRP bars, and loss of axial-load capacity due to concrete crushing. The hysteretic response of each column showed reasonable symmetric lateral load-top drift relationships for loading in the +ve and -ve directions until concrete crushing occurred at one end. Also, it is important to mention that a lateral resistance is developed because of P-Δ effect of the axial load. The corresponding values of the lateral resistance to the required drifts 2.5% and 4% are small. Thus the lateral resistance is ignored in the analysis. **Table 4.3** lists the lateral resistance at 2.5% and 4% drift ratios for all the columns.

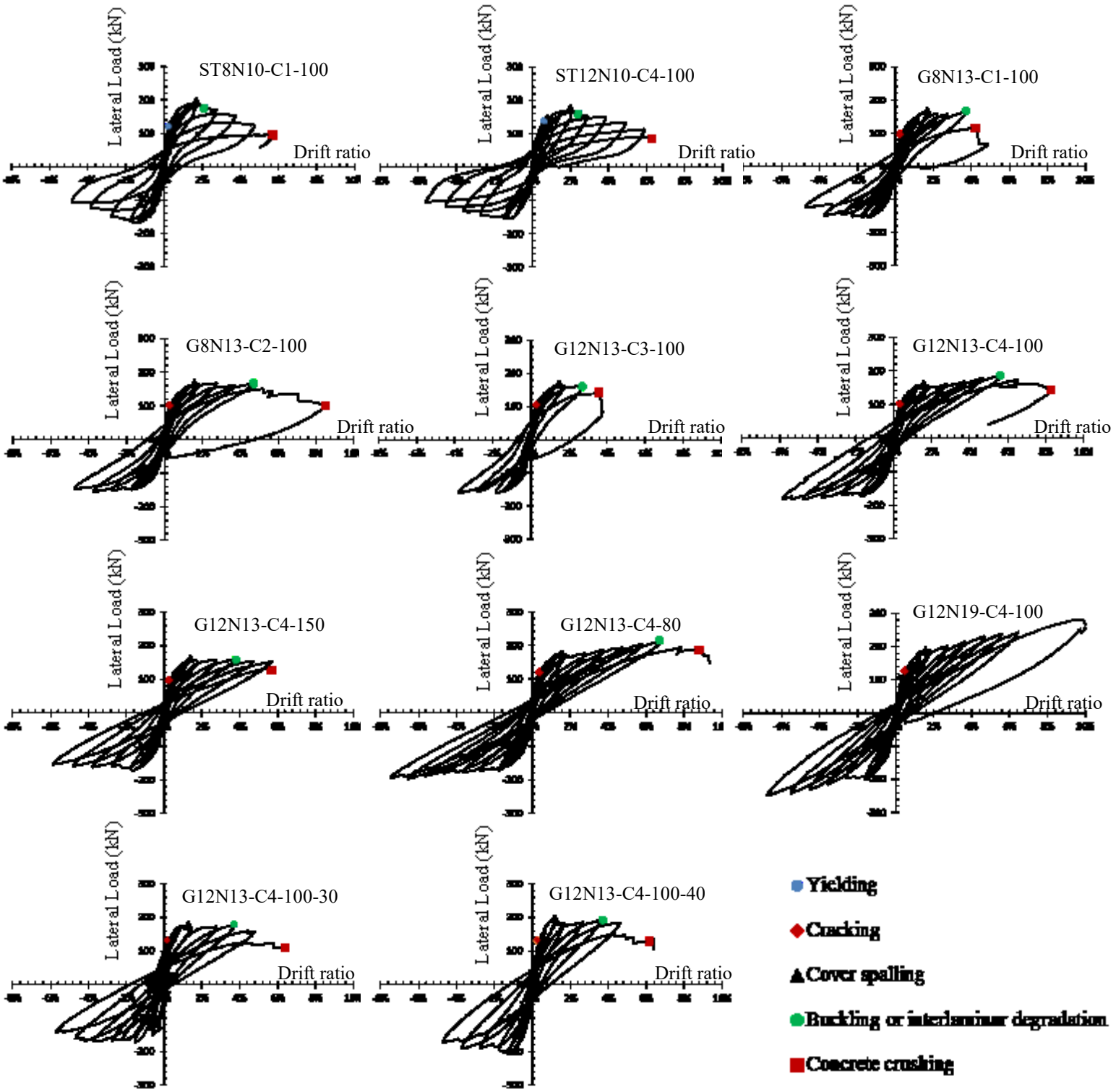

Figure 4.5– Hysteretic response

Table 4.3- The lateral resistance values

Column	Drift ratio 2.5%		Drift ratio 4%	
	The lateral load (kN)	The lateral resistance (kN)	The lateral load (kN)	The lateral resistance (kN)
G8N13-C1-100	150	6	146	14.5
G8N13-C2-100	165	6.6	163	16.2
G12N13-C3-100	150	6	160	15.9
G12N13-C4-100	160	6.4	170	16.9
G12N13-C4-80	170	6.8	179	17.8
G12N13-C4-150	160	6.4	159	15.8
G12N19-C4-100	200	8	221	22
G12N13-C4-100-30	165	6.6	168	16.7
G12N13-C4-100-40	185	7.4	191	19

The response was essentially linear-elastic for all columns up to the formation of the first crack with the GFRP-reinforced columns which evidencing lower initial stiffness than the steel-reinforced ones. Thereafter, cracks started to propagate. The behavior of all the columns was dominated by a flexural response, as evidenced by the typical amount of horizontal cracking aligned with the rectilinear spirals and ties as shown in **Figure 4.6**

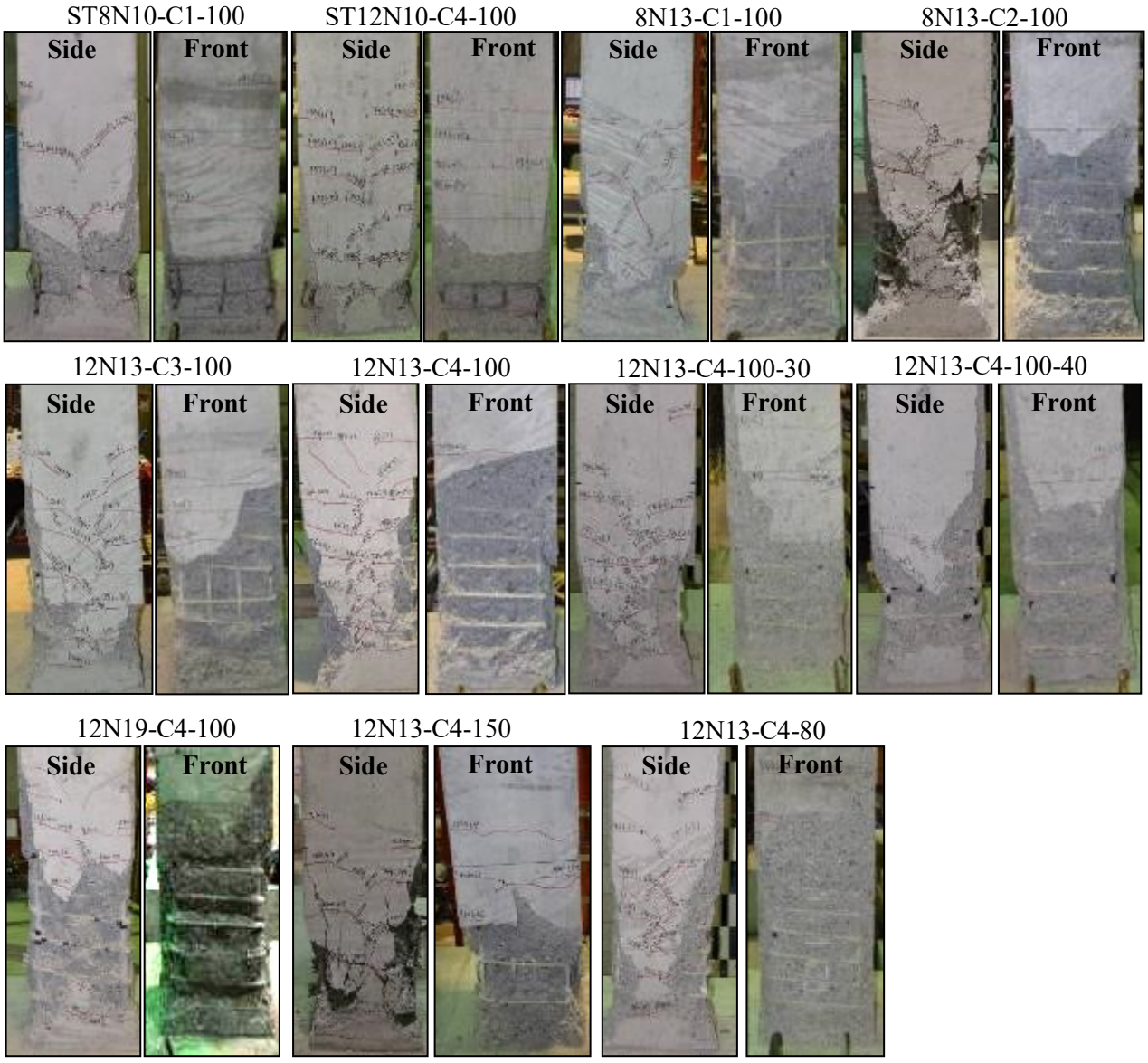

Figure 4.6– Crack pattern (side) and failure and plastic hinge (front)

Under increased displacement, horizontal cracks continued to form up to a height of approximately 60% of the column's effective height (L_c=1650 mm [65 in]) above the column base for well-confined columns, as evidenced in **Figure 4.6**. This relates to photos labelled "side" for columns ST12N10-C4-100, G12N13-C4-80, and G12N19-C4-100. As the confinement level decreased, the cracks propagated up to 50% of L_c in columns G8N13-C2-100, G12N13-C3-100, and G12N13-C4-100 and to 40% for the columns lightly reinforced in the longitudinal or transverse direction and for the columns with higher axial load, such as ST8N10-C1-100, G8N13-C1-100, G12N13-C4-150. , G12N13-C4-100-30, and G12N13-C4-100-40. At the early loading stage, the steel bars in ST8N10-C1-100 and ST12N10-C4-100 yielded at 0.25% and 0.62% drift, respectively.

With further applying of the cyclic load, vertical splitting cracks typically appeared in the columns at the compressed side of the steel- and GFRP-reinforced columns, respectively, as shown in **Figures 4.7a** and **4.8a. Figures 4.7b** and **4.8b** show the spalling of the concrete cover, which became more significant and occurred in all the columns within a range of 1.4% to 1.9% lateral drift.

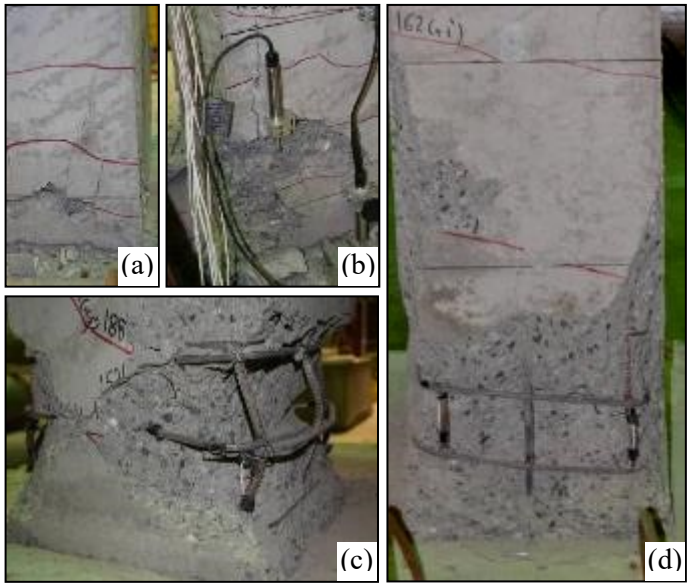

Figure 4.7 – Typical failure progression of the steel-reinforced columns: (a) vertical splitting; (b) spalling of concrete cover; (c) buckling of longitudinal bars; and (d) concrete crushing causing failure.

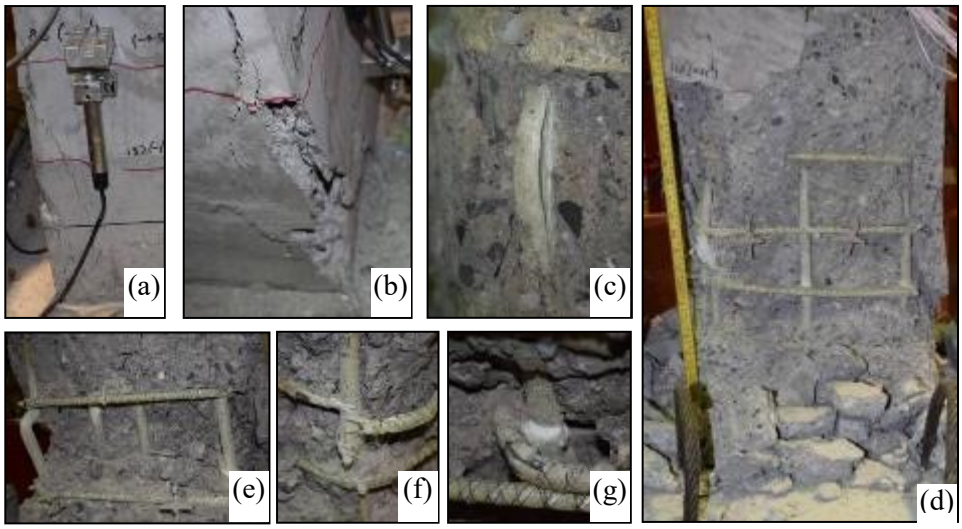

Figure 4.8– Typical failure progression of the GFRP-reinforced columns: (a) vertical splitting; (b) spalling of concrete cover; (c) longitudinal-bar interlaminar degradation; (d) concrete crushing causing failure; (e) fracture of longitudinal bars; (f) rupture of GFRP rectilinear spirals; and (g) rupture of GFRP cross ties.

During the cycle following the concrete-cover spalling, the longitudinal steel bars (**Figure 4.7c**) in ST8N10-C1-100 and ST12N10-C4-100 buckled, as shown in **Figure 4.5**. Although the buckled bars straightened under tension during the reversed load cycle, degradation of the lateral resistance was more pronounced after buckling occurred in the outermost bar. With further cyclic loading, excessive steel-bar buckling was observed until the axial load was lost due to the concrete core crushing (**Figures 4.5**and **4.7d**).

On the other hand, the GFRP-reinforced columns experienced three different behaviors, which can be categorized as follows:

1- Strength degradation followed the concrete-cover spalling. This behavior was observed in the lightly reinforced columns, i.e., G8N13-C1-100, G8N13-C2-100, G12N13-C3-100, and G12M13-C4-150 (**Figure 4.5**).
2- The well-confined columns—such as G12N13-C4-100, G12N13-C4-80, and G12N19-C4-100—experienced a strength gain with a second peak, as shown in **Figure 4.5**. This phenomenon has been reported in axially loaded FRP-reinforced columns (Tobbi et al. 2012).
3- Increasing the axial load to 30% and 40%in for G12N13-C4-100-30 and G12N13-C4-100-40, respectively, controlled the strength gained in column G12N13-C4-100, but both columns reached a plateau after the concrete cover spalled (**Figure 4.5**).

Consequently, the GFRP-reinforced columns had responses similar to their counterpart steel-reinforced columns with similar axial stiffness ($EA \approx 106$ MN), such as comparing ST8N10-C1-100 to G12N13-C3-100. Among the columns with higher axial stiffness ($EA \approx 208$ MN), the GFRP-reinforced columns (G12N19-C4-100) performed better than its counterpart steel-reinforced column (ST12N10-C4-100). Moreover, increasing the longitudinal GFRP bars or reducing the transverse-reinforcement spacing (such as in G12N19-C4-100 and G12N13-C4-80, respectively) enhanced performance as the ultimate strength of the columns increased. Overall, the GFRP bars kept their integrity with no observed degradation until one or two cycles before the failure cycle. The interlaminar degradation of the compressed longitudinal GFRP bars occurred at a various drift levels with a minimum drift value of 2.7% for G12N13-C3-100 and reaching more than 3.7% drift for all the other GFRP-reinforced columns, which is higher than the 2.5% drift recommended by the *National Building Code of Canada* (NBCC 2010) and CSA S806 (2012). In contrast, the steel bars lost their integrity at early drift levels of 2.1% and 2.4% in ST8N10-C1-100 and ST12N10-C4-100, respectively. **Figure 4.8** shows the interlaminar degradation of the GFRP bars.

When the displacement increased, all of the columns lost the axial load due to the concrete core crushing as shown in **Figures 4.7d** and **4.8d**. The failure of the GFRP-reinforced concrete columns was associated with fracturing of compressed longitudinal GFRP bars (**Figure 4.8e**) and rupture of GFRP rectilinear spirals and ties (**Figures 4.8f** and **g**, respectively). There was

one exception: column G12N19-C4-100 reached the limit of the loading setup at 10% lateral drift with no interlaminar degradation or failure. **Table 4.4** provides the failure progression of the test specimens.

Table 4.4 - Failure progression

Specimen	Yielding		Cover Spalling		Buckling		Interlaminar		Concrete Crushing		P_f/P_{max}
	P (kN)	δ %	P (kN)	δ %	P (kN)	δ %	P (kN)	δ %	P (kN)	δ %	
ST8N10-C1-100	120	0.25	190	1.7	176	2.1	N/A		95	5.7	0.50
ST12N10-C4-100	137	0.62	170	1.9	161	2.4			84	6.2	0.49
G8N13-C1-100	N/A		166	1.7	N/A		165	3.7	115	4.2	0.69
G8N13-C2-100			165	1.6			167	4.7	100	8.5	0.60
G12N13-C3-100			167	1.5			160	2.7	140	3.7	0.84
G12N13-C4-100			157	1.6			186	5.6	142	8.3	0.76
G12N13-C4-100-30			171	1.6			178	3.7	111	6.4	0.62
G12N13-C4-100-40			195	1.4			192	3.8	129	6.2	0.66
G12N13-C4-150			161	1.6			158	3.8	125	5.8	0.64
G12N13-C4-80			173	1.6			214	6.7	185	8.8	0.86
G12N19-C4-100			186	1.6			---	---	282[a]	10.1[b]	0.00

[a] Maximum lateral load and drift attained without failure.

The photos in **Figure 4.6** labelled "front" show the appearance of the plastic-hinge zone after all specimens were tested. Generally, based on the damaged region, the higher the confinement level, tie spacing, or the axial load, the larger the column's damaged region. **Figure 4.6** also shows that the damaged zone in all the columns started at a distance of 25 to 30 mm (1 to 1.2 in) above the base stub. This behavior, observed in similar specimens by other researchers (Ali and El-Salakawy 2016; Sheikh and Khoury 1993) has been attributed mainly to the base stub providing confinement to the column sections just above it. Therefore, the moment is calculated at 30 mm above the column–stub interface.

4.5.2 Ductility and Energy Dissipation

Ductility parameters and energy-dissipation capacity are usually used to assess the seismic response of reinforced-concrete members. While the ductility of long-period structures is directly related to the strength-reduction factor used in many codes (CSA S806-12 and NBCC 2010) to calculate the seismic base shear, the energy-dissipation capacity can be used as a response indicator in the design of short-period structures and structures subjected to a long-duration earthquake.

The ductility index is a parameter for ensuring good deformation capacity in RC structures, which is important in areas of earthquake activity where absorbing energy is of prime importance. Conventional ductility indices are defined as the ratio of the final deformation at the ultimate state to the deformation at the first plastic behavior. Therefore, a well-defined explicit relationship must exist between the elastic and inelastic behaviors of GFRP-reinforced columns in order to calculate the ductility index since the ACI 440.1R (2015) and CSA S806 (2012) design codes offer no unified method for assessing the ductility index of FRP-reinforced structures.

The transition from elastic to inelastic deformation should be identified to calculate the ductility parameters. For the steel-reinforced columns, the elastic region ended at the yield-deformation point Δ_y and the inelastic region at the maximum deformation point Δ_u. For GFRP-reinforced columns, the elastic region ended at the start of concrete inelasticity-that is, concrete deterioration at the compressed end of the column-and the inelastic region at the maximum deformation point. The major difference between the steel- and GFRP-reinforced columns is the absence of yielding phenomena in the GFRP bars. For this reason, the transition point between the elastic and inelastic regions in GFRP-reinforced columns is defined herein as the virtual yield deformation point Δ_e. Accordingly, the load-displacement and the moment-curvature curves are used to identify the elastic branch of the idealized curve as shown in **Figure 4.9**. In the load–displacement curve, the elastic branch is secant to the real curve at 65% of the maximum lateral load (P_{max}), and reaches the maximum load to define the virtual yield deformation point Δ_e. Column failure is conventionally defined at the post-peak displacement Δ_u, at which point the remaining capacity of the column has dropped to 80% of the peak load. The moment–curvature curve is used in a similar procedure as shown in **Figure 4.9**.

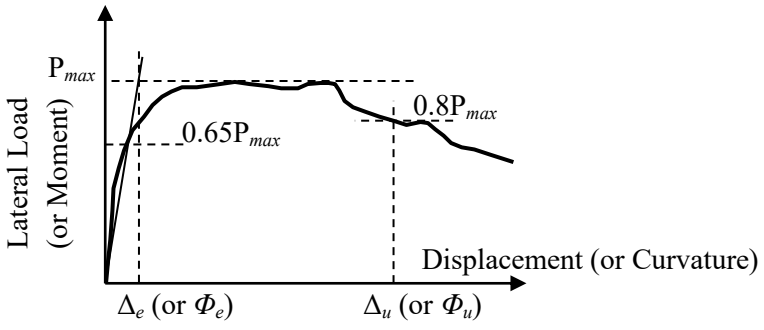

Figure 4.9 – Idealized curve definition

The displacement ductility index (μ_Δ) is defined as:

$$\mu_\Delta = \frac{\Delta_u}{\Delta_y} \text{ for steel or } \mu_\Delta = \frac{\Delta_u}{\Delta_e} \text{ for FRP} \quad (4\text{-}1)$$

, and the curvature ductility index (μ_Φ) is defined as:

$$\mu_\emptyset = \frac{\emptyset_u}{\emptyset_y} \text{ for steel or } \mu_\emptyset = \frac{\emptyset_u}{\emptyset_e} \text{ for FRP} \quad (4\text{-}2)$$

A concept based on deformability rather than ductility was proposed to ensure adequate deformation of FRP-reinforced structures before failing, based on the work reported by Jaeger et al. (1995). The concept was developed for FRP-reinforced beams and slabs. A combination of strength and deformability was incorporated into the deformability factor (*J*), which can be regarded as the ratio of two energy quantities: one associated with the ultimate limit-state condition and the other to the condition when the concrete at the extreme compression fiber reaches its proportional limit. The deformability factor is expressed as follows (Jaeger et al. 1995):

$$J = \frac{M_u \emptyset_u}{M_c \emptyset_c} \quad (4\text{-}3)$$

where *M* and *Φ* are the moment and curvature at service or ultimate, denoted by the subscripts *c* and *u*, respectively. The *Canadian Highway Bridge Design Code* (CHBDC) includes an overall performance factor for FRP-reinforced beams and slabs (CSA S6-14) that combines the strength and deformability given by Eq. (4-3), with the service condition, taken as the point when the maximum concrete compressive strain reaches 0.001.

For the GFRP-reinforced columns, *J* was calculated and resulted in unreliably high values (referred as $J_{0.001}$ in **Table 4.5**). As the moment and curvature were determined at a concrete compressive strain of 0.001 (the recommended value for FRP-reinforced beams and slabs according to CSA S6-14 and CSA S806-12), high values of $J_{0.001}$ were reached due to well-confined concrete, which allowed the concrete compressive strain to reach more than 0.008 at ultimate. Therefore, the deformability factor *J* was recalculated for moment and curvature values corresponding to a concrete compressive strain of 0.0035 ($J_{0.0035}$). **Table 4.5** lists the original $J_{0.001}$ and modified $J_{0.0035}$ deformability factor resulting in a large difference between the two procedures due to the difference in the values of moments and curvatures

corresponding to concrete compressive strains of 0.001 and 0.0035. The calculated $J_{0.0035}$ showed reliable values in comparison to the other procedures (Mohamed et al. 2015).

Table 4.5: Ductility parameters

Specimen	δ_u %	μ_Δ	μ_Φ	J	
				$J_{0.001}$	$J_{0.0035}$
ST8N10-C1-100	5.7	6.6	>7.1	---	---
ST12N10-C4-100	6.2	7.7	>9.0	---	---
G8N13-C1-100	4.2	5.5	>8.2	28.3	5.9
G8N13-C2-100	8.5	10.4	>12.3	41.2	10.1
G12N13-C3-100	3.7	7.8	>9.7	32.9	8.5
G12N13-C4-100	8.3	9.8	>12.5	37.6	10.0
G12N13-C4-100-30	6.4	5.6	>7.9	27.5	6.1
G12N13-C4-100-40	6.2	6.6	>8.5	34.7	6.4
G12N13-C4-150	5.8	7.1	>11.2	31.8	7.3
G12N13-C4-80	8.8	9.8	>10.9	39.5	10.9
G12N19-C4-100	>10	>7.5	>9.9	>33.6	>7.9

The main drawback of using the ductility parameters is the lack of consensus in the research community on a definition of the elastic–plastic transition point in FRP-reinforced concrete members. The maximum interstory drift δ_u is simpler to use and is defined based on the measured displacement at failure as $\delta_u = \Delta_u / L_c$ (**Table 4.5**).

The calculated ductility indices listed in **Table 4.5**; μ_Δ, μ_Φ, J, and δ_u for the GFRP-reinforced columns showed consistency in representing the effect of each studied parameter on the ductility indices. The displacement ductility (μ_Δ) and deformability factor ($J_{0.0035}$) showed reasonable predicted ductility indices while the curvature ductility (μ_Φ) showed higher estimation of the columns' ductility and $J_{0.001}$ might be considered inappropriate due to the confinement level profound in the columns.

Energy dissipation capacity and an adequate ductility level are desirable characteristics in column behavior. Moreover, this capacity is recognized as an important parameter with respect to a structure's seismic performance. Energy dissipation is defined for a cycle *i* by the shaded area as shown in **Figure 4.10** or mathematically as expressed in equations 4.4 and 4.5.

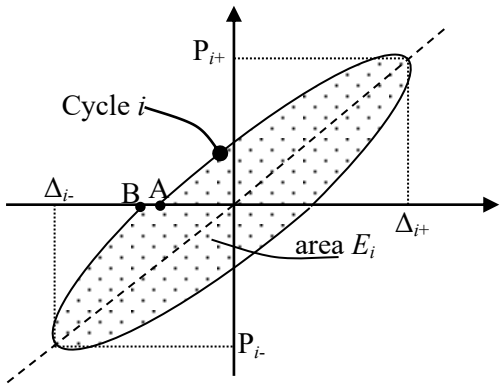

Figure 4.10 – Definition of energy dissipation

$$E_i = \int_A^B F d_u \qquad (4-4)$$

$$E_{iacc} = \sum_1^i E_i \qquad (4-5)$$

Figure 4.11 shows the calculated E_{acc} in each cycle for the tested columns. For drifts lower than 1%, E_{acc} was quite small. For larger drifts, however, a nearly linear increase in the dissipated energy with respect to an increase in drift level can be observed. Close to the final stage, a slight decrease in the tendency rate was observed.

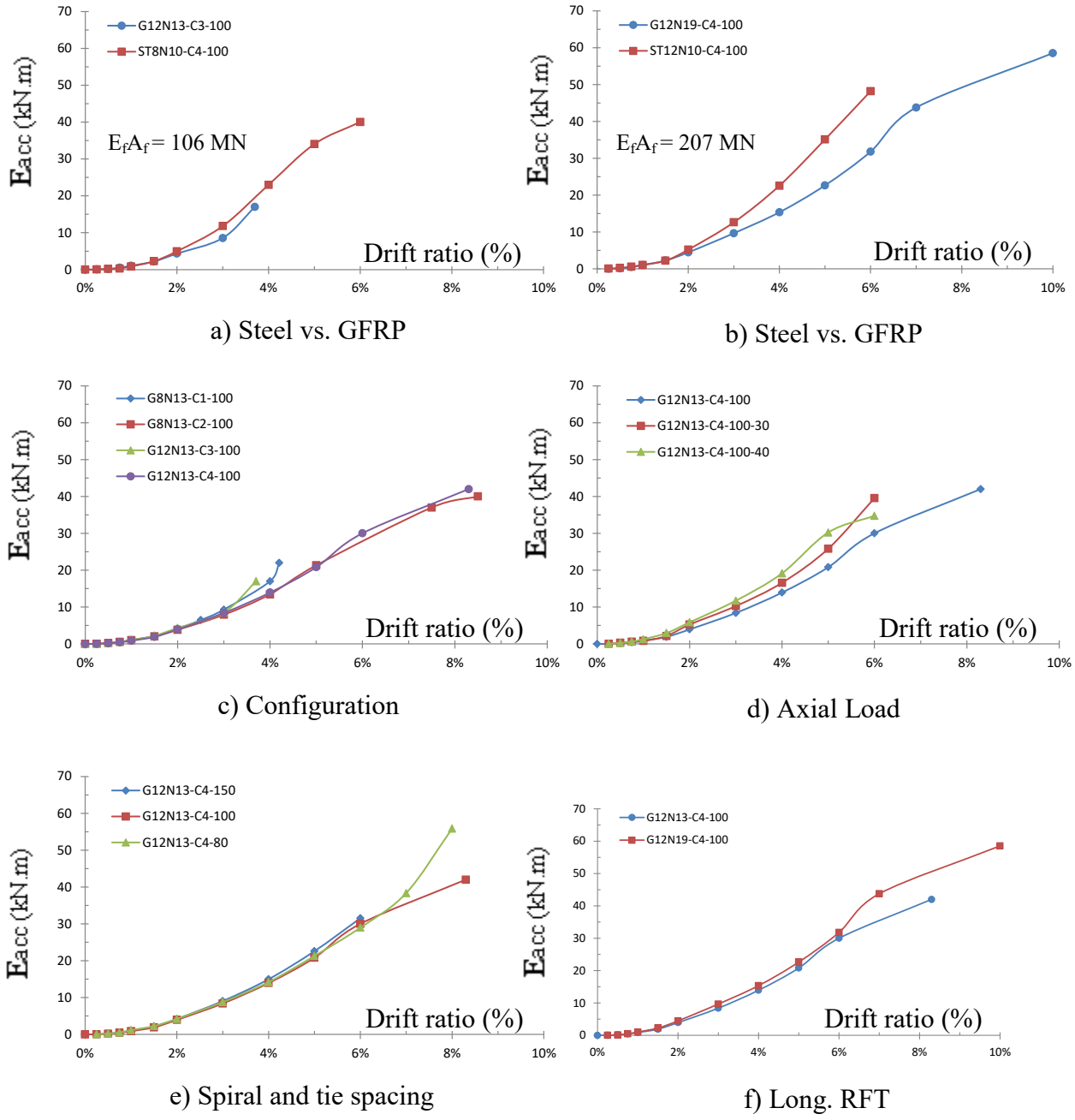

Figure 4.11 – Accumulated energy dissipation

The dissipated energy of the steel- and GFRP-reinforced columns can be compared for lower axial stiffness (≈106 MN) and higher axial stiffness (≈208 MN). Columns ST8N10-C1-100 and G12N13-C3-100 (**Figure 4.11a**), with lower axial stiffness, exhibited similar dissipated energy up to 2% drift, which was prior to the buckling of the steel bars. Thereafter, with increased drift, however ST8N10-C1-100 achieved higher E_{acc} compared to G12N13-C3-100. At 2.5%—corresponding to moderate ductility according to CSA S806-12—the E_{acc} of G12N13-C3-100 was almost 75% that of ST8N10-C1-100, which was expected due to the excessive longitudinal steel-bar buckling occurring after 2% drift led to early degradation of the column, resulting in significant dissipated energy. In contrast, G12N13-C3-100 kept its integrity until a higher drift level (2.7%, corresponding to the interlaminar degradation of longitudinal GFRP bars).

At a higher axial stiffness, however, G12N19-C4-100 exhibited an acceptable tendency compared to ST12N13-C4-100, as shown in **Figure 4.11b**. Up to 2.4% drift, both columns had similar E_{acc}, with ST12N13-C4-100 experiencing more loop opening, but G12N19-C4-100 attaining higher load. The longitudinal steel bars started buckling at 2.4% drift, resulting in ST12N10-C4-100 having a higher E_{acc} than G12N19-C4-100. With the ascending tendency of G12N19-C4-100 after 1.9% drift with continuous load increases until test termination at 10.1% drift and the descending tendency of ST12N10-C4-100 until loss of axial capacity with a 50% reduction of the maximum lateral load, G12N19-C4-100 achieved more than 23% of the dissipated energy attained by ST12N10-C4-100 (refer to **Figure 4.11b**) at failure. Generally, the GFRP columns achieved at least 75% and 70% of the dissipated energy of their counter steel columns at 2.5% and 4% drift ratio respectively, which is considered a satisfactory level of energy dissipation.

Figures 4.11c and **e** show that no clear effect of reinforcement configuration or spiral and tie spacing on the energy dissipation. A slight increase in the dissipated energy due to the increased applied axial load and longitudinal-reinforcement ratio was observed, as shown in **Figures 4.11dand f**, respectively.

4.5.3 Effect of Axial Load

Three axial-load levels of 0.2 $f_c'A_g$, 0.3 $f_c'A_g$, and 0.4 $f_c'A_g$ were applied to G12N13-C4-100, G12N13-C4-100-30, and G12N13-C4-100-40, respectively, to study the effect of axial-load level. A limited increase in strength capacity was observed with increasing axial load, which coincides with the similarity of the estimated plan-sectional analysis flexural strength. Increasing the axial load was found to result in faster deterioration of the concrete core represented by the larger plastic hinge (see **Figure 4.6** image labelled "front") and reduced the ductility performance of the columns (see **Table 4.5**). Similar behavior was reported by Tavassoli et al. (2015) and Ali and El-Salakawy (2016) for laterally loaded circular and square GFRP-reinforced columns, respectively, where specimens with higher axial load showed faster deterioration with lower level of deformability.

4.5.4 Effect of Transverse-Reinforcement Spacing

Increasing the transverse-reinforcement ratio by adjusting the spacing significantly enhanced the ductility and yielded higher strength. Closer transverse-reinforcement spacing resulted in better confinement of the concrete core and delayed the deterioration of either the longitudinal reinforcement or the concrete core. For instance, the drift for column G12N13-C4-80 was almost 50% higher than that of column G12N13-C4-150. Reducing the spacing from 150 mm (5.9 in) to 80 mm (3.15 in) yielded a 33% increase in column strength capacity and delayed the drift corresponding to the interlaminar degradation of longitudinal bars from 3.8% to 6.7% (**Table 4.4** and **Figure 4.5**). Increasing the spacing from 80 mm (3.15 in) to 100 mm (3.94 in) (G12N13-C4-80 and G12N13-C4-100, respectively) resulted in a 13% reduction in column strength capacity with no significant difference in the overall behavior of the two columns (**Table 4.2** and **Figure 4.5**). This could indicate that the maximum spacing requirement by CSA S806-12 (maximum spacing for the specimens is controlled by 6 d_b = 76.2 mm (3 in), where d_b is the longitudinal bar diameter) is restrictive.

4.5.5 Comparison to Design Code

Clause 12.7 in CSA S806 (2012) gives complete detailing and limitations for designing lateral-resisting systems reinforced solely with FRP bars. This information was examined based on the outcomes of the GFRP-reinforced columns tested in this study.

The required area (A_{sh}) of the rectilinear spirals and cross ties provided in the tested GFRP-reinforced columns was calculated as follows:

$$A_{sh} = 14sh_c \frac{f_c^{'}}{f_{fh}} \left(\frac{A_g}{A_c} - 1\right) \frac{P}{P_o} \frac{\delta}{\sqrt{K_c}} \qquad (4-6)$$

where $P/P_o \geq 0.2$ (applied axial load to the column's nominal unconfined axial-load), $(A_g/A_c - 1) \geq 0.3$ (A_g and A_c are the gross and core cross-sectional area of the column); $k_c = 0.15\sqrt{(h_c/s)(h_c/sl)}$, $f_{Fh} = 0.006\,E_f$ or $\phi_f\, f_{fu}$, whichever is less; δ is the drift (0.025 and 0.04 for moderately ductile and ductile lateral-resisting systems, respectively); $f_c^{'}$ is the concrete compressive strength; h_c is the cross-sectional dimension of the column core; s is the spacing of transverse reinforcement, sl is the spacing of tie legs in the cross-sectional plane of the column; E_f and f_{fu} are the modulus of elasticity and ultimate tensile strength of FRP transverse reinforcement, respectively.

All the tested GFRP-reinforced columns were designed using Eq.4-6 to achieve either 2.5% or 4% drift except the columns G8N13-C1-100 and G12N13-C3-100 which had been constructed for comparison (**Table 3.1** and **Figure 3.11c**). The drift that could be achieved by each column according to the transverse reinforcement actually provided was estimated using the back calculation of Eq.4-6. **Figure 4.12** shows the experimentally determined drift of the tested columns against the estimated drift. Columns in lateral-resisting systems should have cross ties, since they greatly enhance overall column behavior. Increasing the transverse reinforcement area by 33% (adding a single-leg cross tie to G8N13-C1-100) clearly enhanced the ductility performance and ultimate drift of G8N13-C2-100 (refer to **Table 4.5** and **Figures 4.5** and **4.12**). Similarly, doubling the transverse-reinforcement area of G12N13-C3-100 (adding a double-leg closed cross tie) enhanced not only G12N13-C4-100's ductility performance and ultimate drift, but also its strength capacity. Generally, all the columns achieved much higher drift than the estimated values, confirming the effectiveness of using GFRP bars in lateral-resisting systems.

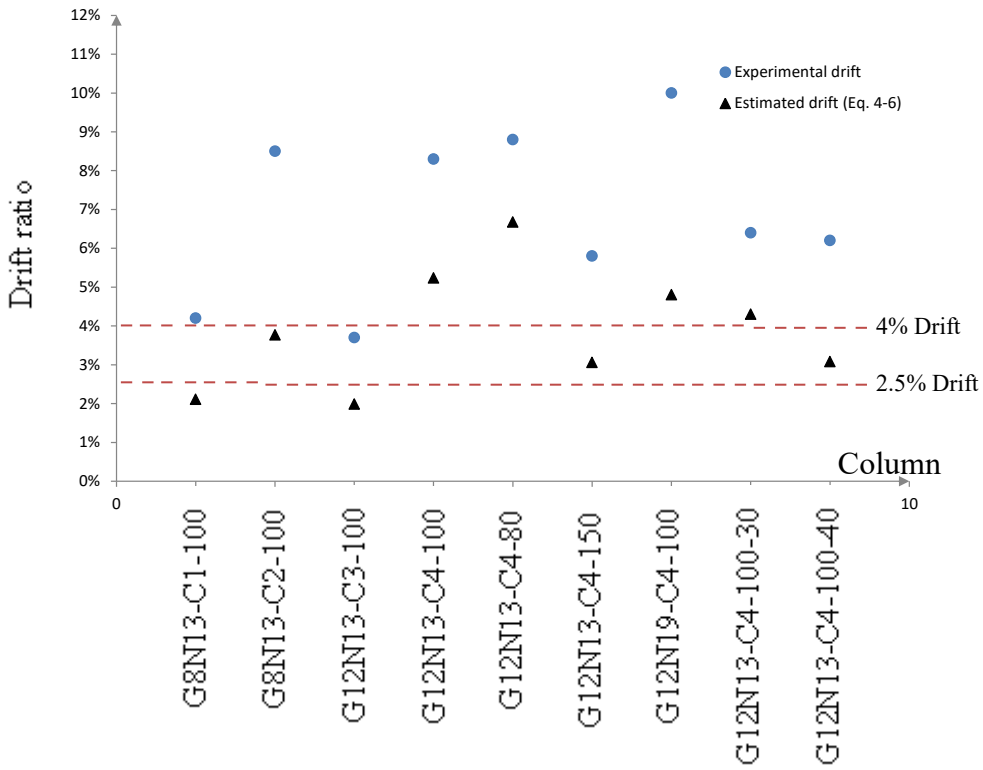

Figure 4.12 – Experimental and estimated drift ratios

The design stress level in FRP transverse reinforcement (f_{fh}) is limited to the least stress corresponding to a strain of 0.006, or the stress corresponding to the failure of the rectilinear spirals or cross ties. The strain limitation (0.006) is usually the predominant parameter in defining stress level due to the high tensile strength of FRP. **Figure 4.13** shows typical hysteretic response of strain in rectilinear spiral and cross ties. The strain increased and fell back to zero in the early stages of loading. As the cover spalled, the concrete core started to have a plastic response with noticeable strain values recorded at zero drift. Thereafter, the strain kept increasing with each cycle.

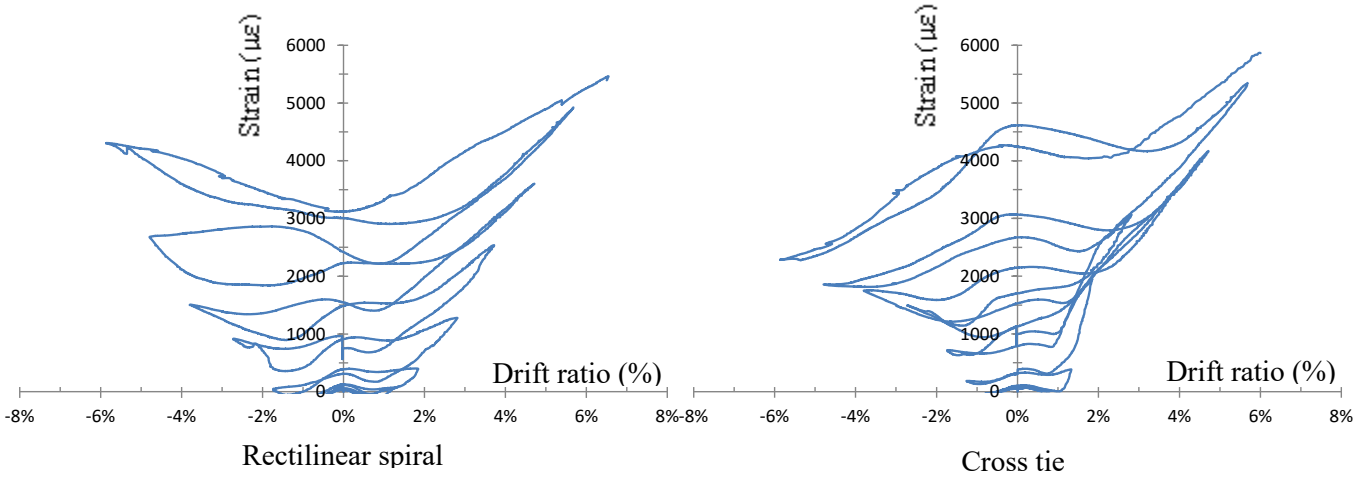

Figure 4.13 – Typical strain in rectilinear spirals and cross ties (G12N13-C4-100)

Figure 4.14 shows the strain values in rectilinear spirals and cross ties that were less than the strain limit of 0.006, confirming that the use of GFRP transverse reinforcement based on Eq. 4-6 effectively confined the concrete core in the post-peak stages. This agrees with the findings of Tobbi et al. 2014. Although Eq. 4-6 estimated similar A_{sh} for G12N13-C4-100 and G12N19-C4-100, the transverse strain was much higher in G12N19-C4-100, reaching 10,400 $\mu\varepsilon$. This could be attributed to the greater longitudinal-bar diameter resulting in increased axial capacity and lateral resistance, as shown in **Table 4.4** and **Figure 4.5**. This, in return, induced higher transverse strains than those attained in G12N13-C4-100 (**Figure 4.14**). Therefore, G12N19-C4-100 having higher transverse-reinforcement area could keep the induced strain within the limit of 0.006. This observation addresses the importance of including the effect of longitudinal bars in calculating the required A_{sh} (Eq.4-6) either as bar diameter or area as well as the number of bars. Moreover, this point confirms the capability of using GFRP bars to carry axial load combined with lateral load.

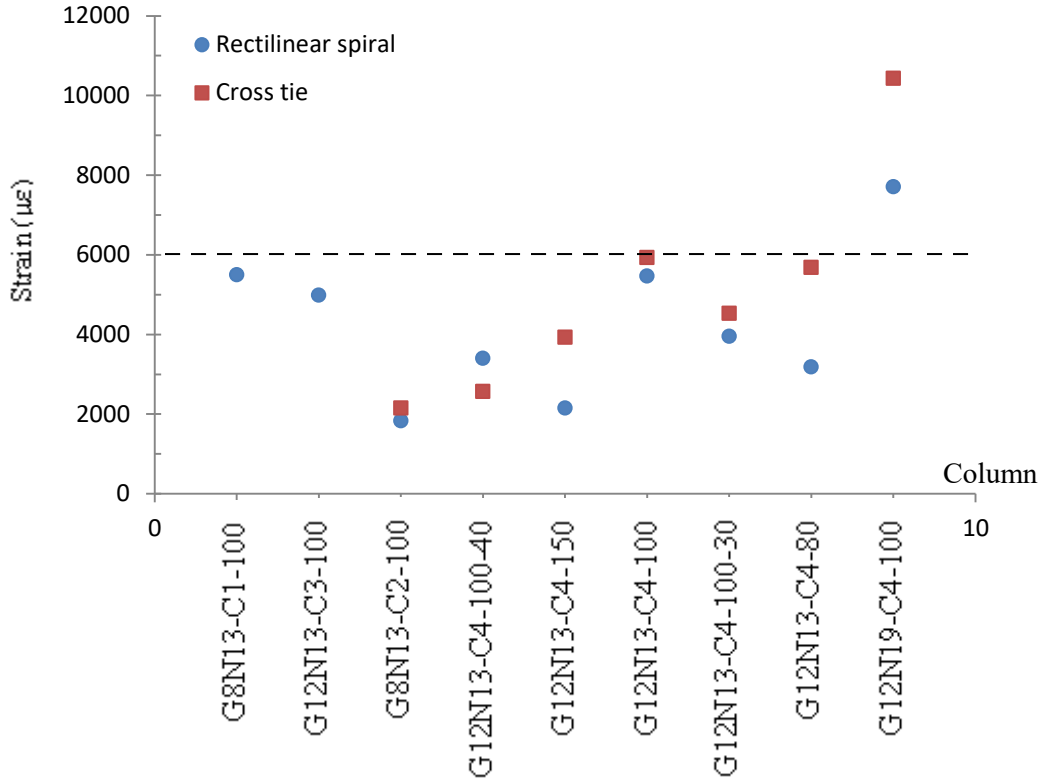

Figure 4.14 – Strain in the rectilinear spirals and cross ties in the tested columns.

4.6 Conclusions

This current study presented a test program aimed at studying the behavior of eleven steel- and GFRP-reinforced columns under simulated earthquake loading. Based on the analysis of the experimental results, the following conclusions were reached:

1. The GFRP reinforcement provided the laterally loaded columns with stable hysteretic behavior, as no strength degradation or slight degradation compared to steel-reinforced columns was observed.
2. The stable behavior enhanced the deformability of the GFRP-reinforced columns as the Δ_u (corresponding to 80% of the post-peak load) was much higher in the GFRP-reinforced columns than in the steel-reinforced ones. This could compensate for the high values of Δ_e comparison to Δ_y.
3. Increasing the axial-load level negatively affected the ductility performance of the GFRP-reinforced columns with negligible strength gain.
4. The detailed and well-confined GFRP-reinforced columns showed acceptable levels of energy dissipation. GFRP-reinforced columns could achieve 75% of the dissipated energy of the steel-reinforced columns.
5. The elastic behavior of the GFRP rectilinear spirals and cross ties enhanced the confinement of the core concrete, delaying crushing. Yielding in the transverse steel reinforcement resulted in early degradation of the core concrete.
6. The achieved drifts for the GFRP-reinforced columns were at least 4% for the columns designed using CSA S806-12 and more than the estimated values, clarifying the conservative limits of Eq. 4-6.
7. The longitudinal bars area should be included in calculating the required transverse reinforcement area, requiring a larger transverse-reinforcement area to comply with the strain limitation of Eq. 4-6
8. It is important to take into account the lateral resistance of P-Δ effect especially in case of higher drift ratios.

Therefore, since the GFRP-reinforced concrete columns attained good strength and deformation capacity as well as reasonable energy dissipation, GFRP reinforcement could be

used in reinforced concrete lateral resisting systems, although further research is needed to implement adequate design guide lines and recommendations for such structural elements.

Chapter 5

Seismic Design of GFRP-Reinforced Concrete Columns Based on Displacement Capacity

Foreword

Authors and Affiliation

- Mohammed Gaber Elshamandy: Ph.D. candidate, Department of Civil Engineering, University of Sherbrooke, Sherbrooke, Quebec, Canada, J1K 2R1, Phone: 819-821-8000,ext.65270;Fax:819-821-7974, E-mail: Mohammed.Mohammed@USherbrooke.ca
- Ahmed Sabry Farghaly: Postdoctoral fellow, Department of Civil Engineering, University of Sherbrooke, Sherbrooke, Quebec, Canada, J1K 2R1, Phone: 819-821-8000, ext. 62967; Fax: 819-821-7974, E-mail: Ahmed.Farghaly@USherbrooke.ca
- Brahim Benmokrane: Professor of Civil Engineering and NSERC Research Chair in FRP Reinforcement for Concrete Infrastructure and Tier-1 Canada Research Chair in Advanced Composite Materials for Civil Structures in Department of Civil Engineering, University of Sherbrooke, Quebec, Canada, J1K 2R1, Phone: 819-821-7758, Fax: 819-821-7974, E-mail: Brahim.Benmokrane@USherbrooke.ca

Journal title: Journal of Composites for Construction

Acceptation state: submitted October 20, 2016.

Reference: Elshamandy, M. G., Farghaly, A. S., and Benmokrane, B., 2016, "Seismic Design of GFRP-Reinforced Concrete Columns Based on Displacement Capacity," *Journal of Composites for Construction*.

5.1 Abstract

The use of fiber-reinforced-polymer (FRP) as reinforcement in concrete structures has been growing rapidly. A potential application of FRP reinforcement is in reinforced concrete frames. However, due to FRP's predominantly elastic behavior, FRP-reinforced members are believed to exhibit low ductility and energy dissipation. Recent experiment results on FRP-reinforced lateral resisting members like shear walls and columns proved the feasibility of using FRP reinforcement without compromising ductility or energy dissipation. Eleven columns were tested to failure under lateral load while subjected to a constant axial load. The experimental studies on glass-FRP (GFRP)-reinforced concrete columns under simulated seismic loads have proven the ability of these structural members to provide large deformations without significant strength loss and acceptable level of energy dissipation compared with steel reinforced concrete columns. This hysteretic performance encouraged to propose a design procedure for such members. The development of design guidelines, however, depends on determining the elastic and inelastic deformation and on assessing the force modification factor and equivalent plastic-hinge length for GFRP-reinforced columns. The experimental results of the GFRP-reinforced columns were used to justify the design guideline proving the accuracy of the proposed design equations.

Keywords: Columns, GFRP bars, idealized curve, force modification factor, virtual plastic hinge length, drift capacity, displacement-based design

5.2 Introduction

Fiber Reinforced Polymers (FRP) composites, in form of reinforcement for concrete structures, have found increasingly wide applications in civil engineering due to many advantages especially their high corrosion resistance and high strength-to-weight ratio, compared with steel reinforcement. These wide applications of FRP composite material especially in harsh environments, are not just as a confining material for concrete in strengthening the existing reinforced concrete members but also as internal reinforcement in new constructions. The different mechanical properties of FRP materials compared to steel, represented by low modulus of elasticity and linear-elastic stress-strain characteristics raise concerns about the applicability of using FRP materials as reinforcement for structures prone to earthquakes. Columns are expected to be the primary elements of energy dissipation in structures subjected to seismic loads. Failure of the columns results in the collapse of these structures. Thus the behavior of columns does plays an essential role for earthquake resistant structures design. Earlier studies of laterally loaded FRP-reinforced columns (Choo et al. 2006, Sharbatdar and Saatcioglu 2009, Tavassoli et al. 2015, Ali and El-Salakawy 2016 and Elshamandy et al. 2015) shows a stable response and high drift ratios with acceptable levels of energy dissipation, confirming the effectiveness of the FRP transverse reinforcement. This played a major role in enhancing the confinement of the concrete core, which delays concrete crushing.

The authors performed an experimental study on nine GFRP-reinforced concrete columns and two steel reinforced concrete columns as control specimens. These columns had been tested under reversed quasi-static cyclic loading. All the columns had an acceptable performance in resisting the simulated seismic loading with adequate deformation (> 4% lateral drift) without significant loss in strength achieving acceptable level of energy dissipation about 75% of the steel reinforced specimens. Tavassoli et al. 2015 concluded that GFRP bars can be successfully used as internal reinforcement in ductile concrete columns. Also Ali and El-Salakawy 2016 concluded that GFRP columns exceeded the limitations of North American building codes with a drift capacity ranged between 8.5 and 12.5 % as well as the GFRP columns deformability replaced successfully the ductility of the steel reinforced concrete columns in dissipating the seismic energy.

Accordingly the primary guidelines for the seismic design of GFRP-reinforced concrete columns need to be investigated. These design guidelines steps involve idealization of load-displacement curve, determination of ductility related force modification factor and plastic hinge length. The proposed design procedure can be used to design the GFRP-reinforced concrete columns when the response is flexure-dominated in regions prone to low to high seismic activities.

5.3 Idealized Load Displacement Curve

Idealizing the nonlinear seismic response behavior of reinforced concrete columns is needed as a simplification for the design approach. The idealized load-displacement response was obtained based on the envelope curve of the hysteretic load-displacement response. Generally to get the idealized bilinear load-displacement curve, two point in the envelope curve need to be identified.

The first point represents the deformation transition from elastic stage to inelastic stage meanwhile the other point represents the end of the inelastic deformation (maximum deformation) and is known as Δ_u. For the steel reinforced concrete columns, the deformation at transition between elastic stage to inelastic stage is known as $\Delta_{y.}$ Δ_y represents the start of longitudinal steel bars yielding. While due to absence of the yielding phenomena in GFRP bars, a hypothetical point called virtual yielding point (Δ_e) representing this transition is adopted. The virtual yielding point is taken as the deformation at the start of permanent deformation for concrete (inelastic deformation). Accordingly, for each column, two deformation points, Δ_e or Δ_y and Δ_u are needed to be identified to produce the bilinear idealized load-displacement curve.

Many previous studies used different idealization methods (Mohamed et al. 2014, Paulay and Priestley 1995, Munoz et al. 2008, Branston et al. 2005, Rogers et al. 2011, Shedid et al. 2009, and Kessler 2009). In this study the equivalent energy elastic plastic method (EEEP) is used. EEEP method was selected because it has been commonly applied to many types of structural members and materials (concrete and steel systems, timber, log, sheet-steel sheathing, and masonry) (Mohamed et al. 2014). Also it is a quite representative for the original load-displacement envelope curve.

To produce the bilinear idealized load-displacement curve for the columns under study using EEEP method, a straight line represents the linear behavior, is taken secant to the envelope curve at first major crack corresponding to 65% of ultimate lateral load for GFRP and steel reinforced concrete columns. The maximum deformation (Δ_u) is taken as the displacement corresponding 20% loss of the ultimate lateral strength (NBCC 2010) for steel columns. However for GFRP columns, the ultimate displacement occurs at the column failure represented in concrete core crushing and longitudinal bars fracture under compression ($\Delta_{capacity}$). For safety issue and avoiding collapse under an earthquake, in this study the allowable maximum displacement (Δ_u) is taken as the displacement corresponding to 4% drift ratio. 4% drift ratio is the allowable drift under seismic loads according to CSA S806-12 for ductile structures. The second straight line (horizontal line) represents the lateral load at the end of the elastic stage and the start of the inelastic deformation, in which areas under the idealized curve and the load-displacement envelop curve are equal as shown in **Figure 5.1**. Well confined concrete core is mandatory so that the concrete can reach the needed strain at the suggested value for the maximum deformation (Δ_u).

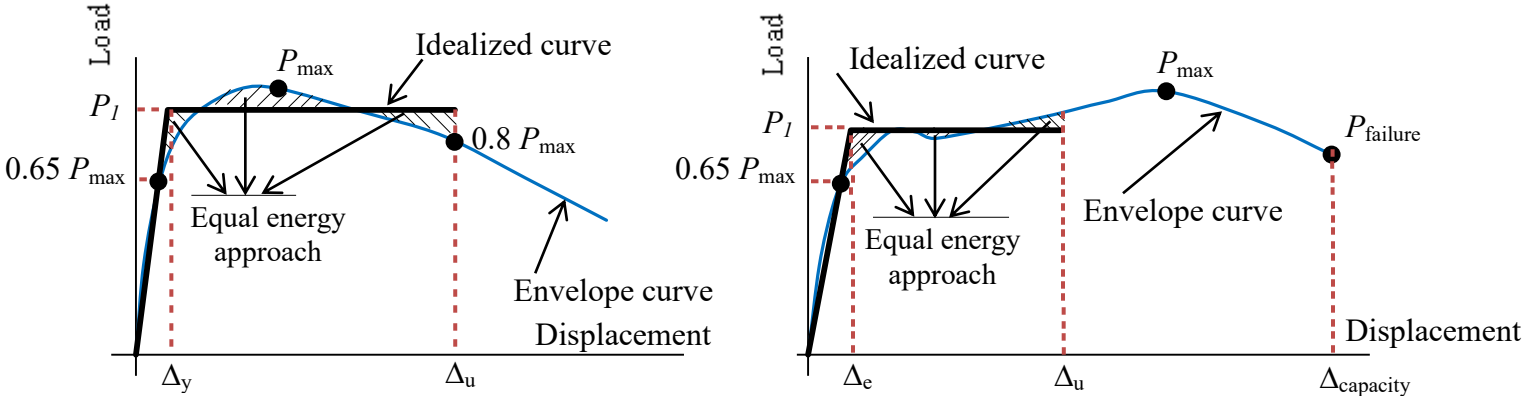

(a) Steel columns (b) GFRP-Columns

Figure 5.1 – Idealized load–displacement curves for tested column specimens

5.4 Force Modification Factor (*R*)

The force modification factor (*R*) is a factor that reflects the ability of a structure to dissipate energy through the inelastic behavior. This factor was used to characterize important aspects for structural members under earthquakes events. It was not just used as deformability factor but it was used also as indicator for energy absorption and the ability to sustain load and stiffness under cyclic loading. NBCC 2010 divides the force modification factor into two factors, the ductility related force modification factor R_d and the over-strength related force modification factor R_o. Generally for reinforced concrete resistant systems, R_d ranges between 5 for very ductile systems and 1.5 for brittle systems. Steel moment resisting frames are considered as ductile systems and can reach R_d equal to 5. Due to shortage of researches for FRP reinforced concrete structural members under seismic loads generally and for GFRP-reinforced concrete columns especially, there is no certain suggested value for R_d. However, to ensure minimum amount of deformability for members reinforced with FRP bars or stirrups, CSA S806-12 set the ductility related force modification factors equal to 2.5 and 4 for shear strength requirements of columns in moderately ductile and ductile moment-resisting frames respectively.

One of the objectives of this study is to propose a suggested value for R_d depending on experimental results of nine tested GFRP-reinforced concrete columns and sixteen other columns tested in previous works (Tavassoli et al. 2015 and Ali and El-salakawy 2016).

5.5 Calculation of R_d

The equal displacement principle is used in the steel reinforced concrete structures in calculation of R_d using the idealized load-displacement curve. The same concept is adopted for GFRP. The designed factored code specified seismic forces should be equal or less than P_1, while P_1 is the maximum elastic load in the idealized load-displacement curve. P_2 is a design seismic force for a structure at maximum deformation for a given seismic map area but corresponds to a fully elastic structural response. P_2 is calculated using equal displacement principle for all of steel and GFRP columns as shown in **Figure 5-2**. Then the ductility related force modification factor is calculated by equation 1 as follows

$$R_d = P_2/P_1 \qquad (5-1)$$

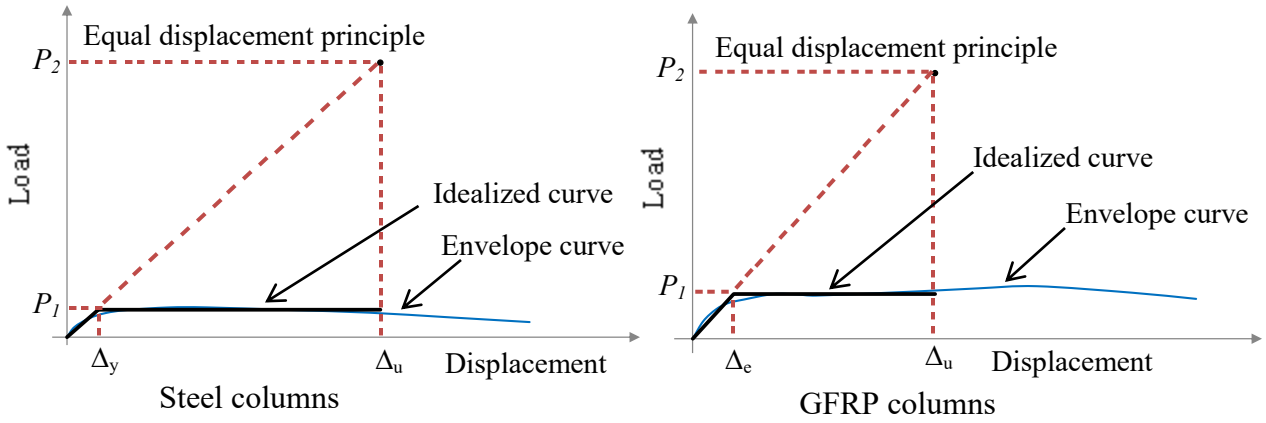

Figure 5-2 – Calculation of ductility-related response modification factor (R_d)

Values of P_1, P_2 and R_d are calculated and listed in **table 5.1** for the eleven columns under study and also for previous studies columns (Tavassoli et al. 2015 and Ali and El-salakawy 2016). The calculated values of R_d show the effects of different parameters. These parameters include the longitudinal and transverse reinforcement ratio, spacing, different types of GFRP bars and stirrups, configuration and axial load level. Generally, it was found that using higher longitudinal or transverse reinforcement ratio or reducing the spacing decreases the value of R_d at the same drift ratio. This may be due to increasing the contribution of the high elastic behavior of FRP bars and stirrups with increasing reinforcement percentage. However, the well confined concrete column core enables the column to undergo higher deformability and drift ratio which is combined with higher values of R_d. Also, higher values for R_d were found with increasing the applied axial load at same drift level meanwhile lower values with increasing the applied axial load at failure drift ratio. Generally with applied axial load equal or higher than 20% of the column axial capacity, values of R_d were higher than 4. This satisfies the specified limits for the design codes CSA S806-12 and NBCC2010 for moderate ductile moment resisting frames and ductile moment resisting frames.

Table 5.1 – Derivation of force modification factors from experimental results

Study	Column	Stirrup diameter	Spacing	A_l/A_g (%)	P/P_o (%)	P_{max}	Δ_e or Δ_y	P_1	Δ_u	P_2	R_d
Current Columns	G8N13-C1-100	9.5	100	0.63	20	166	8.1	146	66	1184	8.1
	G8N13-C2-100	9.5	100	0.63	20	167	9.6	160		1100	6.9
	G12N13-C3-100	9.5	100	0.95	20	167	8.9	154		1069	7
	G12N13-C4-100	9.5	100	0.95	20	186	11.2	158		937	5.9
	G12N13-C4-80	9.5	80	0.95	20	214	13.4	171		842	4.9
	G12N13-C4-150	9.5	150	0.95	20	161	7.1	154		1148	7.5
	G12N19-C4-100	9.5	100	2.14	20	282	25.2	220		453	2.6
	G12N13-C4-100-30	9.5	100	0.95	30	178	16.8	170		665	3.9
	G12N13-C4-100-40	9.5	100	0.95	40	195	11.3	184		1075	5.9
	ST8N10-C1-100	8	100	0.35	20	190	6.4	173	64	1735	10
	ST12N10-C4-100	8	100	0.53	20	170	8.5	142	54	905	6.4
Tavassoli et al. 2015	P28-C-12-50	12	50	2.96	28	72	14.7	69	74	346	5
	P28-C-12-160	12	160	2.96	28	83	14.7	79	46	226	2.9
	P42-B-16-160	15.9	160	2.96	42	71	9.6	68	46	304	4.5
	P42-B-16-275	15.9	275	2.96	42	75	8.4	68	38	248	3.6
	P42-C-12-50	12	50	2.96	42	85	8.7	80	74	676	8.5
	P42-C-12-160	12	160	2.96	42	68	8.5	65	46	337	5.2
	P28-C-16-160	16	160	2.96	28	63	10.2	58	46	236	4.1
	P42-B-12-160	12.7	160	2.96	42	66	6.9	64	36	278	4.4
	P28-B-12-50	12.7	50	2.96	28	87	16.7	82	74	360	4.4
Ali and EL-Salakawy 2016	G-1.3-10-75	9.5	75	1.3	10	175	32.3	144	66	294	2
	G-1.3-10-100	9.5	100	1.3	10	141	26.2	127		319	2.5
	G-1.3-10-150	9.5	150	1.3	10	137	20	127		419	3.3
	G-1.9-10-75	9.5	75	1.9	10	193	37	160		285	1.8
	G-2.9-10-75	9.5	75	2.6	10	202	35	170		321	1.9
	G-1.3-15-75	9.5	75	1.3	15	136	20.5	130		417	3.2
	G-1.3-20-75	9.5	75	1.3	20	161	16.4	144		577	4
	S-1.3-10-75	11.3	75	1.3	10	149	17.4	141	120	971	6.9

By comparing the experimental failure drift ratio and the estimated one using equation 5-2 provided in CSA S806-12, clause 12.7.3.3, it was founded that the equation underestimated drift values compared with the experimental ones for the current columns. The equation neglected the effect of the longitudinal reinforcement ratio. Accordingly proposed equations take into account the influence of the mention parameter represented in equation 5-3 for $0.2 \leq P/Po < 0.3$ and equation 4 for $0.3 \leq P/Po < 0.4$. The proposed two equations had been verified using the experimental test results of the current and past studies.

$$A_{sh} = 14sh_c \frac{f_c^{'}}{f_{fh}} \left(\frac{A_g}{A_c} - 1\right) \frac{P}{P_o} \frac{\delta}{\sqrt{K_c}} \qquad (5-2)$$

$$A_{sh} = 800sh_c \frac{f_c^{'}}{f_{fh}} \left[\frac{A_g}{A_c} - 1\right] \frac{P}{P_o} \frac{A_l}{A_c} \frac{\delta}{\sqrt{K_c}} \qquad (5-3)$$

$$A_{sh} = 600sh_c \frac{f_c^{'}}{f_{fh}} \left[\frac{A_g}{A_c} - 1\right] \frac{P}{P_o} \frac{A_l}{A_c} \frac{\delta}{\sqrt{K_c}} \qquad (5-4)$$

Where P/Po is the applied axial load to axial capacity ≥ 0.2, A_g is the cross sectional area, A_c is the confined concrete core. $\left(\frac{A_g}{A_c} - 1\right) \geq 0.3$. f_{Fh}= 0.006 E_f or $Ø_f f_{Fu}$, whichever is less, K_c = 1.0 for circular spirals and circular hoops, $K_c = 0.15\sqrt{\frac{h_c}{s}\frac{h_c}{s_l}}$ for rectilinear transverse reinforcement, hc is the confined core height, s is the spacing of transverse reinforcement and s_l is the spacing of the tie legs.

Figure 5.3 shows comparison between the experimental drift ratio and the estimated ones using equations 5-2, 5-3 and 5-4. The proposed equations give a more accurate estimation for the drift ratio than the equation which is provided in the design code CSA S806-12. Also, according to CSA S806-12, the design lateral drift ratio shall not be less than 0.04 for columns in ductile moment resisting frames with R_d = 4.0 and 0.025 for columns in moderately ductile moment resisting frames with R_d = 2.5.

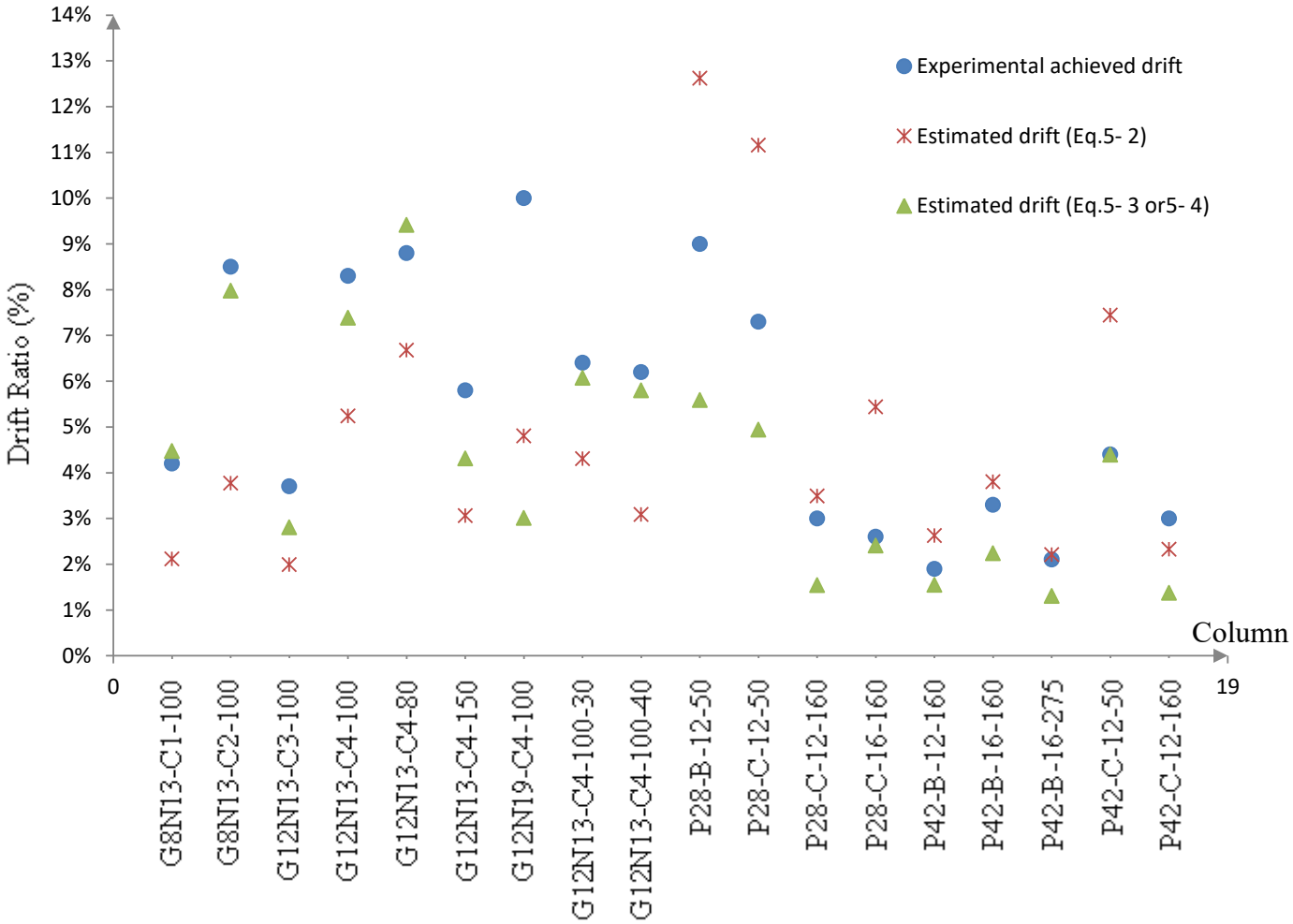

Figure 5.3 – Experimental and estimated drift ratios

5.6 Plastic Hinge Length

Plastic hinge is the region where inelastic deformations and severe damage occurs. It forms at the maximum moments regions of the reinforced concrete column. The deformation capacity of the flexural members is critically affected by the length of the plastic hinge. Well reinforcement details and confinement should be included in this region to survive from severe earthquakes, so identification of this region (length) of plastic hinge is mandatory and considered as the first step to compute the deformation capacity.

Series of LVDTs and strain gauges were used to measure displacements and strains at different levels of the column. The tested GFRP-columns showed very stable seismic behavior and reaching at least 4% drift ratios. The columns behavior was linearly elastic up to 0.65% drift ratio then the flexural cracks initiated. Concrete cover spalling occurred at 2% drift ratio. Then the longitudinal steel started to fail under compression fracture. Finally the concrete column core crushed at 4% drift ratio at least. Also, the behavior of steel reinforced concrete columns was linear elastic up to 0.65% drift ratio, and then the longitudinal steel bars started to yield. Concrete cover splitting occurred at 1.9% drift ratio then the longitudinal steel bars started to buckle at 2.3% drift ratio. Complete longitudinal bars buckling followed by concrete core crushing occurred at 6% drift ratio. The failure of the steel columns is a typical failure in the plastic hinge region as discussed in (Bayrak and Sheikh 2001). Similar progressive failure steps were noted for GFRP and steel columns except yielding of the longitudinal steel bars. High elastic strain values were obtained for GFRP bars. Due to absence of GFRP bars yielding, the concept of plastic hinge is not applied to GFRP-reinforced concrete columns. Meanwhile a virtual plastic hinge concept is used instead to represent the large elastic strains and the permanent deformation of concrete core (Mohamed et al. 2014).

Six LVDTs and strain gauges are used at three different levels of the columns to measure displacement and strains and in turn calculate the curvature at these levels covering the critical region. **Figure 5.4** shows schematic tri-linear shape of the curvature distribution.

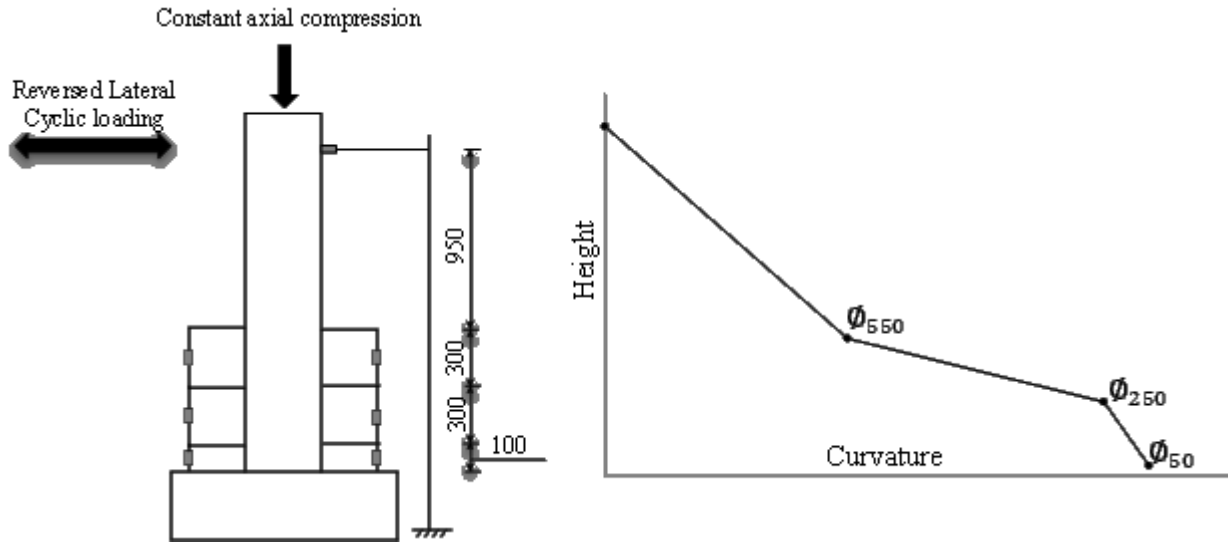

Figure 5.4 – Tri-linear shape of the schematic curvature distribution

Previous studies (Park et al. 1982, Priestley and Park 1987, Paulay and Priestley 1992 and Mohamed et al. 2014) assumed linearly uniform distribution for inelastic curvatures through certain height of the column (plastic hinge length). Following these studies and assumption, the plastic hinge and the virtual plastic hinge lengths can be calculated by integrating the inelastic curvature distribution along the plastic hinge region and redistributing the inelastic curvature to a uniform distribution with a height equal to the plastic hinge length as shown in **Figure 5.5**, and expressed in equation (5-5). The calculated plastic hinge and virtual plastic hinge lengths are listed in **table 5.2**.

$$L_p = \frac{\int \emptyset_i}{\emptyset_i} = \theta_i/(\emptyset_u - \emptyset_e) \qquad (5-5)$$

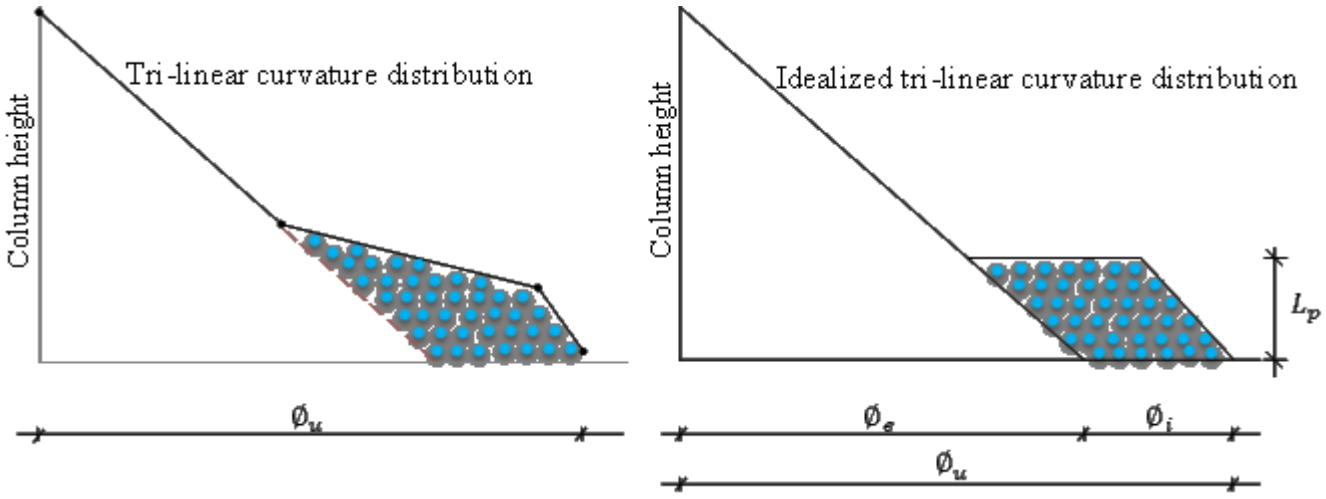

Figure 5.5 – Plastic hinge length

Table 5.2 – Values of Plastic hinge length (all values in mm)

Column	Experimental values	Equ. 5-6	Equ. 5-7	Equ. 5-8	Equ. 5-9	Equ. 5-10	Equ. 5-11	Equ. 5-12 Proposed value
G8N13-C1-100	509	160	208	499	400	212	259	500
G8N13-C2-100	509							
G12N13-C3-100	531							
G12N13-C4-100	645							
G12N13-C4-80	459							
G12N13-C4-150	572							
G12N19-C4-100	347		246	595		211	257	
G12N13-C4-100-30	514		208	499		212	259	
G12N13-C4-100-40	264							
ST8N10-C1-100	219		189	216		214	264	----
ST12N10-C4-100	193							----

Plastic hinge length is really critical for the deformation capacity of flexural members thus many previous researchers studied this length and proposed different values for steel reinforced concrete columns. The plastic hinge length was obtained experimentally (Park et al. 1982). It was suggested that the plastic hinge length could be taken as function of the column overall depth as expressed in Equation 5-6. While Priestley and Park (1987) proposed equation 5-7 which takes into account the shear span of the column and longitudinal bars diameter. In equation 5-7, the first term is accounted mainly for column bending while the second part is accounted bar slip due to the elongation of the longitudinal bars (tensile strain penetration into the joint or the footing). Paulay and Priestley (1992), revised equation 5-7 to include different grades of flexural reinforcement and proposed equation 5-8 then this equation was simplified later to be ≈ 0.5 h. Sheikh and Khoury (1993), and Sheikh et al. (1994) reported that the measured L_p were approximately equal to the overall depth of the tested column as expressed in equation 5-9. Sawyer 1964 proposed equation 5-10 to calculate the plastic hinge length while equation 5-11 was proposed by Mattock (1967).

$$L_p = 0.4\,h \qquad (5-6)$$

$$L_p = 0.08L_c + 6d_b \qquad (5-7)$$

$$L_p = 0.08L_c + 0.022d_b f_y \qquad (5-8)$$

$$L_p = 1.00\,h \qquad (5-9)$$

$$L_P = 0.25d + 0.075L_c \qquad (5-10)$$

$$L_p = 0.5d + 0.05L_{\,c} \qquad (5-11)$$

Where L_c is the shear span; d_b is the longitudinal bar diameter; f_y is steel yielding stress; h is the overall section depth; d is the reinforcement depth.

In this study based on the experimental results of nine GFRP columns, the authors proposed a new empirical equation to estimate a virtual plastic hinge for GFRP-reinforced concrete columns as expressed in equation 5-12.

$$L_p = 1.25\,h \qquad (5-12)$$

All plastic hinge length values using previous equations were calculated and compared with the proposed value in **table 5-2**. It was found that equation 5-8 gives a good acceptable estimation for GFRP-reinforced concrete columns if the yield stress of the longitudinal steel bars is replaced by the ultimate tensile stress of longitudinal GFRP bars. The same equation gives very close values for steel reinforced columns.

5.7 Proposed Provisions for GFRP-Reinforced Concrete Columns

The deformation capacity represented in curvature and drift capacity is very critical demand for all structure members which resist seismic activities especially the columns. To ensure an adequate seismic performance for these columns, the deformation capacity should be designed to satisfy the required deformation demand. This is achieved if the concrete compressive stain capacity is equal or greater than the demanded strain to reach the needed displacement or drift. As the vertical strains are related to curvature capacity, the main expression in deformability design was based on the curvature and can be expressed as follows

$$\emptyset_c \geq \emptyset_d \qquad (5-13)$$

$$\emptyset_c = \varepsilon_{cu}/c \qquad (5-14)$$

Where $\emptyset_c$ is the curvature capacity, $\emptyset_d$ is the curvature demand imposed on the column by the design earthquake, ε_{cu} is the ultimate concrete compressive strain and c is the flexural compression zone length at the critical section as shown in **Figure 5.6**.

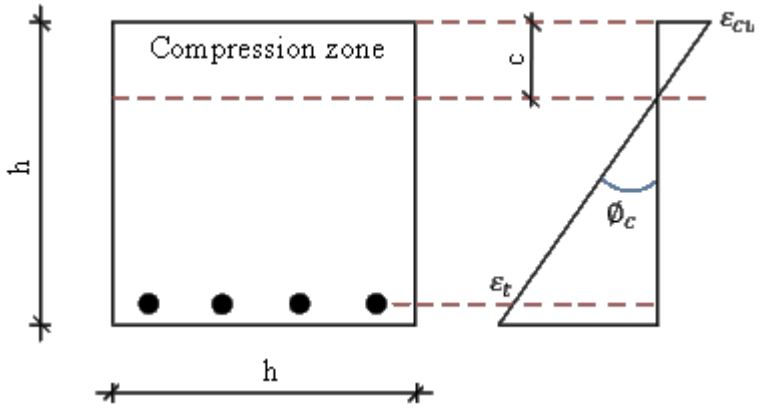

Figure 5.6 – Strain distribution profile

The reinforced concrete columns exposed to earthquakes are required to undergo a large number of inelastic deformations without significant loss in the strength. In steel reinforced concrete columns, the longitudinal steel bars started to yield before the inelastic deformation of concrete occurred (concrete cover splitting). This results in inelastic deformation much higher than the elastic one. Therefore the researchers relay on the inelastic deformation to represent the deformation capacity while the elastic deformation is ignored. In GFRP reinforced concrete columns, the inelastic deformations started with starting of concrete cover deterioration. This means delaying occurrence the inelastic deformation compared with steel columns, and results in high elastic deformation. Applying the same way by ignoring the elastic deformation of GFRP columns is considered conservative by authors for GFRP reinforced concrete columns. At the same time, the main objective of all columns is that the deformation capacity should be equal or higher than the demanded one. Therefore the elastic and inelastic portions are included for the curvature capacity and curvature demand as expressed as follows

$$\emptyset_c = \emptyset_{ec} + \emptyset_{ic} \qquad (5-15)$$

$$\emptyset_d = \emptyset_{ed} + \emptyset_{id} \qquad (5-16)$$

The designers prefer to assess and deal with the total rotation demand and capacity instead of curvatures so equation 5-13, 5-15 and 5-16 are expressed as follows

$$\theta_c \geq \theta_d \qquad (5-17)$$

$$\theta_c = \theta_{ec} + \theta_{ic} \qquad (5-18)$$

$$\theta_d = \theta_{ed} + \theta_{id} \qquad (5-19)$$

The inelastic rotation demand (θ_{id}) can be calculated from the inelastic displacement at the column tip as shown in **Figure 5.7** and expressed in equation 5-20. Assuming linear distribution of elastic curvature, the elastic demand can be calculated as expressed in equation 21.

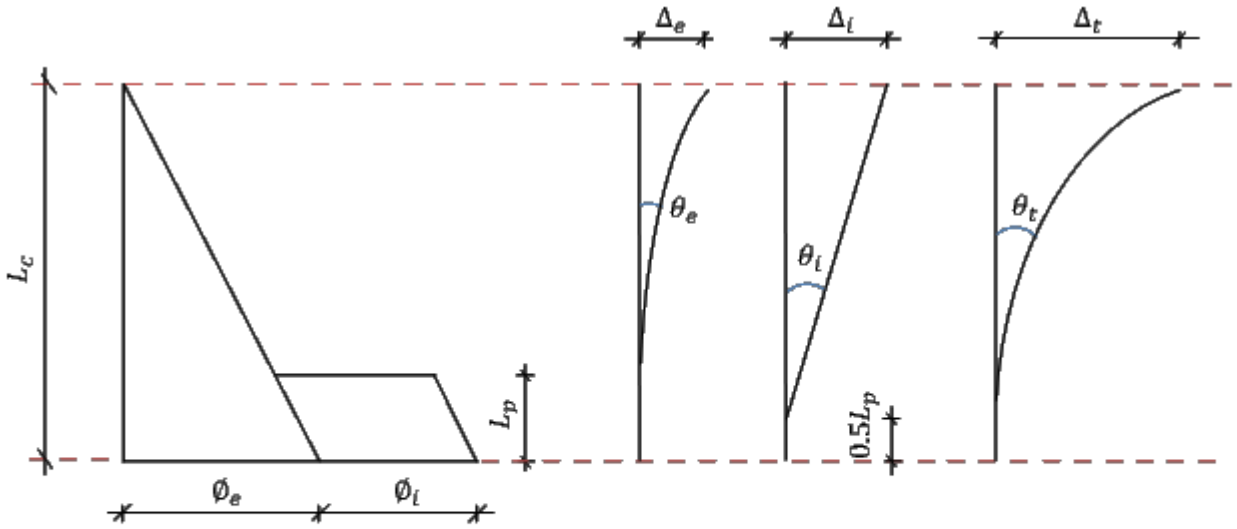

Figure 5.7 – Elastic and plastic displacements and Rotations

$$\theta_{id} = \Delta_{id}/(L_c - 0.5L_p) \qquad (5-20)$$

$$\theta_{ed} = \Delta_{ed}/L_C \qquad (5-21)$$

From equations 5-19, 5-20 and 5-21, the rotation demand can be written in the following form

$$\theta_d = \Delta_{ed}/L_c + \Delta_{id}/(L_c - 0.5L_p) \qquad (5-22)$$

According to CSA A23.3-14, the elastic displacement demand can be estimated as the total displacement divided by the force modification factor, $\Delta_{ed} = \Delta_t/R$, equation 5-22 can be rewritten as follows

$$\theta_d = \Delta_t/RL_c + [\Delta_t(1 - 1/R)/(L_c - 0.5L_p)] \qquad (5-23)$$

After simplifying equation 5-23, the final form can be expressed as follows

$$\theta_d = (\Delta_{ed}/L_c)[(RL_c - 0.5L_p)/(L_c - 0.5L_p)] \qquad (5-24)$$

Similarly, the elastic rotation capacity, the inelastic rotation capacity and the total capacity for columns can be calculated according to Park and Paulay 1975 as follows

$$\theta_{ec} = \emptyset_{ec}(L_c/3) \qquad (5-25)$$

$$\theta_{ic} = L_p(\emptyset_c - \emptyset_{ec}) \qquad (5-26)$$

$$\theta_c = \emptyset_{ec}\left[(L_c/3) - L_p\right] + \emptyset_c L_p \qquad (5-27)$$

5.8 Simplified Proposed Expressions for Designing GFRP-Reinforced Concrete Columns

Careful steps were followed to simplify the proposed design equations for the GFRP-reinforced concrete columns. The proposed design equations simply represent the rotational capacity and demand. To calculate the rotation capacity from equation 5-27, designers need to know the value of the elastic curvature capacity, plastic hinge length and ultimate curvature capacity.

The elastic curvature capacity was calculated experimentally corresponding to the virtual yield point and the values were plotted in **Figure 5.8**. These values for all of the GFRP-reinforced concrete columns are covering different confinement ratio. The elastic curvature is mainly depends on the strain at the end of the elastic stage. This strain at which the concrete started the permanent deformation is depending on the confinement level.

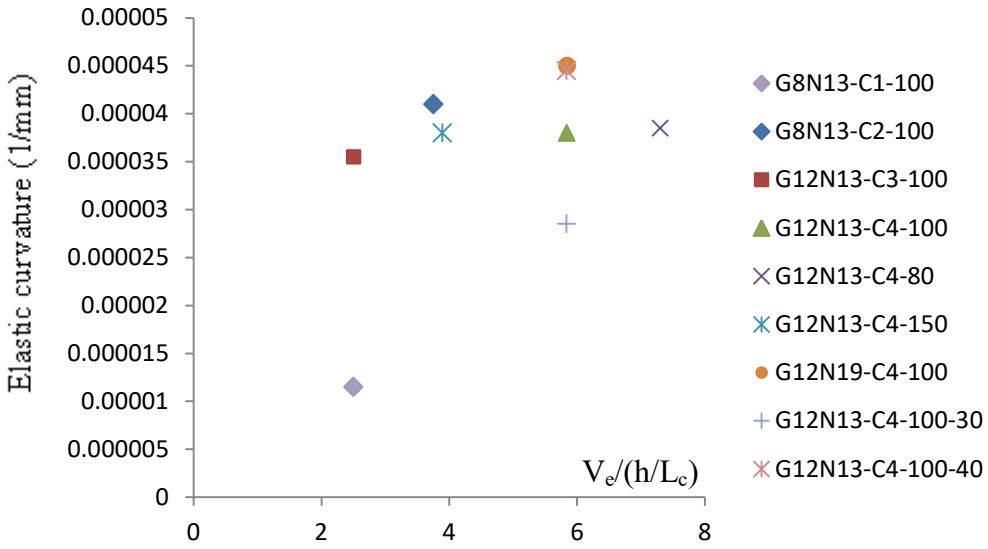

Figure 5.8 – Elastic curvature

Figure 5.8 shows that the elastic curvature values for all the columns ranged between 0.00003 and 0.000045 1/mm as lower and upper limit. The column G8N13-C1-100 is ignored from this estimation as the confinement in this column is not satisfying the recommendation of CSA

S806-12. The values are too close and could be presented as a function of the volumetric transverse reinforcement as 0.000014 $V_e/(h/L_c)$, where V_e is the volumetric reinforcement ratio (%), h is the column depth, L_c is the column shear span. The designers have the ability to choose the lower limit as conservative value for safety issue meanwhile, it was found that the majority of the columns have an elastic curvature equal or over than 0.000014 $V_e/(h/L_c)$ hence the elastic curvature capacity is more represented by equation 5-28.

$$\emptyset_{ec} = 0.000014V_e/\left(\frac{h}{L_c}\right) \qquad (5-28)$$

The plastic hinge length is proposed as mention in previous sections, and can be calculated from equation 5-12. The ultimate curvature capacity can be calculated from equation 5-14 by knowing values of the compression strain of concrete (ε_c) and the compression zone length (c) as shown in **Figure 5.6**. From the experimental results, the confined concrete strain ranged from 4500 to 5300 με for the columns at 2.5%, the minimum drift ratio for moderate ductile moment resisting frames with Rd = 2.5 according to CSA-S806-12. Meanwhile the confined concrete strain ranged from 7000 to 9600 με depending mainly on the axial load level at drift ratio 4%, the minimum drift ratio for ductile moment resisting frames with Rd = 4 according to CSA-S806-12. At failure, the confined concrete strain reached from 9000 to 12000 με for the columns (drift ratio > 4%) . Meanwhile in this study the ultimate curvature capacity was calculated at different strain including 4500, 7000 and 9000, the proposed strain for moderate ductile resisting frames, ductile moment resisting frames and ductile moment resisting frames with axial load level higher than 30% of the axial capacity respectively. The well confined section is necessary to enable the concrete to reach these suggested strain values levels. Finally the compression zone length (c) can be calculated by well-known plane sectional analysis. From equation 5-12, 5-14 and 5-28, the rotational capacity for the GFRP reinforced concrete columns can be calculated from equation 29.

$$\theta_c = [0.000014V_eL_c/h][(L_c/3) - 1.25h] + [1.25h\varepsilon_{cu}/c] \qquad (5-29)$$

Similary from equations 5-12 and 5-24, the rotational demand can be calculated from equation 5-30 as follows

$$\theta_d = (\Delta_{ed}/L_c)\,[(RL_c - 0.625h)/(L_c - 0.625h)] \qquad (5-30)$$

Where the elastic displacement (Δ_{ed}) can be calculated from the nominal strength of the concrete column as follows

$$\Delta_{ed} = P[(L_c^3/3E_cI_e) + (L_c/G_cA_{sh})] \quad (5-31)$$

Where P is the design lateral load, the first part represents the flexural stiffness for the column while the second part represents the shear stiffness. The effective stiffness (E_cI_e) is varying during the loading from uncracked section to fully cracked section; it decreases with increasing the inelastic deformation. The effective stiffness is always taken as percentage of the initial stiffness (E_cI_g). From the experimental results, the effective stiffness is calculated every drift and normalized to the initial stiffness as shown in **Figure 5.9**.

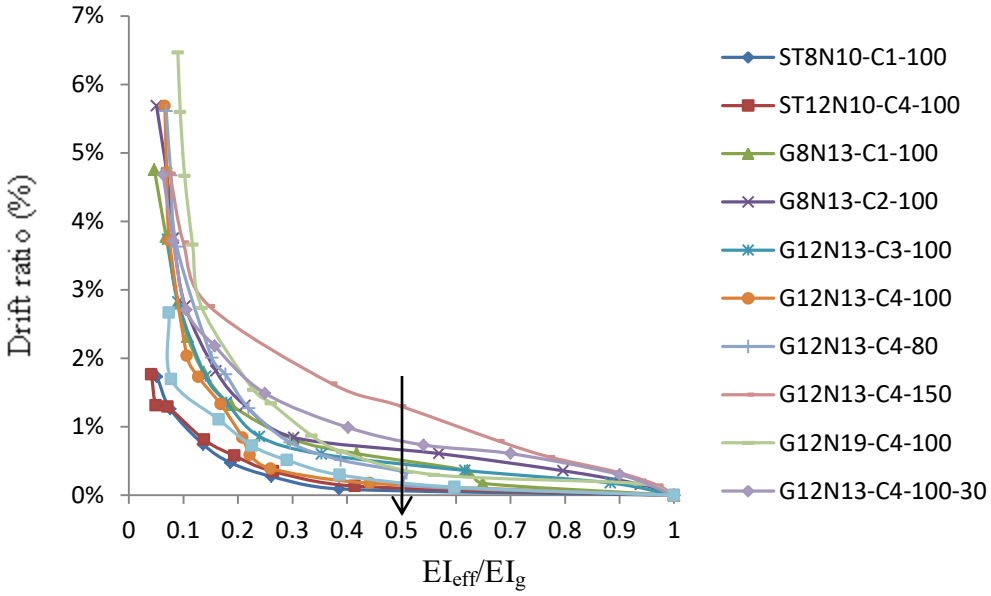

Figure 5.9 – The normalized effective stiffness

A variation in normalized effective stiffness started at 0.5 of the initial flexural stiffness (0.5 E_cI_g), hence 0.5 E_cI_g is suggested for the effective stiffness. While G_c is the shear modulus and it is taken as 40% of the elastic modulus E_c according to FEMA 356, 2000, while Ec is calculated as $4700\sqrt{f_c}$ (Mpa). A_{sh} is the effective shear area of the section and taken as $\frac{5}{6}$ A_g. The rotation capacity values are calculated using the proposed confined concrete strain 4500,

7000, 9000 for moderate ductile moment resisting frames (MDMRF) and the ductile moment resisting frames (DMRF) with axial load level less than 30% of the axial capacity and ductile moment resisting frames for axial load level higher than 30% respectively. Also the calculated rotation capacity including the maximum recorded strain during the experiment and verified by the corresponding experimental drift ratio. Verification of the proposed equations was done using the available previous studies (Ali and El-Salakawy 2016 and Tavassoli et al. 2015). The rotation demand at the proposed strain are calculated and listed with rotation capacity in **table 5.3**.

Table 5.3 – Rotational capacity and demand

Column	Rotation Capacity (%)		θd (%)	Rotation Capacity (%) at ε = maximum recorded strain	Corresponding Experimental drift ratio (%)	Maximum drift(%)	Notes
	at ε = 4500*	at ε = 7000**					
G8N13-C1-100	2.14	3.08	1.90	4.16	4.2	4.2	Proposed for DMRF ***
G8N13-C2-100	2.23	3.17	1.90	5.94	6.7	8.5	Proposed for DMRF
G12N13-C3-100	2.05	2.94	2.35	4.09	3.8	3.8	Proposed for DMRF
G12N13-C4-100	2.28	3.17	2.35	4.97	6.5	8.4	Proposed for DMRF
G12N13-C4-80	2.38	3.27	2.37	5.21	6	9	Proposed for DMRF
G12N13-C4-150	2.14	3.03	2.37	4.43	4.7	5.8	Proposed for DMRF
G12N19-C4-100	2.12	2.94	2.83	4.44	5.2	10	Proposed for DMRF
G12N13-C4-100-30	1.88	3.28	2.66	3.46	4.8	4.8	Proposed for DMRF
G12N13-C4-100-40	1.59	2.82	2.80	3.38	3.8	4.7	Proposed for DMRF
G-1.3-10-75	3.40	4.40	2	4.07	6.5	12.5	Proposed for MDMRF ****
G-1.9-10-75	3.53	4.45	1.7	4.61	6.5	8.5	Proposed for MDMRF
G-2.6-10-75	3.38	4.26	2.1	4.79	6.5	8.5	Proposed for MDMRF
G-1.3-10-100	3.16	4.16	2	3.81	6.5	8.5	Proposed for MDMRF
G-1.3-10-150	2.91	3.91	2	3.57	6.5	8.5	Proposed for MDMRF
G-1.3-15-75	3.11	4.07	2.2	4.31	6.5	8.5	Proposed for MDMRF
G-1.3-20-75	2.85	3.78	3.8	4.59	6.5	8.5	Proposed for DMRF
P28-C-12-50	3.89	4.62	3.00	-*****	-	7.3	Proposed for DMRF
P28-C-12-160	2.11	2.84	1.84	-	-	3	Proposed for MDMRF
P28-C-16-160	2.71	3.42	1.85	-	-	2.6	Proposed for MDMRF
P28-B-12-50	4.19	4.91	3.31	-	-	9	Proposed for DMRF
P42-C-12-50	3.65	4.84	4.38	-	-	4.4	Proposed for DMRF
P42-C-12-160	1.88	3.07	2.68	-	-	3	Proposed for MDMRF
P42-B-12-160	-	-	-	-	-	1.9	******
P42-B-16-160	2.47	3.65	2.89	-	-	3.3	Proposed for MDMRF
P42-B-16-275	-	-	-	-	-	2.1	******

* 4500 με is the proposed confined concrete strain at 2.5% drift ratio.
** 7000 με is the proposed confined concrete strain at 4% drift ratio for axial load level less than 30%, meanwhile 9000 με for 30%<axial load level < 40%. A well designed and detailed section following the CSA S806-12 recommendations and the solved example is mandatory for reaching the proposed strains.
*** DMRF= Ductile moment resisting frame with Rd = 4.
**** MDMRF= Moderate ductile moment resisting frame with Rd = 2.5.
***** Maximum experimental confined concrete strain is not provided.
****** The estimated drift using the proposed equation 5-4 is less than 2.5%, hence the columns can not be used as part of moderate ductile resisting frames according to CSA S806-12.

By comparing the values of rotation capacity and the demanded rotation, satisfying values were found as the rotation capacity is higher than the rotation demand. This confirms capability of using GFRP reinforced concrete columns in structures exposed to earthquakes in region from low to high seismic intensity. Satisfying prediction using the proposed equation for rotation capacity as the values at maximum recorded strain and the corresponding experimental drift ratio are close. The rotation capacity and demand for the columns P42-B-12-160 and P42-B-16-275 were not calculated as the estimated drift ratios using the proposed equation 5-4 are less than 2.5%. A solved example is provided in Appendix A to illustrate the steps in applying the proposed equations.

5.9 Conclusions

The aim of this chapter is to provide design guidelines for GFRP-reinforced concrete columns in regions exposed to low to high earthquakes based on testing of nine GFRP columns to failure under quasi-static cyclic loading. Empirical equations for important parameters needed for the design are proposed. The mains findings during the procedure can be summarized as follows:

1. Due to absence of yielding phenomena in GFRP bars, a virtual yielding point concept was adopted to represent the transition from elastic to inelastic region and was determined as the deformation corresponding to the initiation of concrete inelasticity.

2. The bilinear elastic-plastic curve for load-displacement curve using equal energy principles was found to be quiet representative for the seismic behavior of the GFRP-reinforced concrete columns.

3. The total deformation capacity, including the elastic and inelastic deformation, should be used to compare the total deformation demand and not as in the case of steel reinforcement in which inelastic deformation dominates.

4. The related force modification factor value for most of the columns subjected to 20% axial load or more was greater than 4, satisfying the specified limits in CSA S806-12 and NBCC2010 for moderately ductile moment-resisting frames with R_d equal 2.5 and for ductile moment-resisting frames with R_d equal 4.

5. Two empirical equations Eq. 5-3 and Eq. 5-4 are proposed for calculating the drift ratio for GFRP-reinforced concrete columns subjected to seismic loading with an axial-load equal to or greater than 20% of the axial capacity.

6. The proposed equation, L_p=1.25 h, for calculating the plastic-hinge length is in good agreement with the equation in Paulay et al. (1992) when replacing the yield stress of the longitudinal steel bars with the ultimate tensile stress of longitudinal GFRP bars.

7. The elastic curvature capacity depends mainly on the confinement level. An equation taking into account the volumetric reinforcement ratio and column cross-sectional dimensions to calculate this value is presented.

8. The well confined concrete column core is mandatory to enable the concrete to reach the suggested strain values which is obtained in this study by following CSA S806-12.

9. The simplified proposed equations for calculating the rotation capacity were verified against the available experimental results of laterally loaded columns and found to be higher than the rotation demand.

CHAPTER 6

SUMMARY, CONCLUSIONS AND RECOMMENDATION FOR FUTURE WORK

6.1 Summary

Due to desirable mechanical and physical characteristics including high strength to weight ratio, non-conductivity, electro-magnetic transparency, favorable fatigue strength and low relaxation, FRP materials are widely used as alternative for steel reinforcement in corrosive and harsh environments. However the linear elastic stress-strain curve for FRP bars raises concerns about feasibility of using these materials in structures prone to seismic activities. The current study presented a test program aimed at studying the seismic behavior and performance of nine GFRP reinforced concrete columns under quasi-static reversed cyclic loading simulating the seismic loading. Two steel columns having similar axial stiffness were used as control specimens. The tested parameters including the longitudinal reinforcement ratio, transverse reinforcement spacing, ties configurations and axial load level.

6.2 Conclusions

Based on the analysis of the experimental results, it was found that GFRP reinforced concrete columns can be used as part of the moment resisting frames in structures prone to low to high seismic activities. The study provided design guidelines for GFRP reinforced concrete columns. Empirical equations for parameters needed for the design are proposed. Based on the current study and analysis, the following conclusions were reached:

- The GFRP reinforcement provided the laterally loaded columns with stable hysteretic behavior, as no strength degradation or slight degradation compared to steel-reinforced concrete columns was observed.

- The stable behavior enhanced the deformability of the GFRP-reinforced columns as the Δ_u (corresponding to 80% of the post-peak load) was much higher in the GFRP-

reinforced columns than in the steel-reinforced ones. This could compensate for the high values of Δ_e compared to Δ_y.

- Increasing the axial-load level negatively affected the ductility performance of the GFRP-reinforced columns with negligible strength gain.

- The detailed and well-confined GFRP-reinforced columns showed acceptable levels of energy dissipation. GFRP-reinforced columns could achieve 75% of the dissipated energy of the steel-reinforced columns.

- The elastic behavior of the GFRP rectilinear spirals and cross ties enhanced the confinement of the concrete core, delaying crushing. Yielding in the transverse steel reinforcement resulted in early degradation of the concrete core.

- The achieved drifts for the GFRP-reinforced columns were at least 4% and greater than the estimated values using CSA S806-12, clarifying the conservative limits of Eq. 4-6.

- The longitudinal bars area should be included in calculating the required transverse reinforcement area, requiring a larger transverse-reinforcement area to comply with the strain limitation of Eq. 4-6

- It is important to take into account the lateral resistance of P-Δ effect of the axial load especially in case of higher drift ratios.

- Due to absence of yielding phenomena in GFRP bars, a virtual yielding point concept was adopted to represent the transition from elastic to inelastic region and was determined as the deformation corresponding to the initiation of concrete inelasticity.

- The bilinear elastic-plastic curve for load-displacement curve using equal energy principles was found to be quite representative for the seismic behavior of the GFRP-reinforced concrete columns.

- The total deformation capacity, including the elastic and inelastic deformation, should be used to compare the total deformation demand and not as in the case of steel reinforcement in which inelastic deformation dominates.

- The related force modification factor value for most of the columns subjected to 20% axial load or more was greater than 4, satisfying the specified limits in CSA S806-12 and NBCC2010 for moderately ductile moment-resisting frames with R_d equal 2.5 and for ductile moment-resisting frames with R_d equal 4.

- Two empirical equations Eq. 5-3 and Eq. 5-4 are proposed for calculating the drift ratio for GFRP-reinforced concrete columns subjected to seismic loading with an axial-load equal to or greater than 20% of the axial capacity.

- The proposed equation, L_p=1.25 h, for calculating the plastic-hinge length is in good agreement with the equation in Paulay et al. (1992) when replacing the yield stress of the longitudinal steel bars with the ultimate tensile stress of the longitudinal GFRP bars.

- The elastic curvature capacity depends mainly on the confinement level. An equation taking into account the volumetric reinforcement ratio and column cross-sectional dimensions to calculate this value is presented.

- The well confined concrete column core is mandatory to enable the concrete to reach the suggested strain values which is obtained in this study by following CSA S806-12.

- The simplified proposed equations for calculating the rotation capacity were verified against the available experimental results of laterally loaded columns and found to be higher than the rotation demand.

6.3 Recommendations For Future Work

Based on the findings and conclusions of the current study which state the applicability of using GFRP materials as reinforcement in structures prone to seismic activities and provide simplified design guidelines, the following recommendations are made:

- Additional experimental work on different concrete dimensions is required to study the effect of different aspect ratios and shear span length.

- It is recommended to investigate the behavior of GFRP reinforced concrete columns using ultra high performance fiber reinforced concrete (UHPFRC).
- It is recommended to investigate the behavior of GFRP reinforced concrete columns using splices for the longitudinal bars.
- There is a need to develop a confinement model for FRP reinforced concrete columns.
- Experimental study on complete full scale FRP reinforced concrete frame under simulated seismic loading will provide a great assessment for the seismic performance.

SOMMAIRES, CONCLUSIONS ET RECOMMENDATION POUR LA RECHERCHE FUTURE

6.4 Sommaire

Grâce aux propriétés mécaniques et physiques souhaitées des matériaux en PRF, incluant un rapport résistance/poids élevé, conductivité nulle, une conductance électromagnétique nulle, une bonne résistance à la fatigue et une faible relaxation, les PRF sont largement utilisés comme alternative pour le renforcement en acier dans des environnements corrosifs et difficiles. Cependant, la courbe contrainte-déformation élastique et linéaire pour les barres de PRF suscite des inquiétudes quant à la faisabilité de l'utilisation de ces matériaux dans des structures sujettes aux activités sismiques. Cette étude présente un programme d'essai visant à étudier le comportement sismique et la performance de neuf colonnes en béton armé de PRFV sous un chargement cyclique inversé quasi-statique simulant une charge sismique. Deux colonnes en acier ayant une rigidité axiale similaire ont été utilisées comme spécimens de référence. Les paramètres testés sont : le taux d'armature longitudinal, le taux d'armature transversal, la configuration de la section ainsi que le niveau de charge axiale.

6.5 Conclusions

Sur la base de l'analyse des résultats expérimentaux, il a été constaté que les colonnes en béton armé de PRFV pouvaient être utilisées pour résister aux moments dans des structures sujettes à des activités sismiques faibles à élevées. L'étude a fourni des directives de conception pour les colonnes en béton armé en PRFV. Des équations empiriques pour les paramètres importants nécessaires à la conception sont proposées. Sur la base de l'étude et de l'analyse actuel, les conclusions suivantes ont été tirées :

- Le renforcement en PRFV a fourni aux colonnes chargées latéralement une stabilité à travers la réponse hystérétique, car aucune dégradation (ou mineure) a été observé par rapport aux colonnes renforcées d'acier.
- L'amélioration de la stabilité en déformabilité des colonnes renforcées de PRFV due à Δu (correspondant à 80% de la charge post-pic) était beaucoup plus élevée dans les

colonnes renforcées de PRFV que dans celles renforcées d'acier. Ceci pourrait compenser les valeurs élevées de Δe comparées à Δy.

- L'augmentation du niveau de charge axiale affecte négativement la performance en ductilité des colonnes renforcées de GFRP avec un gain de résistance négligeable.
- Les colonnes renforcées de PRFV bien conçues et confinées ont montré des niveaux acceptables de dissipation d'énergie. Les colonnes renforcées de PRFV pourraient atteindre jusqu'à 75% de l'énergie dissipée par rapport à l'armature en acier.
- Le comportement élastique des étriers en PRFV a favorisé le confinement du noyau de béton, retardant l'éclatement du béton. La plastification du renfort en acier transversal a entraîné une dégradation précoce du noyau de béton.
- Les déplacements latéraux obtenus pour les colonnes renforcées de PRFV étaient au moins 4% supérieures aux valeurs estimées en utilisant la norme CSA S806-12, clarifiant les limites conservatrices de l'équation 4-6.
- La configuration des barres longitudinales devrait être incluse dans le calcul de l'aire du renforcement transversale requise, nécessitant une zone de renforcement transversale plus grande pour se conformer à la limitation de la contrainte de l'équation 4-6.
- En raison de l'absence du phénomène de plastification dans les barres de PRFV, un concept de point de plastification virtuel a été adopté pour représenter la transition de la région élastique à la région inélastique et à déterminer la déformation correspondant à l'initiation du comportement non-linéaire du béton.
- La courbe élasto-plastique bilinéaire pour la relation charge-déplacement utilisant des principes d'énergie égale a été jugée très représentative pour le comportement sismique des colonnes en béton renforcé de PRFV.
- La capacité de déformation totale, y compris la déformation élastique et inélastique, doit être utilisée pour comparer la demande en déformation. Ce n'est pas la même comparaison avec l'armature en acier dans laquelle la déformation inélastique domine.
- La valeur du facteur de modification de la force sismique correspondante pour la plupart des colonnes soumises à une charge axiale de 20% ou plus était supérieure à 4, satisfaisant aux limites spécifiées dans CSA S806-12 et NBCC2010 pour des cadres

rigides à ductilité modérée pour un Rd égale à 2,5 et pour des cadres rigides ductiles avec un Rd égale à 4.

- Deux équations empiriques, Eq. 5-3 et Eq. 5-4, sont proposés pour calculer le rapport de déplacement latéral pour les colonnes en béton armé de PRFV soumises à une charge sismique et une charge axiale égale ou supérieure à 20% de la capacité axiale.
- L'équation proposée, Lp = 1,25 h, pour le calcul de la longueur de rotule plastique est en accord avec l'équation de Paulay et al. (1992) en utilisant la limite d'élasticité des barres d'acier longitudinales par la contrainte de traction ultime des barres longitudinales de PRFV.
- La capacité en courbure élastique dépend principalement du niveau de confinement. Une équation tenant compte du taux d'armature volumétrique et des dimensions de la section transversale de la colonne pour calculer cette valeur est présentée.
- Le noyau de béton doit être bien confiné pour atteindre des valeurs de contrainte suggérées.
- Les équations proposées simplistes pour le calcul de la capacité en rotation inélastique ont été vérifiées par rapport aux résultats expérimentaux disponibles et sont plus élevées que la demande de rotation pour les colonnes chargées latéralement.

6.6 Recommendations pour la recherche future

Sur la base des observations et des conclusions de la présente étude indiquant l'applicabilité de l'utilisation de matériaux de PRFV comme renforcement dans des structures sujettes à des activités sismiques, les recommandations suivantes sont formulées:

- Des travaux expérimentaux supplémentaires sur différentes dimensions de béton sont nécessaires pour éliminer l'effet des différents aspects étudiés ainsi la longueur de cisaillement.
- Il est recommandé d'étudier le comportement des colonnes de béton armé en PRFV en utilisant du béton à ultra hautes performances fibrés (BUHPF).
- Il est recommandé d'étudier le comportement des colonnes en béton armé de PRFV en utilisant des chevauchement pour les barres longitudinales pour simuler la réalité.

- Il est nécessaire de développer un modèle de confinement pour les colonnes en béton armé en PRFV.
- Faire une étude expérimentale sur un cadre rigide en béton armé de FRP à grande échelle, sous charge sismique simulée, fournissant une excellente évaluation de la performance sismique.

REFERENCES

ACI Committee 318 (2011). “Building Code Requirements for Structural Concrete and Commentary (ACI 318-11).” *ACI*, Farmington Hills, MI 48331

ACI Committee 318 (2005). “Building Code Requirements for Structural Concrete and Commentary (ACI 318-05).” *ACI*, Farmington Hills, MI, 430 pp.

ACI Committee 318 (1995). “Building Code Requirements for Structural Concrete and Commentary (ACI 318-95).” *ACI*, Farmington Hills, MI, 369 pp.

ACI Committee 440, 2004, ―Guide Test Methods for Fiber-Reinforced Polymers (FRPs) for Reinforcing or Strengthening Concrete Structures (ACI 440.3R-04).‖ *ACI*, Farmington Hills, MI, 40 pp.

ACI Committee 440 (2015). “Guide for the design and construction of concrete reinforced with FRP Bars (ACI 440.1R-15).” *ACI*, Farmington Hills, MI, 44 pp.

ACI Committee 440 (2007). “Report on Fiber-Reinforced Polymer (FRP) Reinforcement Concrete Structures (ACI 440R-07).” *ACI*, Farmington Hills, MI, 100 pp.

Afifi, M., Mohamed, H., and Benmokrane, B. (2014) “Axial Capacity of Circular Concrete Columns Reinforced with GFRP Bars and Spirals,” *Journal of Composites for Construction*, 18 (1), 04013017

Aldulaijan S. U., Nanni A., Alzahrani M. M., and Bakis C. E. (1996). “Bond Evaluation of Environmentally Conditioned GFRP/Concrete System.” *Advanced Composite Materials in Bridges and Structures (ACMBS-2), Canadian Society for Civil Engineering*, Montreal, Quebec, 845-852.

Ali, M. and El-Salakawy, E. (2016). "Seismic Performance of GFRP-Reinforced Concrete Rectangular Columns." *Journal of Composites for Construction*, 20 (3), 04015074.

Alsayed, S. H.; Al-Salloum, Y. A.; Almusallam, T. H.; and Amjad, M. A. (1999). "Concrete Columns Reinforced by GFRP Rods," *Fourth International Symposium on Fiber-Reinforced Polymer Reinforcement for Reinforced Concrete Structures, SP-188*, American Concrete Institute, Farmington Hills, Mich., pp. 103-112

ASTM, 2011, ―Standard Test Methods for Tensile Properties of Fiber-Reinforced Polymer Matrix Composite Bars,‖ *ASTM D7205-11*, American Society for Testing and Materials, Conshohocken, USA, 13 p.

Bae S. and Bayrak O. (2008). "Plastic Hinge Length of Reinforced Concrete Columns." *ACI Structural Journal*, 105 (3), 290-300.

Bakis, C. E., Bank, L. C., Brown, V. L., Cosenza, E., Davalos, J. F., Lesko, J. J., Machida, A., Rizkalla, S. H., and T. C. Triantafillou, T. C. (2002). "Fiber-Reinforced Polymer Composites for Construction—State-of-the-Art Review," *Journal of Composites for Construction*., 6 (2), pp. 73-87.

Bakis C. E., Freimanis A. J., Gremel D., and Nanni A. (1998). "Effect of Resin Material on Bond and Tensile Properties of Unconditioned and Conditioned FRP Reinforcement Rods." *Proceedings of the First International Conference on Durability of Composites for Construction*, Sherbrooke, Quebec, 525-535.

Bank L. C. (1993). "Properties of FRP Reinforcement for Concrete." *Elsevier*, Amsterdam, 42, 59-86.

Bank L. C., Puterman M., and Katz A. (1998). "The Effect of Material Degradation on Bond Properties of FRP Reinforcing Bars in Concrete." *ACI Materials Journal*, 95 (3), 232-243.

Bayrak O. and Shamim A. S. (1998). "Confinement Reinforcement Design Considerations for Ductile HSC Columns." *Journal of Structural Engineering*, *ASCE*, 124 (9), 999-1010.

Bayrak, O., and Sheikh, S.A. (2001) "Plastic Hinge Analysis", *Journal of Structural Engineering*, *ASCE*, 127 (9), 1092-1100.

Benmokrane B. (1997). "Bond Strength of FRP Rebar Splices," *Proceedings of the Third International Symposium on Non-Metallic (FRP) Reinforcement for Concrete Structures (FRPRCS-3)*, Japan Concrete Institute, Tokyo, Japan, 2, 405-412.

Branston, A. E., Boudreault, F. A., and Rogers, C. A., (2005). "Method for the Design of Light Gauge Steel Frame/Wood Panel Shear Walls," *Advances in Steel Structures*, *Elsevier*, 2, 1347-1352.

Caballero K. E., Bonet J. L., Avarro J. N., and Marti J. R. (2012)."Behavior of Steel-Fiber-Reinforced Normal-Strength Concrete Slender Columns under Cyclic Loading." *Engineering Structures*, 39, 162-175.

CAN/CSA A23.3-14 (2014)."Design of Concrete Structures", *Canadian Standards Association*, Mississauga, Ontario. 295 pp.

CAN/CSA S6-14, 2014, "Canadian Highway Bridge Design Code," *Canadian Standards Association*, Mississauga, Ontario, Canada, 1078 pp.

CAN/CSA S806-12 (2012). "Design and Construction of Building Structures with Fiber-Reinforced Polymers." *Canadian Standards Association* Rexdale, Ontario.208 pp.

CAN/CSA S806-02. (2002). "Design and Construction of Building Components with Fiber-Reinforced Polymers." *Canadian Standards Association*, Rexdale, Ontario. 206 pp.

Canadian Network of Centres of Excellence on Intelligent Sensing for Innovative Structures, *ISIS*-2007 Design Manual No. 3

Choo C., Harik I., and Gesund H. (2006). "Strength of Rectangular Concrete Columns Reinforced with Fiber-Reinforced Polymer Bars." *ACI Structural Journal*, 103 (3), 460-466.

De Luca, A.; Matta, F.; and Nanni, A., 2010, "Behavior of Full-Scale Glass Fiber-Reinforced Polymer Reinforced Concrete Columns under Axial Load," *ACI Structural Journal*, 107 (5), pp. 589-596.

Deniaud C. and Neale K. W. (2005). "An Assessment of Constitutive Models for Concrete Columns Confined with Fiber Composite Sheets." *Composite Structures*., 73 (3), 318-330.

Dong S., G., Yu F. W., Gang W., and Zhi S. W. (2012). "Plastic Hinge Analysis of FRP Confined Circular Concrete Columns." *Construction and Building Materials*, 27, 223-233.

Ehsani M. R., Saadatmanesh H., and Tao S. (1996). "Bond Behavior and Design Recommendations for Fiber-Glass Reinforcing Bars." *Proceedings of the First International Conference on Composites in Infrastructure (ICCI-96)*, Tucson, Ariz., 466-476.

El-Salakawy, E., Benmokrane, B., El-Ragaby, A., and Nadeau, D. (2005). "Field Investigation on the First Bridge Deck Slab Reinforced with Glass FRP Bars Constructed in Canada," *Journal of Composites for Construction*., 9 (6), pp. 470-479.

Elshamandy, M., Farghaly, A. S., and Benmokrane, B. (2015). "Simulated Seismic Behavior of GFRP-Reinforced Concrete Columns." *The 11th Canadian Conference on Earthquake Engineering, Canadian Association for Earthquake Engineering (11CCEE)*, Victoria, BC, Canada, 21 – 24 July, 8 p.

Faza S. S. and GangaRao H. V. (1990). "Bending and Bond Behavior of Concrete Beams Reinforced with Plastic Rebars." *Transportation Research Record* 1290, 185-193.

Fédération Internationale du Béton, fib, (2007). "FRP reinforcement in RC structures," Task Group 9.3, Lausanne, Switzerland.

FEMA 356, (2000). "Prestandard and Commentary for the Seismic Rehabilitation of Buildings." *Federal Emergency Management Agency*, Washington, DC, 518 pp.

Fischer G. and Li V. C. (2003). "Intrinsic Response Control of Moment-Resisting Frames Utilizing Advanced Composite Materials and Structural Elements." *ACI Structural Journal*, 100 (2), 166-176.

Freimanis A. J., Bakis C. E., Nanni A., and Gremel D. (1998). "A Comparison of Pullout and Tensile Behaviors of FRP Reinforcement for Concrete." *Proceedings of the Second International Conference on Composites in Infrastructure*, Tucson, Ariz, 2, 52-65.

Fukuyama H., and Masuda Y. (1995). "Structural Performances of Concrete Frame Reinforced with FRP Reinforcement." Non-Metallic (FRP) Reinforcement for Concrete Structures. Edited by Taerwe. E&FN Spon, London, pp. 275-286.

Gajalakshmi P. and Helena H. J. (2012). "Behavior of Concrete-Filled Steel Columns Subjected to Lateral Cyclic Loading." *Journal of Constructional Steel Research*, 75, 55-63.

Grira M., and Saatcioglu M. (1998) "Innovative Approaches to Column Confinement." Ph.D. Thesis, Dept. of Civil Engineering, University of Ottawa, Ottawa.

Hasaballa, M. H. (2009). "Seismic Behavior of Exterior GFRP Reinforced Concrete Beam-Column Joints." M.Sc. Thesis, University of Manitoba, Winnipeg, Manitoba, Canada.

Ho J. C. M. (2011). "Limited Ductility Design of Reinforced Concrete Columns for Tall Buildings in Low to Moderate Seismicity Regions," *Structural Design of Tall and Special Building*, 20 (1), 102–120.

Hwang S. and Yun H. (2004). "Effects of Transverse Reinforcement on Flexural Behavior of High-Strength Concrete Columns." *Engineering Structures*, 26 (1), 1-12.

Kassem, C.; Farghaly, A. S.; and Benmokrane, B. (2011). "Evaluation of Flexural Behavior and Serviceability Performance of Concrete Beams Reinforced with FRP Bars," *Journal of Composites for Construction*, 15 (5), pp. 682-695.

Kessler, S. (2010). "A Study of the Seismic Response Modification Factor for Log Shear Walls," MSc thesis, Kansas State University, Manhattan, KS, 113 pp.

Kobayashi K. and Fujisaki T. (1995). "Compressive Behavior of FRP Reinforcement in Non-Prestressed Concrete Members." *Non-metallic (FRP) Reinforcement For Concrete Structures*, Edited by Taerwe. E&FN SPon, London, 267-274.

Mady M., Elragaby A., and Elsalakawy E. (2011). "Seismic behavior of beam-column joints reinforced with GFRP bars and stirrups." *Journal of Composites for Construction*, 15 (6), 875-886.

Mallick P. K. "Fiber Reinforced Composites, Materials, Manufacturing, and Design." Marcell Dekker, Inc., New York, 1988, 469 pp.

Mattock, A. H. (1967). "Discussion of 'Rotational Capacity of Reinforced Concrete Beams' by W.G. Corley," *Journal of the Structural Division*, 93 (2), pp. 519-522.

Mohamed, N., Farghaly, A. S., Benmokrane, B., and Neale, K. W. (2014). "Drift Capacity Design of Shear Walls Reinforced with GFRP Bars." *ACI Structural Journal*, 111 (6), 1397-1406.

Mohamed N., Farghaly A. S., Benmokrane B., and Neale K. W. (2014). "Experimental Investigation of Concrete Shear Walls Reinforced with Glass-Fiber-Reinforced Bars under Lateral Cyclic Loading." *Journal of Composites for Construction*, 18 (3), A4014001.

Mohamed, N.; Farghaly, A. S.; and Benmokrane, B. (2015). "Aspects of Deformability of Concrete Shear Walls Reinforced with Glass Fiber–Reinforced Bars," *Journal of Composites for Construction*, 19 (5), p. 06014001

Mortezaei A. and Ronagh H. R. (2013). "Plastic Hinge Length of Reinforced Concrete Columns subjected to Both Far-Fault and Near-Fault Ground Motions having Forward Directivity." *The Structural Design of Tall and Special Buildings*, 22 (12), 903 – 926.

Mosley C. P. (2002). “Bond Performance of Fiber Reinforced Plastic (FRP) Reinforcement in Concrete,” MSc thesis, Purdue University, West Lafayette, Ind.

Munoz, W., Salenikovich, A., Mohammad, M., Quenneville, P. (2008) “Determination of yield point and ductility of timber assemblies: in search for a harmonised approach.” Proc *of Meeting 41 of CIB-W18*, St Andrews, Canada.

Nanni A., Nenninger J., Ash K., and Liu J. (1997). “Experimental Bond Behavior of Hybrid Rods for Concrete Reinforcement.” *Structural Engineering and Mechanics*, 5 (4), 339-354.

National Building Code of Canada (NBCC) (2010). "Canadian Commission on Building and Fire Codes." *National Research Council of Canada,* Canada.

National Building Code of Canada (NBCC) (2005). "Canadian Commission on Building and Fire Codes." *National Research Council of Canada,* Canada.

Ozbakkaloglu T. and Saatcioglu M. (2007). “Seismic Performance of Square High-Strength Concrete Columns in FRP Stay-in-Place Formwork.” *Journal of Structural Engineering*, 133 (1), 44-56

Pantelides C. P., Gibbons M. E., and Reaveley L. D. (2013). “Axial Load Behavior of Concrete Columns Confined with GFRP Spirals.” *Journal of Composites for Construction*, 17 (3), 305-313

Paramanantham N. (1993). “Investigation of the Behavior of Concrete Columns Reinforced with Fiber Reinforced Plastic Rebars.” MSc Thesis, Lamar University, Beaumont, Texas.

Park, R., and Paulay, T. (1975). “Reinforced Concrete Structures”, John Wiley and Sons, New York, 769 pp.

Park, R., Priestley, M. J. N., and Gill, W. D. (1982). “Ductility of Square-Confined Concrete Columns,” *Journal of Structural Division*, ASCE, 108 (4), pp. 929-950.

Paulay, T., and Priestley, M. J. N. (1992). "Seismic Design of Reinforced Concrete and Masonry Buildings", John Wiley and Sons, New York, 767 pp.

Paulay T., and Priestley M. J. N. (1995). "Seismic Design of Reinforced Concrete and Masonry Buildings." John Wiley and Sons, 735 pp.

Phillips L.N. "Design with Advanced Composite Materials", 1989, Springer-Verlag.

Priestley, M. J. N., and Park, R. (1987). "Strength and Ductility of Concrete Bridge Columns under Seismic Loading," *ACI Structural Journal*, 84 (1), 61-76.

Purba B. K. and Mufti A. A. (1999). "Investigation of the Behavior of Circular Concrete Columns Reinforced with Carbon Fiber Reinforced Polymer (CFRP) Jackets." *Canadian Journal of Civil Engineering*, 26, 590–596.

Rogers, C. A., Balh, N., Ong-Tone, C., Shamim, I., and DaBreo, J., (2011). "Development of Seismic Design Provisions for Steel Sheet Sheathed Shear Walls," *Proceedings of the Structures Congress*, ASCE, Las Vegas, NV, pp. 676-687.

Saatcioglu M. and Baingo D. (1999) "Circular High-Strength Concrete Columns under Simulated Seismic Loading." *Journal of Structural Engineering*, 125 (3), 272-280.

Said A. M. and Nehdi M. L. (2004). "Use of FRP for RC Frames in Seismic Zones: Part II. Performance of Steel-Free GFRP-Reinforced Beam-Column Joints." *Applied Composite Materials,* 11, 227-245.

Samuel Y. L., Tzu L. W., Tony C. L., Shamim A. S., and Raymond W.(2011). "Interlocking Spiral Confinement for Rectangular Columns." *Concrete International*, 33 (12).

Sawyer, H. A., "Design of Concrete Frames for Two Failure Stages, (1964). " *Proceedings of the International Symposium on Flexural Mechanics of Reinforced Concrete*, ASCE-ACI, Miami, FL, pp. 405-431.

Shamim A. S. and Yeh C. C. (1990). "Tied Concrete Columns under Axial Load and Flexure." *Journal of Structural Engineering*, 116 (10), 2780-2800

Shan B., Xiao Y., and Guo Y. (2006). "Residual Performance of FRP-Retrofitted RC Columns after Being Subjected to Cyclic Loading Damage." *Journal of Composites for Construction*, 10 (4), 304-312.

Sharbatdar M. K. (2003). "Concrete Columns and Beams Reinforced with FRP Bars and Grids under Monotonic and Reversed Cyclic Loading." Ph.D. Thesis, University of Ottawa, Ottawa, Canada.

Sharbatdar, M. K.; and Saatcioglu, M., 2009, "Seismic Design of FRP Reinforced Concrete Structures," *Asian Journal of Applied Sciences*, 2 (3), pp. 211-222

Sharbatdar M. k., Saatcioglu M., and Benmokrane B. (2011). "Seismic Flexural Behavior of Concrete Connections Reinforced with CFRP Bars and Grids." *Composite Structures*, 93 (10), 2439-2449.

Sheikh, S. A.; and Khoury, S. S., 1993, "Confined Concrete Columns with Stubs," *ACI Structural Journal*, 90 (4), pp. 414-431.

Sheikh, S. A., Shah, D. V., and Khoury, S. S. (1994). "Confinement of High-Strength Concrete Columns," *ACI Structural Journal*, 91 (1), pp. 100-111.

Shield C., French C., and Hanus J. (1999). "Bond of GFRP Rebar for Consideration in Bridge Decks." Fourth International Symposium on Fiber Reinforced Polymer Reinforcement for Reinforced Concrete Structures, *ACI* SP-188, 393-406.

Tavassoli, A., Liu, J., and Sheikh, S. (2015) "Glass Fiber-Reinforced Polymer-Reinforced Circular Columns under Simulated Seismic Loads," *ACI Structural Journal*, 112 (9), pp. 103-114.

Tighiouart B., Benmokrane B., and Mukhopadhyaya P. (1999), "Bond Strength of Glass FRP Rebar Splices in Beams Under Static Loading." *Construction and Building Materials*, 13 (7), 383-392.

Tobbi H., Farghaly A. S., and Benmokrane B. (2012). "Concrete Columns Reinforced Longitudinally and Transversally with Glass Fiber-Reinforced Polymer Bars." *ACI Structural Journal*, 109 (4), 551-558.

Tobbi, H.; Farghaly, A. S.; and Benmokrane, B., 2014, "Strength Model for Concrete Columns Reinforced with Fiber-Reinforced Polymer Bars and Ties," *ACI Structural Journal*, 111 (65), pp. 789-798.

Wambeke B. and Shield C. (2006). "Development Length of Glass Fiber Reinforced Polymer Bars in Concrete." *ACI Structural Journal*, 103 (1), 11-17.

Wu W. P. (1990). "Thermomechanical Properties of Fiber Reinforced Plastic (FRP) Bars." PhD Dissertation, West Virginia University, Morgantown, West Virginia, 292pp.

Yamakawa T. and Fujisaki T. (1995). "A study on Elasto-Plastic Behavior of Structural Walls Reinforced by CFRP Grids." *Non-metallic (FRP) Reinforcement for Concrete Structures*, Edited by Taerwe. E&FN SPon, London, 306-313.

Yun H. W. (2003). "Full-Scale Experimental and Analytical Studies on high-Strength Concrete Columns." Ph.D. Thesis, University of Southern California, USA.

Zadeh, H. J.; and Nanni, A., 2013, "Design of RC columns using glass FRP reinforcement," *Journal of Composites for Construction*, 17 (3), pp. 294-304.

Zafra R., G. and Kawashima K. (2009). "Analysis of Carbon Fiber Sheet-Retrofitted RC Bridge Columns under Lateral Cyclic Loading." *Journal of Earthquake Engineering*, 13 (2), 129-154.

APPENDIX

SOLVED EXAMPLE

Design of GFRP-reinforced concrete columns satisfying the seismic requirements for ductile moment-resisting frames (Rd = 4)

Data

The mechanical properties of the reinforcement used are as follows:

- Longitudinal reinforcement (#4 GFRP bars)
  Bar diameter = 12.7 mm, bar nominal cross-sectional area = 126.7 mm^2, Efrp = 69.6 GPa, f_{frpu} = 1392 MPa, ε_{frpu} = 0.02
- Transverse reinforcement (#3 GFRP stirrups and ties)
  Stirrup/tie diameter = 9.5 mm, Stirrup/tie nominal cross-sectional area = 71.3 mm^2, E_{frp} = 52 GPa, f_{frpu} = 962 MPa, ε_{frpu} = 0.0185
- The vertical load needed to be carried = 1120 kN, concrete strength = 41 MPa, column height = 1.65 m

Design

Assume a square concrete section = *Ag,*

$$A_g = 400mm * 400mm \quad (32)$$

Nominal load = *Po*,

$$P_O = 0.85 * A_c f_c^{`} = 0.85 * 400 * 400 = 5576\ kN \quad (33)$$

Axial-load percentage = *P/Po,*

$$P/Po = 1120/5576 = 0.2 \quad (34)$$

(lies in the proposed range of applied axial load)

From CSA S806-12, clauses 8.4.3.7and 8.4.3.10:

Longitudinal reinforcement area=A_l,

$$A_l = 1\%\ A_g = 0.01 * 400 * 400 = 1600\ mm^2 \quad (35)$$

Assume 12#4.

From CSA-S806-12, clauses 8.4.3.14, 8.4.3.15, 8.4.6, 12.7.2.3, 12.7.3.4, and 12.7.4.4; assume spacing (s) = 80 mm

Using closed internal stirrups 9.5 mm in diameter; check the volumetric ratio against CSA S806-12, clause 8.4.3.13

$$V_e(\%) \geq \left(f_c^{`}/f_{fh}\right)\left(A_g/A_c - 1\right)(P/P_o) \quad (36)$$

where *Ve (%)* is the volumetric reinforcement ratio

$V_e(\%) = 1.77\% > 0.6\% \ldots\ldots\ldots\ldots ok$

Checking the lateral drift ratio using Eq. 3

$$K_C = 0.15\left[\sqrt{\frac{h_c h_c}{s\, s_l}}\right] \quad (37)$$

$$K_C = 0.15 * \left[\sqrt{\frac{350 * 350}{80 * 117}}\right] = 0.54$$

$$A_{sh} = 800\, s\, h_c\left[f_c^{`}/f_{fh}\right]\left[(A_g/A_c) - 1\right][P/P_O][A_l/A_c]\left[\delta/\sqrt{K_C}\right] \quad (38)$$

$284 = 800 * 80 * 350 * [41/300][(400^2/350^2) - 1] * 0.2 * [1519/350^2] * [\delta/0.7366]$

$\delta = 0.09 > 0.04$

Using plane sectional analysis and interaction diagram, assume the confined concrete strain = 7000 με, as recommended.

The corresponding moment to the axial load (1120 kN) is = 298.16 kN.m.

The lateral nominal load = 180.7 kN; $\varepsilon_c/c = 55.2\ \mu\varepsilon/mm$

Calculation of rotation capacity

$$V_e(\%) * (L/h) = 7.3 \quad (39)$$

Using Eq. 29

$$\theta_c = [0.000014 V_e L_c/h][(L_c/3) - 1.25h] + [1.25h\varepsilon_{cu}/c] \quad (29)$$

$\theta_c = (0.000014 * 7.3)(550 - 1.25 * 400) + ((1.25 * 400 * 55.2)/10^6)$

$\theta_c = 0.0327 = 3.27\%$

Calculation of rotation demand

Using Eq. 31, calculate the elastic deformation.

$$\Delta_{ed} = P[(L_c^3/3E_cI_e) + (L_c/G_cA_{sh})] \quad (31)$$

where P is the lateral design force ≤ the lateral nominal load. In this study, for safety, P will be taken as the lateral nominal load = 180.7 kN.

Rd = 4 for ductile moment-resisting frames

$$\Delta_{ed} = 180700\ [(1650^3/(3 * 30000 * 1.067 * 10^9)) + (1650/(12020 * 137600))]$$

$$\Delta_{ed} = 8.62\ mm$$

From Eq. 30

$$\theta_d = (\Delta_{ed}/L_c)\ [(RL_c - 0.625h)/(L_c - 0.625h)] \quad (30)$$

$$\theta_d = [8.62/1650][(4 * 1650 - 0.625 * 400)/(1650 - 0.625 * 400)]$$

$$\theta_d = 0.237 = 2.37\%$$

Since $\theta_c > \theta_d$, the proposed column can be used as part of the ductile moment-resisting frame.